NASA-CR-190624

P 165

TRACE GAS AND AEROSOL TRANSPORTS INTO AND OUT OF THE AMAZON BASIN

NASA Cooperative Agreement NCC1-106

Semi-Annual Report
for the period

1 September 1991-31 May 1992

Submitted by

Michael Garstang
Principal Investigator

Department of Environmental Sciences
University of Virginia
Charlottesville, VA 22903

July 1992

(NASA-CR-190624) TRACE GAS AND AEROSOL TRANSPORTS INTO AND OUT OF THE AMAZON BASIN Semiannual Report, 1 Sep. 1991 - 31 May 1992 (Virginia Univ.) 165 p

N92-31153

Unclas

G3/45 0115075

LOW-LEVEL NOCTURNAL WIND MAXIMUM OVER THE CENTRAL AMAZON BASIN

STEVEN GRECO[1], STANLEY ULANSKI[2], MICHAEL GARSTANG and SAMUEL HOUSTON[3]

[1]*Department of Environmental Sciences, University of Virginia, Charlottesville, VA 22903, U.S.A.*
[2]*Department of Geology and Geography, James Madison University, Harrisonburg, VA 22807, U.S.A.*
[3]*Hurricane Research Division, NOAA, Miami, FL, 33149, U.S.A.*

(Received in final form 13 June, 1991)

Abstract. A low-level nocturnal wind maximum is shown to exist over extensive and nearly undisturbed rainforest near the central Amazon city of Manaus. Analysis of meteorological data collected during the 1985 and 1987 Amazon Boundary Layer Experiments (ABLE 2A and 2B) indicates the presence of this nocturnal wind maximum during both the wet and dry seasons of the Central Amazon Basin. Daytime wind speeds which are characteristically 3–7 m s^{-1} between 300 and 1000 m increase to 10–15 m s^{-1} shortly after sunset. The wind speed maximum is reached in the early evening, with wind speeds remaining high until several hours after sunrise. The nocturnal wind maximum is closely linked to a strong low-level inversion formed by radiational cooling of the rainforest canopy. The night-time inversion extends up to 300 m with strong vertical shear of the horizontal wind below the inversion top and uniformly strong horizontal winds above the inversion top. Frictional decoupling of the air above the inversion from the rough forest below, however, is responsible for only part of the observed increase. Surface and low-level pressure gradients between the undisturbed forest and the large Amazon river system and the city of Manaus are shown to be responsible for much of the nocturnal wind increase. The pressure gradients are interpreted as a function of the thermal differences between undisturbed forest and the river/city. The importance of both the frictional decoupling and the horizontal pressure gradient suggest that the nocturnal wind maximum does not occur uniformly over all Amazonia. We suspect that stronger low-level winds are pervasive under clear skies and strong surface cooling and that, in many places (i.e., near rivers), local pressure gradients enhance the low-level nocturnal winds.

1. Introduction

The lower atmosphere of the global tropics is generally embedded within the equatorial trough and is mainly thought to be a region of low wind speed; note the widely-used term 'doldrums'. It came, therefore, as a considerable surprise to these investigators to find low-level, nocturnal wind speeds in the near-equatorial central Amazonian rainforests to be in excess of 15 m s^{-1} during both the wet and dry seasons.

Equatorial continental regions of the earth's surface beyond the immediate environs of a few cities and settlements remain relatively inaccessible. The rainforest, with its attendant size (canopies at 40 to 50 m) and biological and physical conditions, presents a hostile environment, particularly in the wet season, for scientific measurements. Despite these obstacles, considerable work has been done in equatorial rainforests. Most has focussed upon the biological aspects of this large and diverse ecosystem. The work that has dealt with the atmosphere has

Boundary-Layer Meteorology **58**: 91–115, 1992.

been mainly directed at the larger scale dynamics. In the Amazon Basin, for example, several researchers (Kousky, 1979; Kousky and Ferreira, 1981; Kousky and Kagano, 1981; Paegle, 1987; Salati and Vose, 1984; Silva Dias *et al.*, 1987; Nobre *et al.*, 1987) have been responsible for pioneering work. The British-Brazilian experiments of the early 1980's (Shuttleworth *et al.*, 1984, 1985) were the first in Amazonia to address the detail of the hydrologic cycle and the micrometeorology of the rainforest.

In 1985 and 1987, the U.S. National Aeronautics and Space Administration (NASA), as part of its Global Tropospheric Experiment (GTE), joined with the Brazilian Instituto de Pesquisas Espaciais (INPE) and the Instituto Nacional de Pesquisas da Amazonia (INPA) to mount two major experiments in central Amazonia. These experiments, called the Amazon Boundary Layer Experiments (ABLE), were conducted in the dry (July–August 1985) and wet (April–May 1987) seasons and were directed at establishing the base atmospheric chemistry state over the forest and wetlands of the Amazon basin (Harriss *et al.*, 1988, 1990; Garstang *et al.*, 1990). We shall draw upon these experiments to document the structure and nature of the nocturnal velocity field in the boundary layer over the rainforest of central Amazonia.

The occurrence of a pronounced nocturnal wind maximum over the central Amazon basin (CAB) was first noted by Greco *et al.* (1989). Garstang *et al.* (1990) and Oliveira (1990) have also discussed this feature. In this paper, we shall describe the nocturnal evolution of the boundary-layer winds together with the associated temperature and pressure fields. We shall then present a mechanism which accounts for the night-time wind speed maximum in the first kilometer above the forest.

Nocturnal low-level jets and wind maxima have been documented in many locations around the globe (Bonner, 1968; Wipperman, 1973). The low-level jet of the Great Plains region of the United States has been extensively studied by among others, Hoecker (1963, 1965); Blackadar (1957); Wexler (1961) and Bonner (1968). Other mid-to-higher latitude nocturnal low-level jets have been detected in southeastern Australia (Clarke *et al.*, 1971), southern England (Thorpe and Guymer, 1977), northwestern Germany (Kraus *et al.*, 1985), the United States Gulf coast (Hsu, 1979), and the coastal regions of northeastern United States and the Canadian Maritimes (Dickerson and Neumann, 1982). In the tropical and subtropical regions of the world, however, only a few documented cases of low-level nocturnal jets or wind maxima are in existence. DeSouza *et al.* (1971) showed remarkable accelerations below 500 m over the island of Barbados (near 13° N, 60° W). These accelerations were not, however, strictly nocturnal. In the Daly Waters region of Australia (16°16′ S, 133°23′ E), Clarke and Brook (1979), Brook (1985), and Garratt (1982, 1985) all have documented a nocturnal jet based upon measurements from the 1974 Korrin expedition. Virji (1981) found a nocturnal jet in the western Amazon basin near the foothills of the Andes.

Although these strong nocturnal winds form in numerous and varied locations,

they have a number of common features. The nocturnal wind maxima all form shortly before or after sunset, within the nocturnal planetary boundary layer (often at heights between 300–700 m above ground level), and can reach speeds which are 2–3 times larger than daytime values. Each low-level jet or wind maximum, however, may owe its origin to a different mechanism or set of mechanisms.

One of the mechanisms most often responsible for nocturnal maxima is the inertial oscillation induced when frictional constraint imposed by daytime turbulence is released by the formation of an inversion near sunset (Blackadar, 1957). This allows the wind above the inversion to reach supergeostrophic levels. Other prime mechanisms include: winds associated with surface radiational cooling over sloping terrain (Lettau, 1967, 1983; Zeman, 1979); advective accelerations (Paegle and Rasch, 1973); variations in the synoptic-scale geostrophic wind (Mahrt, 1981); and the generation of mesoscale pressure gradients in response to heating and cooling over sloping or non-uniform terrain (McNider and Pielke, 1981).

The ABLE, located in the CAB essentially on the equator, precludes inertial oscillation (period too long), Coriolis force (approaches zero for horizontal motion) or terrain (large-scale slope $\leq 1:2000$ km) as forces driving the nocturnal maxima of the low-level wind. However, horizontal surface temperature gradients produced by the confluence of the large Negro and Solimoes rivers to form the Amazon may play a role in generating the nocturnal wind maxima of the CAB. In addition, the effective removal of surface frictional drag by the formation of a low-level nocturnal radiation inversion may also be responsible for the increase in horizontal wind speed between day and night.

2. Experimental Design and Data Collection

A manned tethersonde and radiosonde station was operated in ABLE 2A from July 15 to August 7, 1985 at Ducke Forest Reserve, approximately 20 km northeast of Manaus, Brazil (Figures 1 and 2). Vertical profiles of temperature, horizontal wind speed and direction, pressure, and humidity up to 1000 m were taken by a sonde-equipped tethered balloon. The ascent rate of the balloon was 1 m s^{-1} and measurements of horizontal velocity were made every 2 m and those of temperature, humidity and pressure every 4 m. Each sounding lasted between 15 and 20 min and both up and down profiles were taken. Three to four vertical soundings were made during most hours. In addition to the tethersondes, rawinsondes using a high-resolution Atmospheric Instrumentation Research (AIR) sonde and a digital recording and processing system were launched every three hours. These rawinsondes ascended to 500–400 mb and provided measurements of wind speed and direction, temperature, and specific humidity. Hours of operation were mainly confined to the daytime, except for six days when measurements were taken throughout the 24 h. The data from these six days will be a main focus in this paper.

In the ABLE 2B wet season experiment, from April 1 to May 14, 1987, Ducke

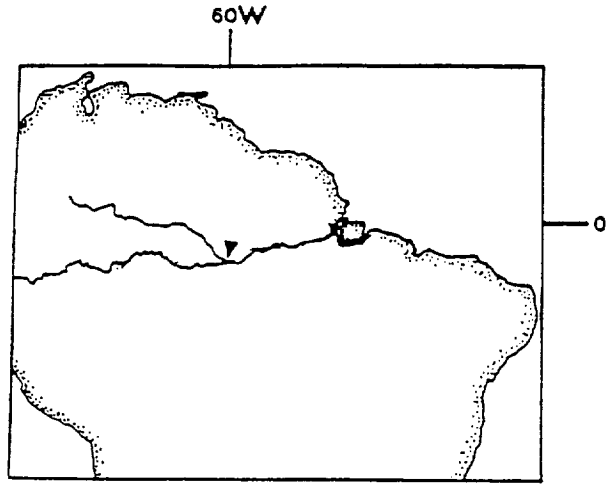

Fig. 1. Location of the ABLE 2A and 2B experiments within the central Amazon basin as indicated by the darkened triangle.

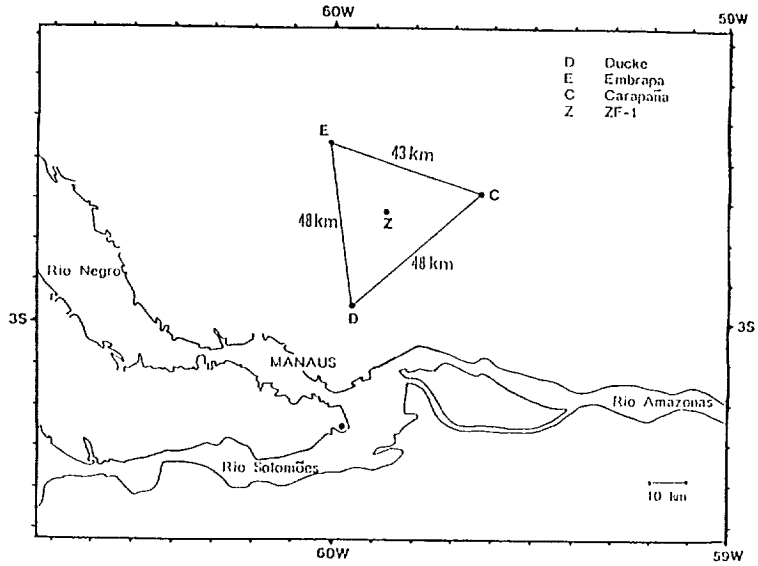

Fig. 2. Orientation, dimensions, and location relative to the Amazon river system of the mesoscale triangle network (blackened triangle in Figure 1) employed during ABLE 2B.

Reserve was one of three sonde-equipped stations forming a mesoscale triangle of approximately 1000 km^2 (Figure 2). The mesoscale network consisted of 3 stations (Ducke, Embrapa, and Carapaña) located at the triangle corners and one station (ZF-1) located in the center. The tethered balloons ascended up to 500 m at Carapaña and Embrapa and up to 1000 m at Ducke. No balloons were launched from ZF-1. Vertical profiles of the boundary layer during ABLE 2B were not

obtained as often as during the earlier dry season experiment. At most, 2–3 vertical profiles were taken during each hour of observation and there were many periods of up to 2 hours without a vertical tethersonde profile. Reasons for this included logistics, different experimental objectives, and preventive maintenance on strained equipment. Rawinsonde launches occurred 4 times a day at Ducke and Carapaña (0800, 1100, 1400, and 1700 LST) and 6 times a day at Embrapa (2000, 0200, 0800, 1100, 1400, and 1700 LST).

The four stations shown in Figure 2 were also equipped with Portable Automated Mesonet (PAM) systems mounted on 45 m towers, placing them 5 m above the forest canopy. Measurements of horizontal wind speed and direction, temperature, humidity, and pressure were taken at a frequency of 1 Hz and compiled into 1 min averages.

Similar to ABLE 2A, most of the ABLE 2B experiment was conducted during the daytime. However, a four-day period of continuous 24-h operation was carried out near the end of the experiment to examine the structure and evolution of the transition (dusk, dawn) and night-time boundary layer during the wet season.

3. Observed Boundary-Layer Structure

3.1 ABLE 2A

Meteorological conditions during the 1985 ABLE 2A experiment were typical of the CAB dry season when undisturbed conditions with suppressed convection tend to dominate. Night-time observations in the dry season were taken on 6 occasions: July 25–26, July 26–27, July 30–31, July 31–August 1, August 1–2, and August 2–3. With the exception of the initial night-time observation period (July 25–26), the tethersonde data coverage was fairly continuous throughout the night.

Composite soundings for the ABLE 2A experiment were created from the 3-hourly rawinsonde launches made at Ducke Reserve. Figure 3 displays the composite wind speed profiles below 700 mb for soundings taken at 2000, 0200, 0800 and 1400 LST.* Between midafternoon (1400 LST) and early evening (2000 LST), there is a noticeable increase in wind speed throughout the lower troposphere. The strongest increase is found below 1000 m/900 mb where winds increase from 4–5 to 7–8 m s^{-1} with a nose-like feature found between 950–900 mb at 2000 LST. After this initial acceleration, the winds below 1000 m remain relatively constant through most of the night before decelerating after sunrise.

The composite wind profiles from the rawinsonde shown in Figure 3 offer some evidence of a boundary-layer nocturnal low-level jet or wind maximum (WM hereafter). However, the rawinsonde speeds are averaged over a depth of 200–300 m and give a smoothed profile of the boundary-layer winds, which perhaps

* Since sunrise and sunset in the ABLE mesoscale triangle region (2–3 °S latitude) is near 6 a.m. and 6 p.m. during the entire year, and the subject of this paper is closely tied to the diurnal cycle, we shall use Local Standard Time (60th meridian) throughout.

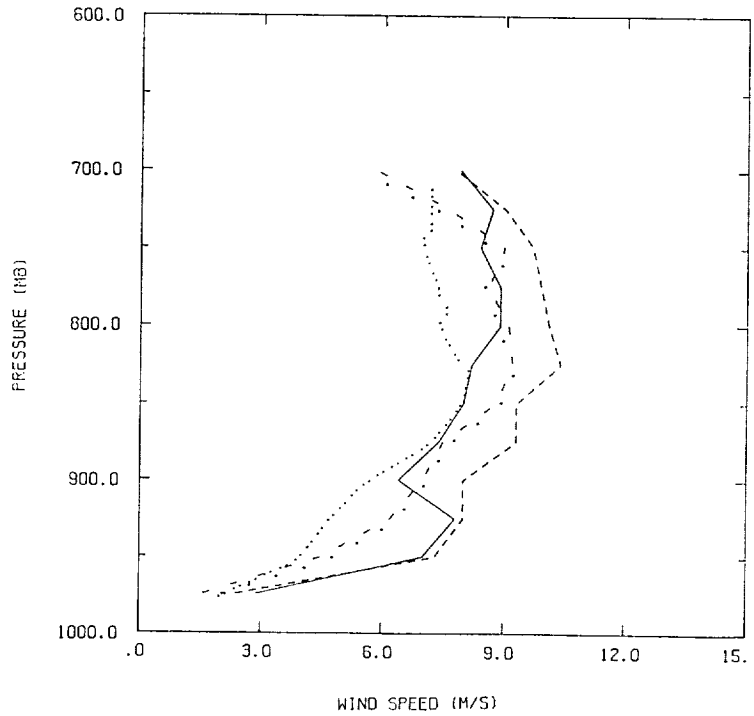

Fig. 3. Composite rawinsonde wind speed profiles measured during ABLE 2A at Ducke Reserve for 0800 LST (dash-dot), 1400 LST (dotted), 2000 LST (solid) and 0200 LST (dashed).

does not capture the full extent of the nocturnal wind speeds. Table I shows a comparison between rawinsonde and tethersonde measured wind speeds at similar heights and near-coincident times. During the afternoon (1400 LST), there is little difference between the values of wind speed measured by tethersondes and by rawinsondes. This is mainly an indication of the well-mixed afternoon boundary layer. At night (0200 LST), however, the rawinsondes, unlike the finer resolution tethersonde, are unable to capture the strong nocturnal winds and their vertical shear. This is illustrated by the 2–5 m s^{-1} difference between the tethersonde and rawinsonde wind measurements. The absence of detailed measurements with high vertical resolution in the lower atmosphere of the CAB before the ABLE may be a reason why a nocturnal WM has not been previously detected.

However, as seen in the 0200 LST rawinsonde composite wind speeds for all 6 nights and the 3 nights with a strong nocturnal WM (Figure 4), the rawinsondes, despite their poor vertical resolution, are still able to capture the nocturnal WM on nights when the tethersonde data indicated the existence of a strong maxima. On nights when the WM is more modest, the rawinsonde smooths the vertical profile to the point where any evidence of a nocturnal WM is lost. To document the existence of this WM, we shall concentrate on the more detailed measurements taken by the tethered balloons.

TABLE I

Average wind speed values in the 1000–900 mb layer as measured by near-coincident tethersondes ($\bar{T}$) and rawinsondes ($\bar{R}$) at Ducke during ABLE 2A. Several times are given and a mean difference ($\overline{T-R}$) is calculated

	No. of rawinsondes launched	Rawinsonde ($\bar{R}$ in m s^{-1})	Tethersonde ($\bar{T}$ in m s^{-1})	$\overline{T-R}$ (m s^{-1})
1400 LST				
975 mb	12	2.9	3.9	1.0
950 mb	13	4.9	4.4	−0.5
925 mb	13	4.7	4.7	0.1
900 mb	11	5.6	6.4	0.8
2000 LST				
975 mb	4	3.5	8.0	4.6
950 mb	6	7.0	8.6	1.5
925 mb	6	7.8	9.1	1.2
900 mb	3	3.7	8.8	5.6
0200 LST				
975 mb	5	2.4	8.2	5.8
950 mb	6	7.3	9.5	2.2
925 mb	6	8.0	10.5	2.5
900 mb	2	6.6	8.5	1.9
0800 LST				
975 mb	8	1.8	5.6	3.9
950 mb	11	4.1	6.6	2.6
925 mb	10	5.4	7.9	2.6
900 mb	9	5.0	9.1	3.6

Tables IIa–b summarize the salient features of the diurnal evolution of the boundary-layer wind and temperature tethersonde profiles for the 5 cases (omitting the August 2–3 synoptic event) of day-to-night operations. The nocturnal WM and a surface-based temperature inversion exist on all 5 nights, although with varying intensities. In addition, there is in all 5 cases a common wind direction shift from SE/ESE to NE/ENE between day and night. The wind shift is especially strong during the 3 nights with substantial increase of wind speed from day to night (July 30–31, July 31–August 1, August 1–2).

The night-time feature illustrated in Table II and Figures 3 and 4 is examined in greater depth by concentrating on 2 cases of a strong nocturnal WM.

After a one-day suspension of operations, observations resumed at 1800 LST on July 30. The formation of a strong surface-based temperature inversion (+2.5 °C/150 m) shortly after sunset can be seen in Figure 5a. This inversion lasts throughout the night, weakening only slightly by 0600 LST. The top of the inversion is situated near 380 m above mean sea level (MSL) or 300 m above ground level (AGL) (Ducke is 78 m above MSL). This inversion is much stronger than the one noted on the partly cloudy nights of July 25–26 and 26–27 due to the

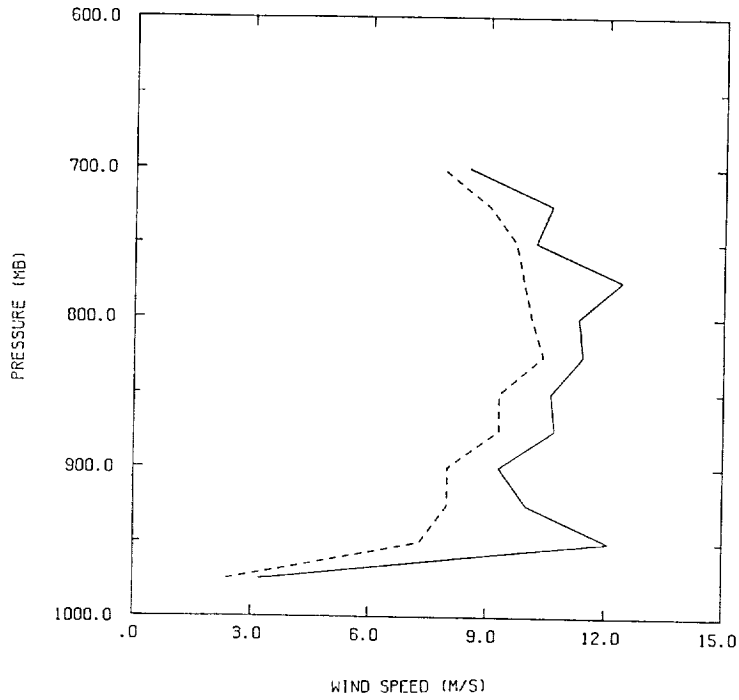

Fig. 4. 0200 LST composite rawinsonde wind speed profiles during ABLE 2A at Ducke for: all six nights (dashed); and the three nights with strong nocturnal wind accelerations (solid).

more intense radiative cooling produced by the clear skies which were noted by weather observations.

A large increase in horizontal wind speed at and above the inversion top accompanies the stable conditions in the lower 300 m. As illustrated by Figure 5b, winds above the top of the inversion increase from 6–12 m s^{-1} near 1800 LST to 12–15 m s^{-1} through the night. These winds are uniformly strong up to at least 1000 m. Below the inversion top, there is a layer of strong vertical wind shear with winds increasing from near calm at the surface to 11–13 m s^{-1} at 300 m AGL. The nocturnal inversion and WM, along with the separation of layers noted on July 30–31 are all stronger than during the nights of July 25–26 and 26–27 when broken cloudiness lasted throughout 0200 LST (see Table II).

Similar to the July 25–26 and 26–27 cases, however, the stronger horizontal winds continue through 0900–1000 LST of the next morning (July 31) until the inversion breaks down and adiabatic lapse rates resume (Figures 6a, b). After 1000 LST, turbulent mixing and surface heating once again produce a well mixed layer with wind speeds of <7 m s^{-1}. Shortly before sunset, the surface-based inversion has once again formed. With the inversion formation, a significant increase in the wind speed is seen before 1800 LST with winds reaching 9 m s^{-1} between 250 and 400 m AGL.

TABLE II

Tethersonde-measured boundary-layer temperature (°C) and wind conditions ($m\,s^{-1}$ and degrees) at Ducke during 5 nights of ABLE 2A operation. Conditions are noted for the surface, inversion top (300 m) and 700 m

	7/25–7/26	7/26–7/27	7/30–7/31	7/31–8/1	8/1–8/2
(a) *Temperature*					
1600 LST					
sfc	28.7	27.5	25.4	29.8	–
300 m	27.0	26.4	27.3	28.5	–
700 m	23.4	22.8	24.5	24.7	–
0000 LST					
sfc	22.1	22.7	23.9	22.7	22.2
300 m	23.2	23.3	26.4	26.7	26.0
700 m	23.1	21.7	23.7	23.9	24.2
0800 LST					
sfc	23.6	22.5	23.7	22.2	21.3
300 m	23.8	24.0	26.0	26.2	25.0
700 m	21.9	22.3	23.1	23.3	23.8
1200 LST					
sfc	26.4	28.3	29.4	–	30.6
300 m	24.6	26.7	27.7	–	28.8
700 m	21.8	23.1	23.9	–	24.7
(b) *Wind*					
1600 LST					
sfc	2.4/84	1.1/106	1.1/95	4.2/94	–
300 m	3.8/106	3.1/70	7.3/98	6.3/114	–
700 m	4.7/111	2.6/25	12.0/87	7.0/95	–
0000 LST					
sfc	0.4/80	1.2/50	2.0/55	0.5/44	1.2/10
300 m	4.5/–	4.7/66	11.7/59	10.1/90	7.9/11
700 m	9.5/94	5.8/103	10.7/92	10.8/85	11.7/10
0800 LST					
sfc	2.3/45	2.1/52	3.4/50	0.6/80	0.6/344
300 m	6.3/50	8.4/44	11.9/74	10.6/90	7.4/345
700 m	8.5/93	8.7/63	12.0/80	8.8/96	9.5/0
1200 LST					
sfc	4.1/26	2.6/130	5.3/120	–	4.5/150
300 m	5.1/30	3.8/148	3.8/48	–	7.5/136
700 m	7.5/33	4.1/90	4.1/90	–	7.9/135

The night of July 31–August 1 was almost identical to the previous night (Figures 7a, b). Clear skies and radiation cooling enhance the surface-based temperature inversion which extends up to 300–320 m AGL and lasts the entire night. This inversion exhibits a lapse rate of +1–2°/100 m and also weakens slightly by morning. Strong nocturnal winds develop above the inversion top with speeds of 10–14 $m\,s^{-1}$ between 300 and 1000 m. Once again, strong stratification is seen with

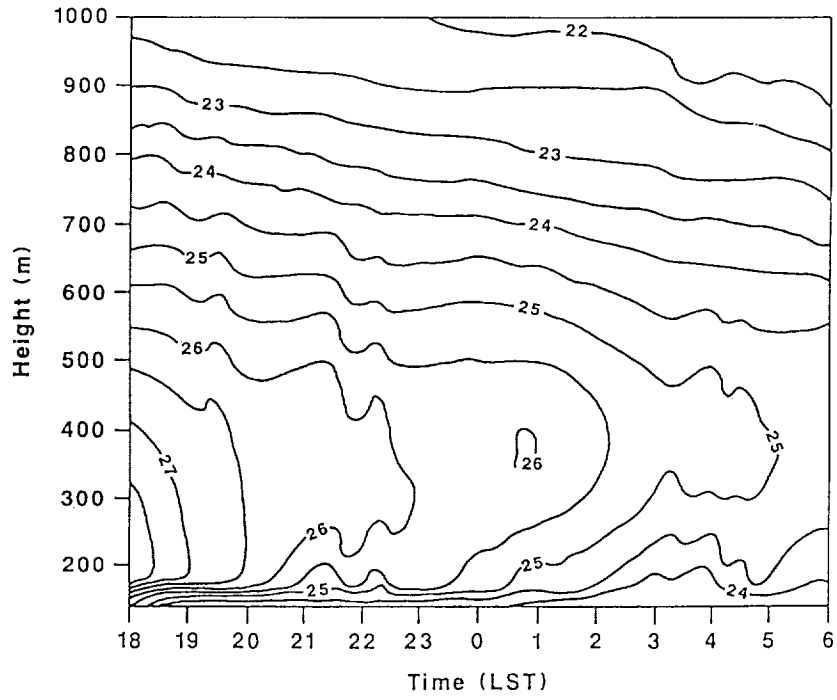

(a)

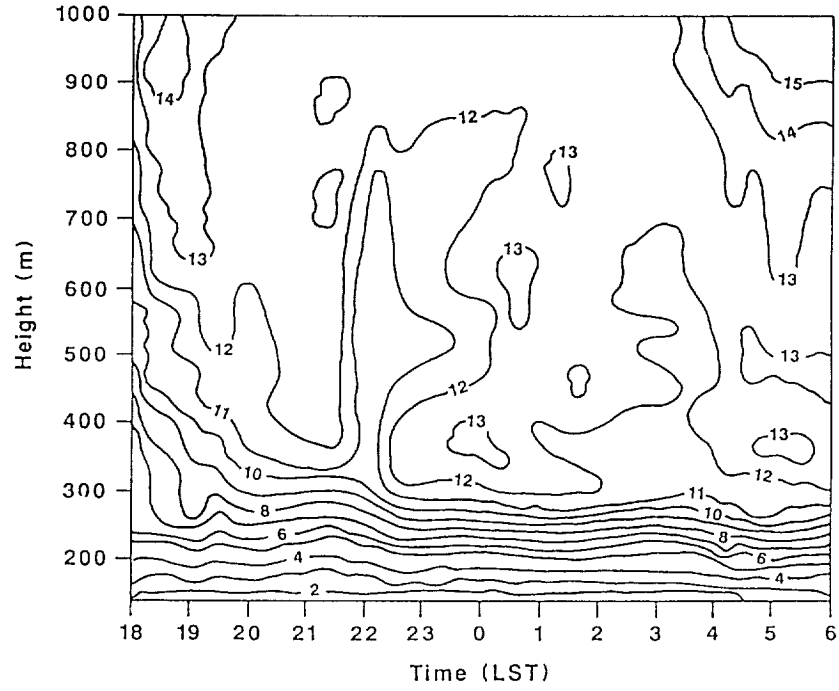

(b)

Fig. 5. Time-height contours of (a) temperature and (b) wind speed measured by tethersonde at Ducke during July 30–31, 1985. Height is in meters above mean sea level (Ducke is 78 m above MSL).

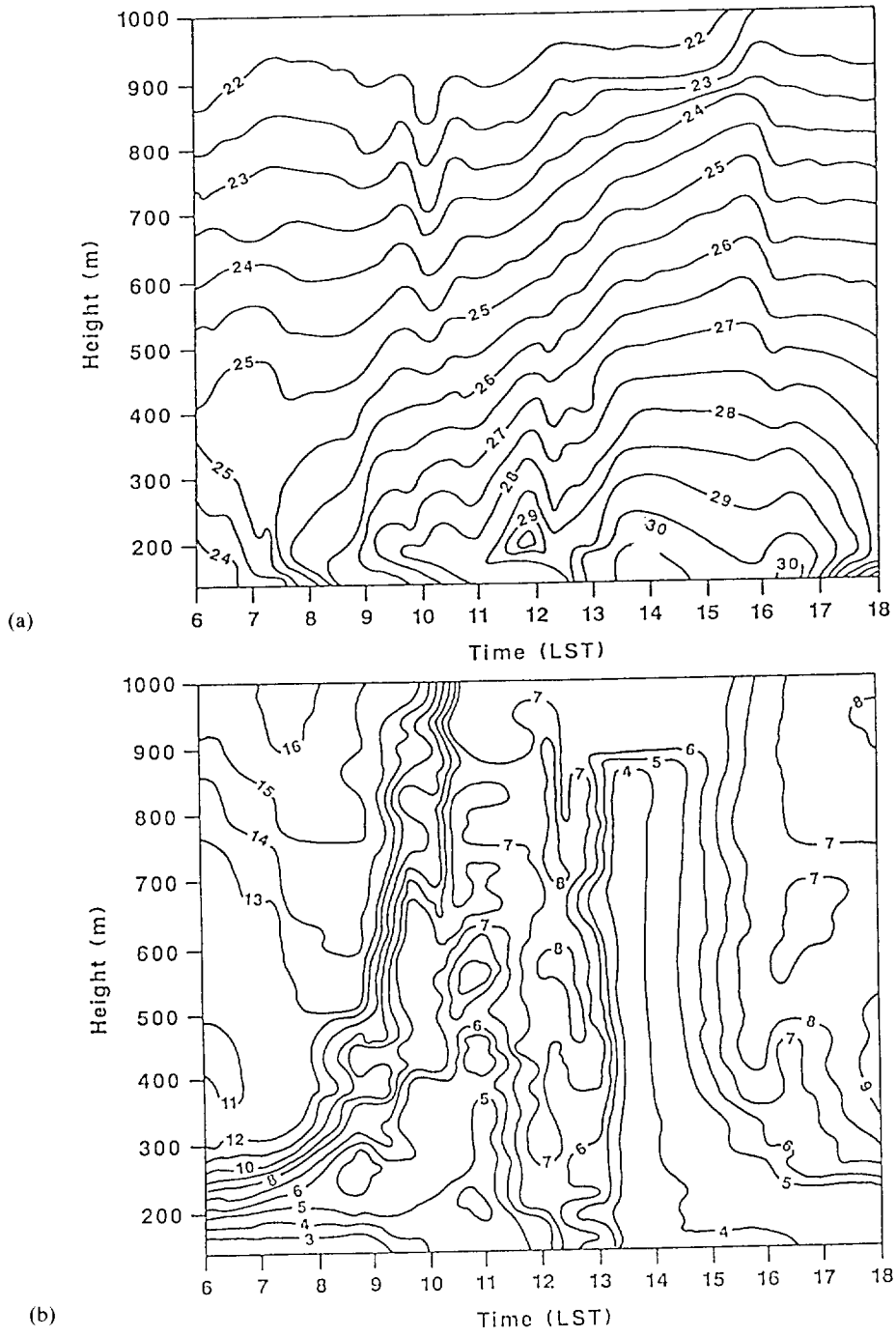

Fig. 6. Same as Figure 5, but for July 31, 1985.

the inversion separating the lower atmosphere into two layers. Strong wind shear exists between these two layers.

3.2. ABLE 2B

The rainfall of the April–May 1987 wet season was organized on scales ranging from the convective to the synoptic, with most of the rain (80%) produced by meso- to synoptic-scale systems originating in the eastern Amazon basin and the northern Atlantic coast of Brazil (Greco *et al.*, 1990). However, Greco *et al.* (1990) also show that 40% of the days were dominated by fairly undisturbed conditions with only scattered airmass-type convection. These days are similar to the ABLE 2A dry season period. With this in mind, a goal of this work was to see if the nocturnal WM seen during ABLE 2A also existed during the wet season. In addition, with the expansion of the data gathering network to 3 manned stations during ABLE 2B, the spatial extent of this phenomenon could be examined.

The 24 h of continuous observations began at 0600 LST, May 5 and ended at 1500 LST, May 9. Tethersonde and rawinsonde measurements were taken at all three corner stations of the mesoscale network (Figure 2). As an example, we shall present a series of tethersonde profiles for May 5–6, a day and night characterized by generally undisturbed conditions similar to the dry season.

Figures 8a, b and 9a, b show tethersonde profiles of temperature and wind speed at Ducke during the afternoon of May 5 and the night of May 5–6. In the late afternoon (1706 LST), the wind speeds through the entire surface-1000 m layer are 3–7 m s^{-1}. No inversion is present and the near-surface (approximately 20 m) temperature is 28 °C. By 2219 LST (Figure 9a), a strong surface-based inversion (+1–2 °C/100 m) is in place, extending up to 250 m AGL; wind speeds above the inversion top have increased to 8–12 m s^{-1} (Figure 9b). Although slightly weaker than during ABLE 2A, night-time wind speeds during the wet season are twice as high as daytime values. Below the inversion top, strong wind shear is also present. The inversion and strong low-level winds continue through the night (0432 LST) before diminishing after sunrise (0712, 0807 LST). These characteristics are very similar to those observed during the dry season and are substantiated by further wet season cases not shown.

Examination of the tethersoundings at the other stations in Figure 2 shows that the low-level nocturnal WM develops over the entire area. Figures 10a, b illustrate the evolution of the surface-based inversion and significant day-to-night wind speed increase which occurred at Carapaña during the evening of May 5. Above the inversion top, wind speeds increase to near 11 m s^{-1}. Due to equipment failure, no tethersonde data exist after 0100 LST on May 6. Nocturnal WM similarly evolve over Embrapa but with evidence that the nocturnal maxima at both Carapaña and Embrapa are not as large as at Ducke.

The greatest difference seen between the wet and dry season development of the nocturnal WM is related to the increase of disturbed weather during the wet season. More frequent and larger amounts of cloudiness reduce nocturnal cooling

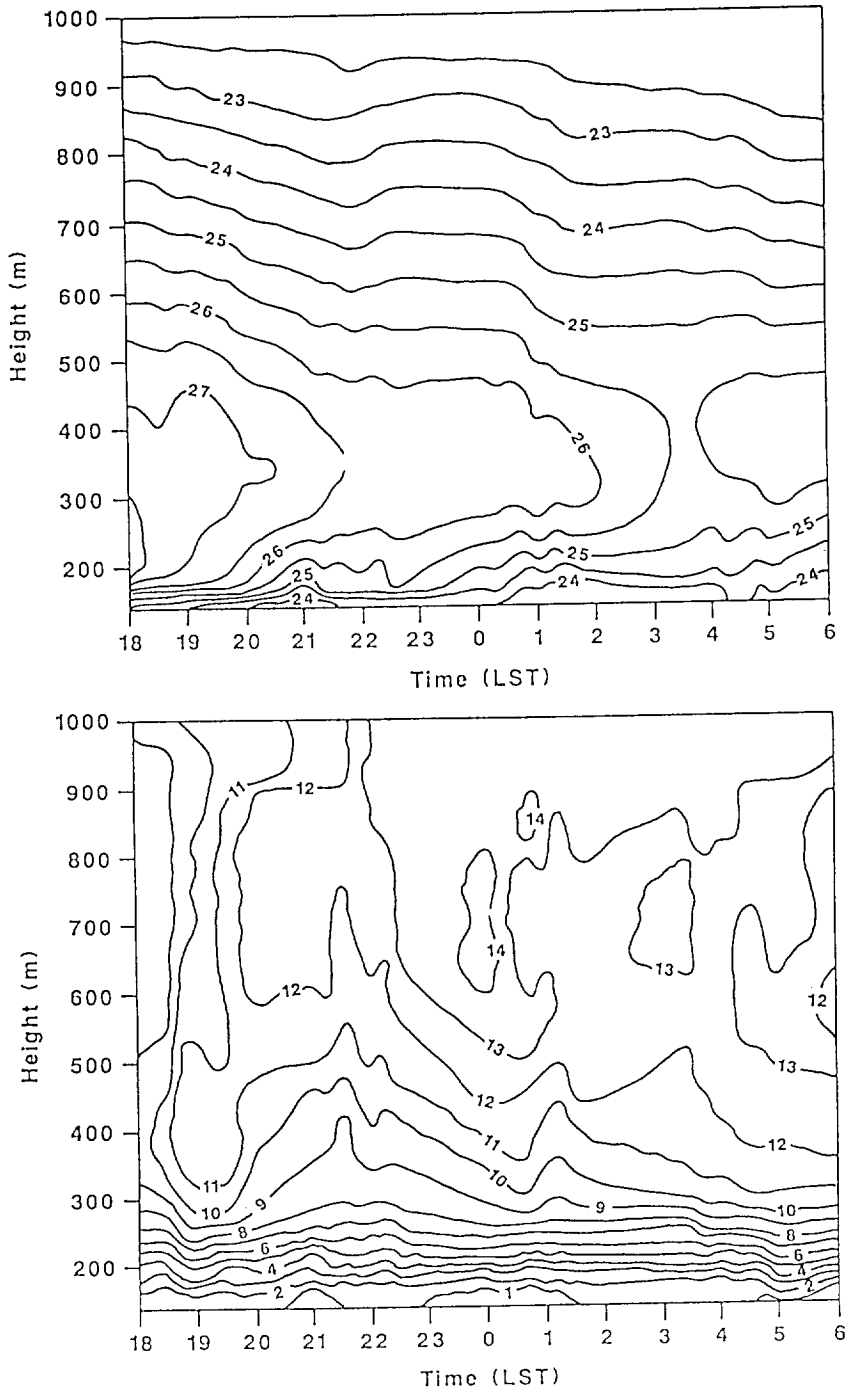

Fig. 7. Same as Figure 5, but for July 31–August 1, 1985.

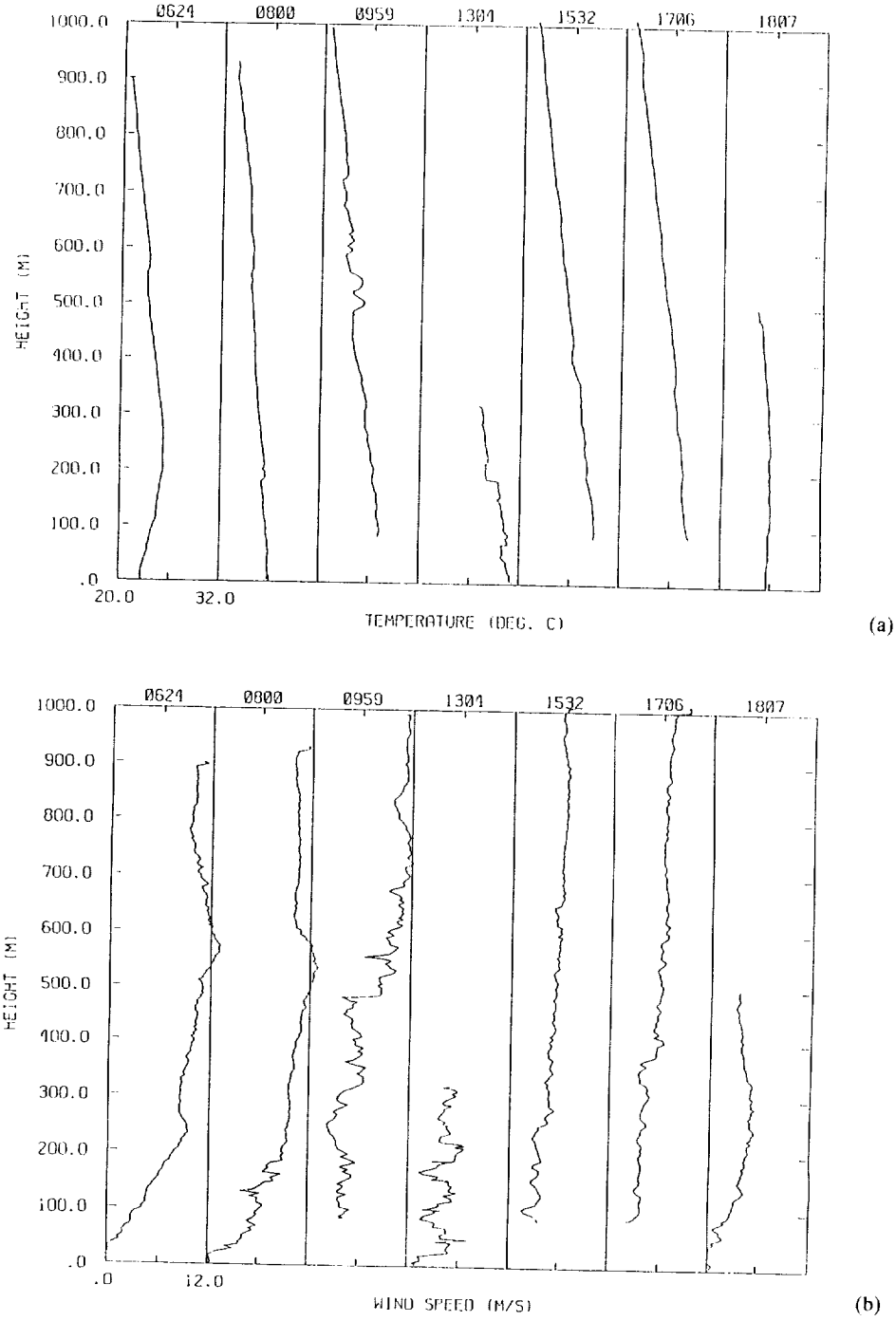

Fig. 8. Vertical profiles of (a) temperature and (b) wind speed measured by tethersonde at Ducke during May 5, 1987. Height is in meters above ground level.

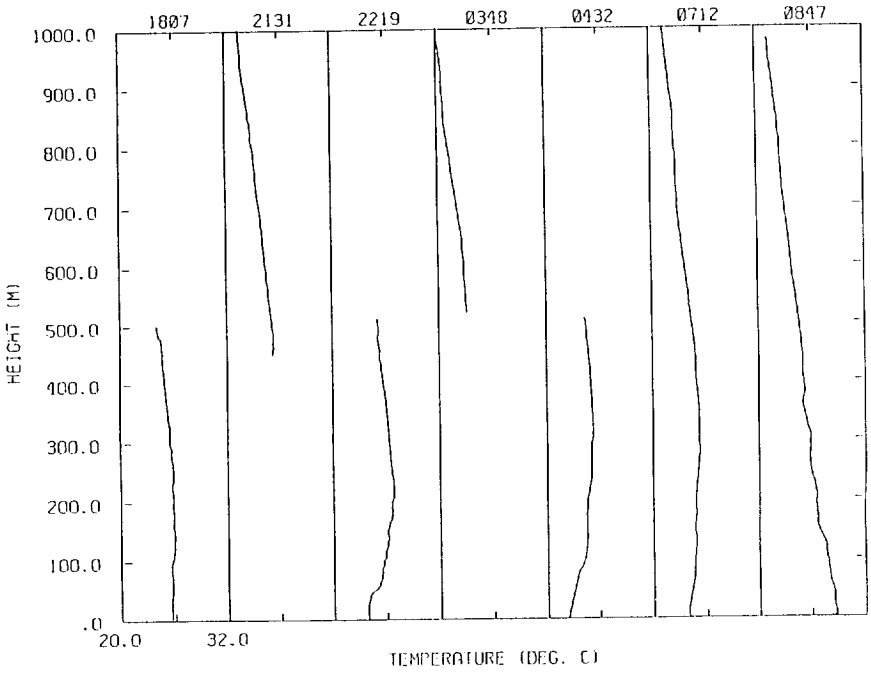

(a)

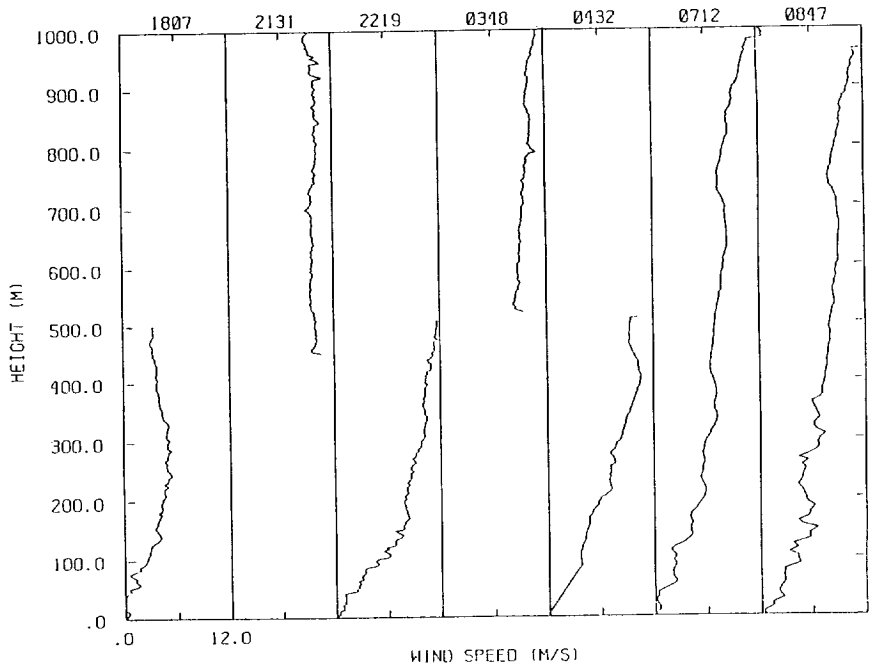

(b)

Fig. 9. Same as Figure 8, but for May 5–6, 1987.

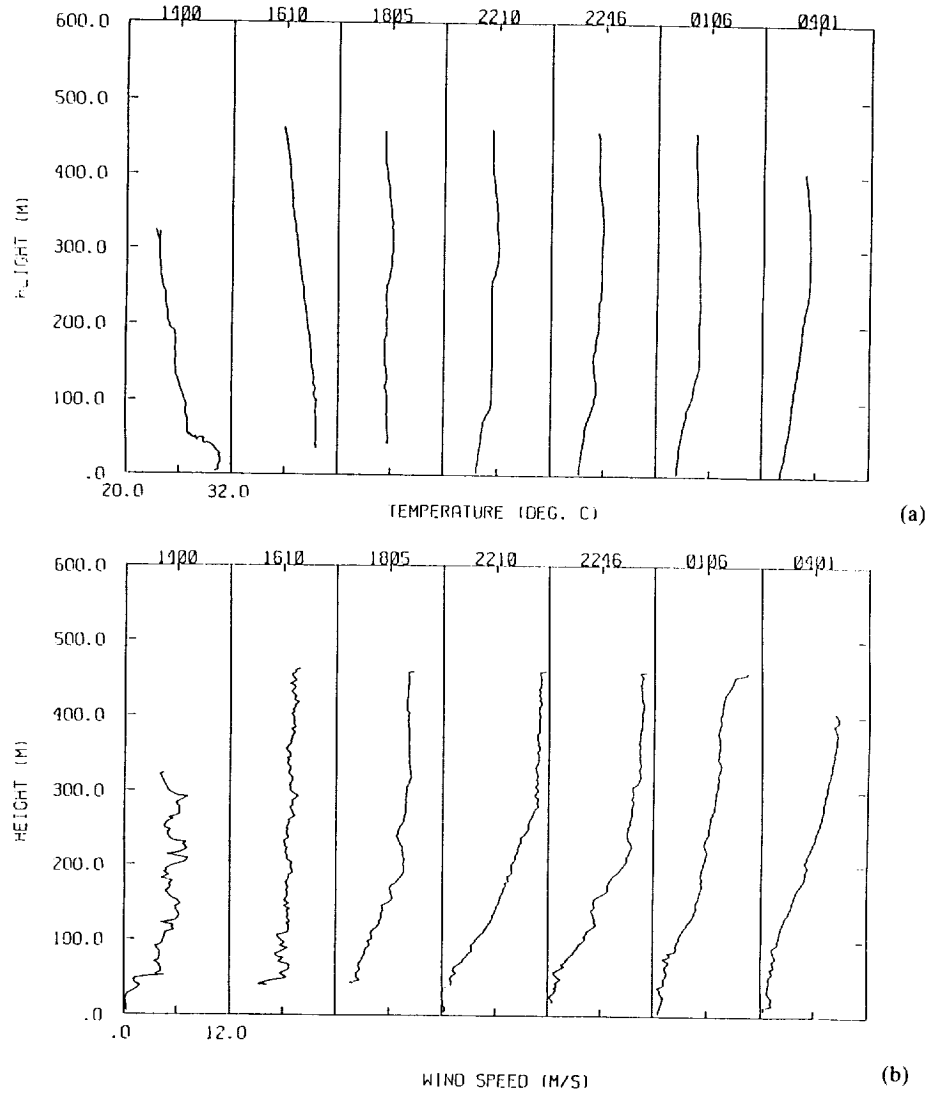

Fig. 10. Vertical profiles of (a) temperature and (b) wind speed measured by tethersonde at Carapaña during May 5–6, 1987. Height is in meters above ground level.

and the intensity of the inversion and thus the associated maxima in the wet season.

Another factor influencing the magnitude of the nocturnal WM is the prevailing wind direction. Figures 11a–c present a 24-h time series contour of rawinsonde-measured wind direction on, respectively, May 5–6, 6–7, and 7–8 at Ducke. The nights of May 5–6 and 6–7 were characterized by a strong low-level nocturnal WM. On May 5–6, there was a shift from a southerly component before 1700 LST to a more northerly component during the night and early morning. A shift in

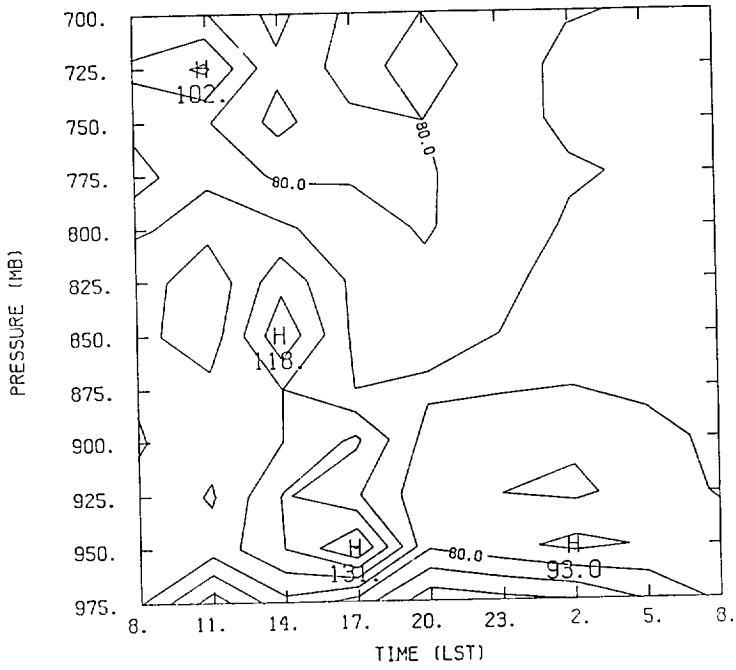

Fig. 11a.

Fig. 11. Time-height contours of rawinsonde measured wind direction at Ducke during (a) May 5–6, 1987, (b) May 6–7, 1987, and (c) May 7–8, 1987.

boundary-layer winds from ESE to ENE also occurs on May 6–7, as does a significant nocturnal WM. In contrast, Figure 11c shows that, on a night with a relatively weak WM (May 7–8), the predominant wind direction in the boundary layer after sunset was 85–120°. Wind directions measured at Carapaña and Embrapa reveal the same wind shifts as found at Ducke.

4. Mechanism for the Observed Nocturnal Wind Maximum

A necessary condition shown in Section 3 for a strong nocturnal WM is the establishment of a surface-based inversion near or after sunset. This inversion, which extends up to 300 m AGL, is produced by significant radiative cooling at the surface during nights with clear or mostly clear skies.

With the formation of the inversion, a two-layered fluid is established during the night-time hours. Below the inversion top is a layer of strong wind shear and mechanical turbulence as winds increase from near calm at the surface to 10–12 m s^{-1} at the inversion top. The layer above the inversion top is effectively decoupled from turbulence and surface frictional affects within the inversion layer. Such decoupling leads to a relative maxima of the winds above the inversion.

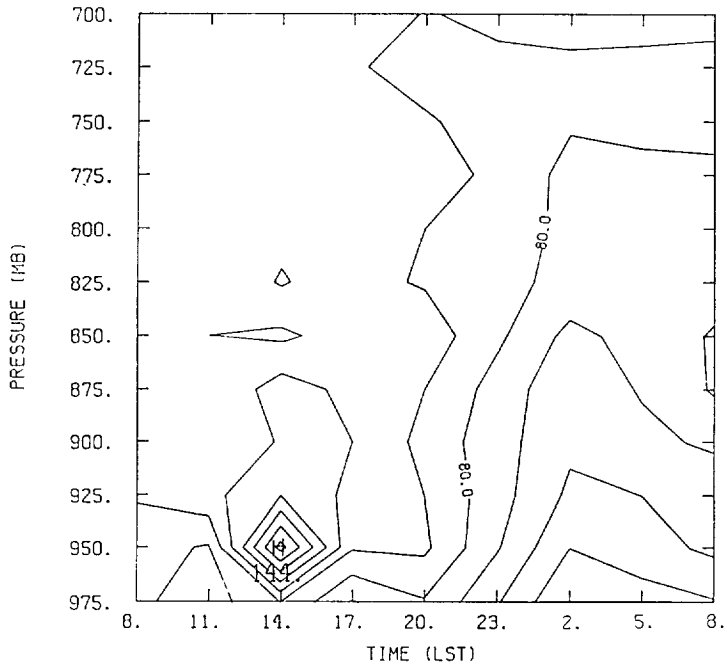

Fig. 11b.

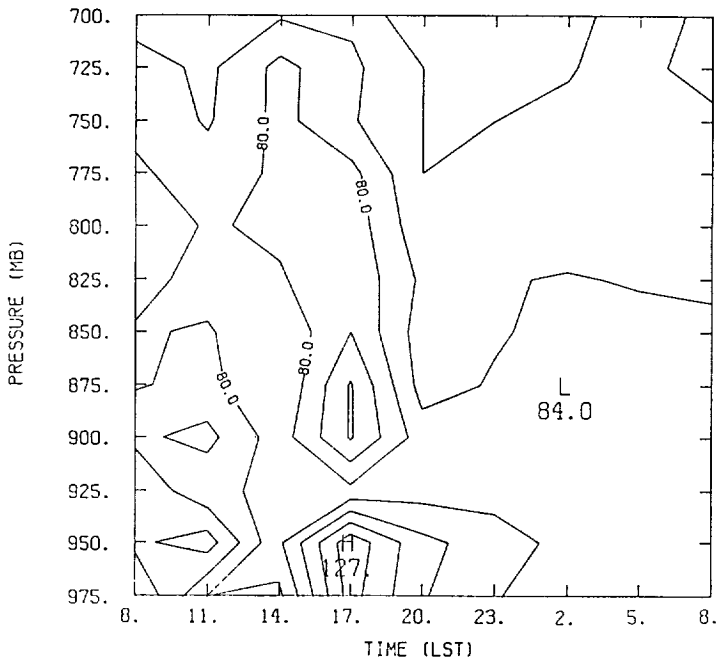

Fig. 11c.

The wind speed increase associated with the frictional decoupling is not, however, sufficient to account for the observed nocturnal WM.

The strength of the nocturnal maxima of the wind is also controlled by a thermally-driven pressure gradient and associated wind generated between the forest sites and the nearby Negro–Solimoes–Amazon river system in the presence of the frictional decoupling. The river-land circulation mechanism was also proposed by Oliviera (1990). Figure 2 shows that Ducke is approximately 20 km north of the river system while Carapaña is more than 50 km from the Amazon river. The rivers reach widths of >15 km near their confluence and the temperature difference between the air over the rivers and that over the undisturbed forest is potentially large enough to generate an observed mesoscale circulation.

With only indirect measurements (aircraft) made over the rivers, Ducke-Carapaña is used as a measure of the river-to-forest gradients in surface temperature and pressure. Ducke, which lies 20 km north and east of the rivers and north of the City of Manaus, will be under the influence of both the rivers and the city. Carapaña, however, lying 65 km upwind of the city and 45 km north of the Amazon is regarded as a representative rainforest site.

Airborne radiometric temperatures taken during the ABLE 2A and 2B experiments show the rivers to be 2–3 °C cooler than the forest canopy during the day and 6–8 °C warmer at night. Figure 12 shows a 24-h time series of the ABLE 2B composite horizontal temperature and pressure differences between Ducke and Carapaña (D–C) at the surface as measured by PAM towers. During the night (1800 LST–0600 LST), it is warmer at Ducke than at Carapaña. After 0800 LST, the gradient starts decreasing but it is not until 1000–1100 LST when it is warmer over the Carapaña forest site (C) than at the Ducke river/city site (D). The forest station reaches its maximum temperature at 1400 LST and is warmer than Ducke until 1700 LST. The similarity in the trends and slight lag (~1 h) between Δt and ΔP indicates that the pressure gradient is controlled by horizontal temperature differences between the land/forest and river/city at night.

The pressure gradient (D–C) becomes negative and reaches a maximum (−0.25 mb/50 km) during the late afternoon and early evening (1900 LST). This maximum in surface horizontal pressure gradient coincides with the increase in wind speeds. The negative pressure gradient between Ducke and Carapãna implies that the wind generated by the pressure gradient force should be directed from Carapaña (higher pressure) to Ducke (lower pressure). This is indeed the case. As illustrated in Figure 11, on the two nights with the strongest WM, a wind shift occured from ESE to ENE during the period of the intensifying pressure gradient. With a wind direction from the ENE, the air will be directed from Carapaña to Ducke. Figure 12 indicates that, for the remainder of the night and early-to-late morning, the pressure gradient, like the temperature gradient, is fairly constant (−0.08 to −0.14 mb over 50 km). During this period, the nocturnal winds shown in Section 3 remain strong but with no large increases. Late morning to early

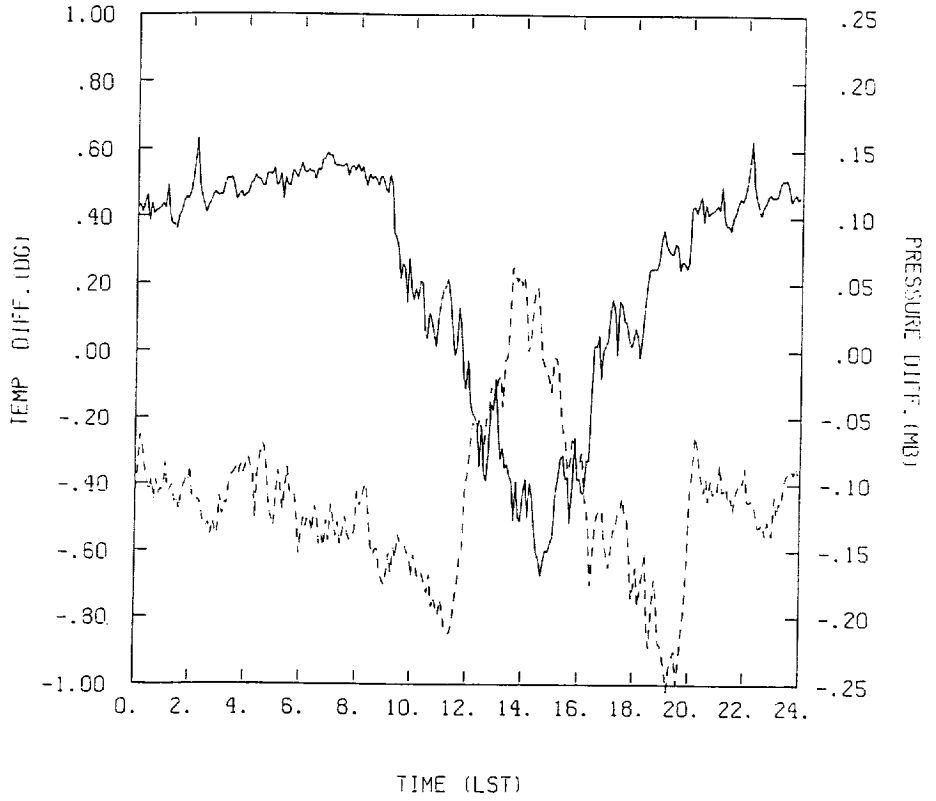

Fig. 12. ABLE 2B daily time-series composite of the temperature (solid) and pressure (dashed) differences between Ducke and Carapaña (D–C) as measured by the PAM towers. Pressure and temperature values were recorded every minute.

afternoon sees a reversal in both temperature and pressure gradients along with a diminishing of the boundary-layer winds.

The horizontal acceleration of the wind can be expressed in the usual fashion:

$$\frac{d\mathbf{v}}{dt} = \frac{-1}{\rho}\nabla P - f\mathbf{K} \times \mathbf{V} + \mathbf{F}. \tag{1}$$

For the purpose of this paper, we shall represent the frictional drag within the tropical PBL in the simplified form

$$\mathbf{F} = -a\mathbf{V}, \tag{2}$$

where "a" is a frictional coefficient with some dependence upon wind speed, surface roughness and static stability. Neglecting the Coriolis effect as very small near the equator, the equation of motion reduces to:

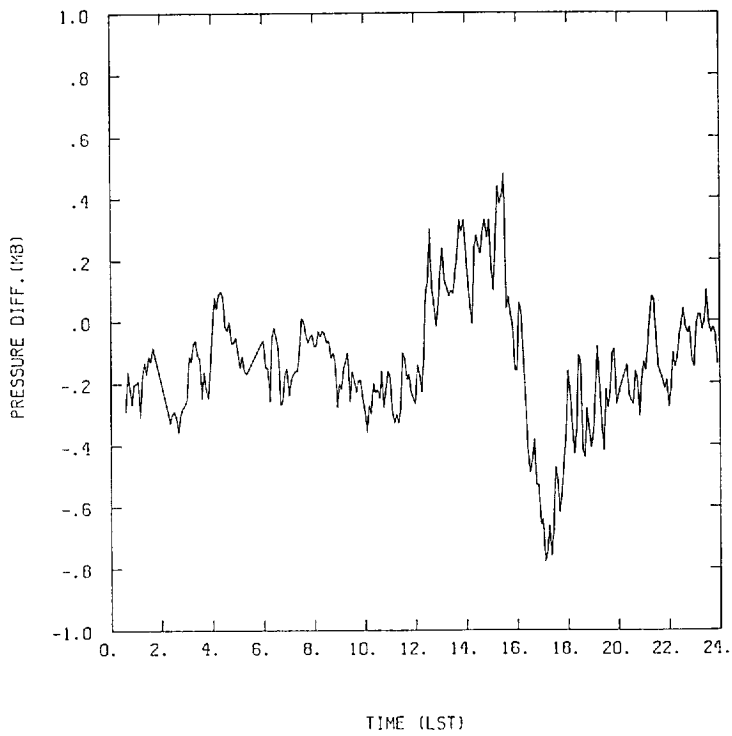

Fig. 13. Daily time-series of the pressure difference between Ducke and Carapaña (D–C) as measured by the PAM towers on May 5, 1987.

$$\frac{\mathrm{d}v}{\mathrm{d}t} = \frac{-1}{\rho}\nabla P - a\mathbf{V} . \tag{3}$$

After a large initial acceleration near sunset, the wind speed throughout the PBL was shown above to remain relatively constant during the night. With the acceleration near zero at night, Equation (3) reduces to

$$\frac{-1}{\rho}\nabla P = -a\mathbf{V} . \tag{4}$$

From the PAM-measured surface pressure at Ducke (D) and Carapaña (C), it was seen that the D–C pressure difference during the late afternoon/early evening period of wind increase varied between 0.15 and 0.60 mb, significantly higher than seen in the composite (Figure 12). As an example, the PAM-derived pressure difference between Ducke and Carapaña on May 5 is shown in Figure 13. After the early evening WM, ΔP values remain fairly constant through the next morning for all 3 cases, with mean values of 0.15, 0.25 and 0.20 mb on, respectively, May 5–6, May 6–7 and May 7–8.

The frictional coefficient "a" can thus be calculated for these cases using Equa-

TABLE III

Observed pressure differences (D–C) and wind accelerations along with predicted values of total wind acceleration, acceleration by the pressure gradient force, and deceleration by friction. Computed using the simplified model proposed in Section 4

	May 5–6	May 6–7	May 7–8
Ave. nocturnal ΔP	0.15 mb	0.25 mb	0.20 mb
Ave. nocturnal wind speed	11 m s^{-1}	11 m s^{-1}	6 m s^{-1}
a	2.8×10^{-5} s^{-1}	4.7×10^{-5} s^{-1}	6.9×10^{-5} s^{-1}
Observed Day/Night dv/dt	5 m s^{-1} in 4 h	5 m s^{-1} in 4 h	3 m s^{-1} in 4 h
Ave. ΔP during wind speed increase	0.30 mb	0.30 mb	0.20 mb
V during wind speed increase	7 m s^{-1}	7.5 m s^{-1}	5 m s^{-1}
Accel. by PGF (in 4 h)	9 m s^{-1}	9 m s^{-1}	6 m s^{-1}
Damping by Fric. (in 4 h)	4.7 m s^{-1}	5.1 m s^{-1}	3.4 m s^{-1}
Calculated Day/Night dv/dt	4.3 m s^{-2} in 4 h	3.9 m s^{-2} in 4 h	2.6 m s^{-2} in 4 h

tion (4) and the mean nocturnal values of ΔP and observed wind speeds. These results are summarized in Table III for Ducke. With the mean value of the frictional coefficient "a" from the three nights, a predicted day-to-night increase can be calculated using Equation (3) and the observed ΔP and wind speed during the nocturnal maxima period. These values are also summarized in Table III.

Predicted values of wind speed increases during the period of acceleration on all 3 nights are within 1.5 m s^{-1} of the observed wind increases (see Table III). The results suggest that the initial forcing of the WM is due to the increase produced by a combination of the thermal/pressure gradients between Carapaña (forest) and Ducke (river/city), and the decrease in the frictional forcing. Through most of the night, little wind increase is observed as the pressure gradient and frictional forces are in near-equilibrium.

After sunrise, a decrease in wind speed responds to the imbalance between the frictional and pressure gradient terms. Figures 12 and 13 show that the pressure remains higher at Carapaña than at Ducke through midday, well after the observed decrease of the wind. This decrease in wind speed between the surface and 1000 m is caused by the increase in friction resulting from the destruction of the surface-based inversion by strong surface heating and recoupling through turbulence to the rough forest. This decrease can be explained by Equation (3) in terms of a higher daytime value of the frictional coefficient "a" than used during the night.

As an example, an observed decrease of 2.5 m s^{-1} was noted at the inversion top by Ducke tethersondes between 0627 and 1027 LST on May 7–8. Using a value of $a = 1 \times 10^{-4}$ (slightly higher than the night values) and $\bar{v} = 5.2$ m s^{-1} and $\overline{\Delta P} = 0.20$ mb during the decrease period, the increase by the pressure gradient force is 6 m s^{-1} and the frictional decrease is 7.6 m s^{-1}. The calculated total decrease of 1.6 m s^{-1} per 4 h is only 1 m s^{-1} below the observed deceleration (Table III).

5. Summary and Conclusions

A nocturnal wind maximum in the atmosphere below 1000 m is observed over the extensive and nearly undisturbed rainforest north and east of the central Amazon city of Manaus. Wind speeds which are characteristically less than 5 m s^{-1} at 3–500 m above the canopy during the day, increase to 10–15 m s^{-1} after sunset. A maximum is reached during the early evening, after which wind speeds remain high until after dawn.

The nocturnal wind maxima occur during both the dry and wet seasons of central Amazonia, and are closely linked to the formation of a strong low-level inversion. The inversion is due to radiational cooling of the rainforest canopy and is strongly controlled by cloudiness. Thus, nocturnal inversions and associated wind increases are more frequent in the dry than in the wet season. The intensity of the nocturnal wind maximum is also influenced by the prevailing wind direction. Wind shifts observed during the times of wind speed increases suggest that the forcing is related to surface pressure gradients.

Surface pressure gradients are observed and interpreted as a function of surface thermal gradients between undisturbed forest and the large river system and the City of Manaus. The surface pressure gradients are shown to be responsible for part of the observed increases in wind speed between day and night. Frictional decoupling of the air above the inversion from the rough forest below must be called upon to explain the total increase.

The dual nature of the nocturnal wind maximum depending upon both the existence of a horizontal pressure gradient and frictional decoupling would suggest that the phenomenon is not uniformly occurring over the vast reaches of Amazonia. We suspect, however, that in many places local pressure gradients are enhancing the low level nocturnal winds and that, in general, stronger winds in the lower atmosphere are pervasive when strong surface nocturnal cooling exists. Thus, the phenomenon has seasonal characteristics which relate to cloudiness. We also suspect that in the dry season, in particular, strong low-level nocturnal winds over wide regions of Amazonia are important in terms of advection of air above the surface-based inversion. The finding that biomass burning products were, for example, very widely dispersed over the Amazon basin early in the dry season of ABLE 2A may be largely due to this process.

Acknowledgements

We wish to acknowledge the broad support of NASA in the GTE-ABLE program. We would also like to give special thanks to Ms. Mary Morris for doing an excellent job in proofreading, typing and formatting this manuscript.

References

Blackadar, A. K.: 1957, 'Boundary-Layer Wind Maxima and their Significance for the Growth of Nocturnal Inversions', *Bull. Amer. Meteorol. Soc.* **38**, 283–290.

Bonner, W. D.: 1968, 'Climatology of the Low Level Jet', *Mon. Wea. Rev.* **96**, 83–95.

Brook, R. R.: 1985, 'The Koorin Nocturnal Low Level Jet', *Boundary-Layer Meteorol.* **32**, 133–154.

Clarke, R. H. and Brook, R. R.: 1979, 'The Koorin Experiment', Australian Government Publishing Service, Bureau of Meteorology, Canberra, Australia, 359 pp.

Clarke, R. H., Dyer, A. J., Brook, R. R., Reid, D. G., and Troup, A. J.: 1971, 'The Wangara Experiment: Boundary-Layer Data', Tech. Paper No. 19, Division of Meteorological Physics, CSIRO, Australia.

DeSouza, R. L., Aspliden, C. I., Garstang, M., LaSeur, N. E., and Hsueh, Y.: 1971, 'A Low-Level Jet in the Tropics', *Mon. Wea. Rev.* **99**, 559–563.

Dickerson, R. B. and Neumann, H. H.: 1982, 'The Occurrence of Nocturnal Low-Level Jets in New England and the Canadian Maritimes', *Atmos.-Ocean* **20**, 287–300.

Garratt, J. R.: 1982, 'Observations in the Nocturnal Boundary Layer', *Boundary-Layer Meteorol.* **22**, 21–48.

Garratt, J. R.: 1985, 'The Inland Boundary Layer at Low Latitudes', *Boundary-Layer Meteorol.* **32**, 307–327.

Garstang, M., Ulanski, S., Greco, S., Scala, J., Swap, R., Fitzjarald, D., Martin, D., Browell, E., Shipman, M., Connors, V., Harriss, R., and Talbot, R.: 1990, 'The Amazon Boundary Layer Experiment (ABLE 2B): A Meteorological Perspective', *Bull. Amer. Meteorol. Soc.* **71**, 19–31.

Greco, S., Garstang, M., Ulanski, S., Houston, S., and Swap, R.: 1989, 'Local Circulations over the Central Amazon Basin', *Proc. Third International Conf. on Southern Hemisphere Meteorology and Oceanography*, pp. 213–215.

Greco, S., Swap, R., Garstang, M., Ulanski, S., Shipham, M., Harriss, R. C., Talbot, R., Andreae, M., and Artaxo, P.: 1990, 'Rainfall and Surface Kinematic Conditions over Central Amazonia during ABLE 2B', *J. Geophys. Res.* **95**, 17001–17014.

Harriss, R., Wofsy, S., Garstang, M., Browell, E., Molion, L., McNeal, R., Hoell, J., Bendura, R., Beck, S., Navarro, R., Riley, J., and Snell, R.: 1988, 'The Amazon Boundary Layer Experiment (ABLE 2A): Dry Season', *J. Geophys. Res.* **93**, 1351–1360.

Harriss, R., Garstang, M., Wofsy, S., Beck, S., Bendura, R., Coelho, J., Drewry, J., Hoell, J., Matson, P., McNeal, R., Molion, L., Navarro, R., Rabine, V., and Snell, R.: 1990, 'The Amazon Boundary Layer Experiment: Wet Season 1987', *J. Geophys. Res.* **95**, 16721–16736.

Hoecker, W. H.: 1963, 'Three Southerly Low-Level Jet Systems Delineated by the Weather Bureau Special Pibal Network', *Mon. Wea. Rev.* **91**, 573–582.

Hoecker, W. H.: 1965, 'Comparative Physical Behavior of Southerly Boundary-Layer Wind Jets', *Mon. Wea. Rev.* **93**, 133–144.

Hsu, S. A.: 1979, 'Mesoscale Nocturnal Jet-Like Winds within the Planetary Boundary Layer over a Flat, Open Coast', *Boundary-Layer Meteorol.* **17**, 485–494.

Kousky, V. E.: 1979, 'Frontal Influence on Northeast Brazil', *Mon. Wea. Rev.* **107**, 1140–1153.

Kousky, V. E. and Ferreira, N. J.: 1981, 'Interdiurnal Surface Pressure Variation in Brazil: Their Spatial Distributions, Origins and Effects', *Mon. Wea. Rev.* **109**, 1999–2008.

Kousky, V. E. and Kagano, M.: 1981, 'A Climatological Study of the Tropospheric Circulation over the Amazon Region', *Acta Amazonica* **11**, 743–758.

Kraus, H., Malcher, J., and Schaller, E.: 1985, 'A Nocturnal Low-Level Wind during PUKK', *Boundary-Layer Meteorol.* **31**, 187–195.

Lettau, H. H.: 1967, 'Small to Large-Scale Features of Boundary Layer Structure over Mountain Slopes', *Proc. Symp. Mount. Meteor.*, Atmos. Sci. Paper No. 122, Colorado State University.

Lettau, H. H.: 1983, 'Thoughts on Priorities in Boundary-Layer Research', *Boundary-Layer Meteorol.* **25**, 429–432.

Mahrt, L.: 1981, 'The Early Evening Boundary Layer Transition', *Quart. J. Roy. Meteorol. Soc.* **107**, 329–343.

McNider, R. and Pielke, R.: 1981, 'Diurnal Boundary-Layer Development over Sloping Terrain', *J. Atmos. Sci.* **38**, 2198–2210.

Nobre, C. A., Silva Dias, P., dos Santos, M. A. R., Cohen, J., da Rocha, J. P., Guedes, R., Ferreira, R., and dos Santos, J. A.: 1987, 'Mean Large Scale Meteorological Aspects of ABLE 2B', Paper presented at Spring AGU Meeting, Baltimore, MD.

Oliveira, A. P.: 1990, 'Planetary Boundary Layer Dynamics over the Amazon Rain Forest', Ph.D. dissertation, College of Sciences and Mathematics, Department of Atmospheric Sciences, State University of New York at Albany, 295 pp.

Paegle, J.: 1987, 'Interactions between Convective and Large-Scale Motions over Amazonia', in R. Dickerson (ed.), *The Geophysiology of Amazonia: Vegetation and Climate Interactions*, Wiley Intersciences, New York, pp. 347–390.

Paegle, J. and Rasch, G. E.: 1973, 'Three-Dimensional Characteristics of Diurnally Varying Boundary-Layer Flows', *Mon. Wea. Rev.* **101**, 746–755.

Salati, E. and Vose, P. B.: 1984, 'Amazon Basin: A System in Equilibrium', *Science* **225**, 129–138.

Shuttleworth, W. J., Gash, J., Lloyd, J., Moore, C. J., Robert, C. J., Filho, A., Fisch, G., Filho, V., Ribeiro, M., Molion, L., Sa de Abreu, L., Nobre, C., Cabral, O. M. R., Pitel, S. R., and Moraes, J. C.: 1984, 'Observation of Radiation Exchange above and below Amazonian Forest', *Quart. J. Roy. Meteorol. Soc.* **110**, 1163–1169.

Shuttleworth, W. J., Gash, J., Lloyd, J., Moore, C. J., Robert, C. J., Filho, A., Fisch, G., Filho, V., Ribeiro, M., Molion, L., Sa de Abreu, L., Nobre, C., Cabral, O. M. R., Pitel, S. R., and Moraes, J. C.: 1985, 'Daily Variations of Temperature and Humidity within and above Amazonian Forest', *Weather* **40**, 102–108.

Silva Dias, P., Benatti, J. P., and Kousky, V.: 1987, 'Diurnally Forced Tropical Tropospheric Circulation over South America', *Mon. Wea. Rev.* **115**, 1465–1478.

Thorpe, A. J. and Guymer, T. H.: 1977, 'The Nocturnal Jet', *Quart. J. Roy. Meteorol. Soc.* **103**, 633–653.

Virji, H.: 1981, 'A Preliminary Study of Summertime Tropospheric Circulation Patterns over South America Estimated from Cloud Winds', *Mon. Wea. Rev.* **109**, 599–610.

Wexler, H.: 1961, 'A Boundary Layer Interpretation of the Low-Level Jet', *Tellus* **13**, 368–378.

Wippermann, F.: 1973, 'Numerical Study on the Effects Controlling the Low-Level Jet', *Beitr. Phys. Atmos.* **46**, 137–154.

Zeman, O.: 1979, 'Parameterization of the Dynamics of Stable Boundary Layer and Nocturnal Jets', *J. Atmos. Sci.* **36**, 792–804.

Table of Contents

SUMMARY

Research under Agreement NCC1-106 during the interim period 1 October 1991 to 31 May 1992 has continued to use the data collected during all three ABLE missions (ABLE I, 1984; ABLE IIa, 1985; and ABLE IIb, 1987).

The work reported upon in this interim period follows the description provided in the previous progress report (September 1991), i.e., global interactions between the rain forest of the Amazon Basin and local and regional processes interior to the Basin itself. The progress in each of these two areas during this reporting period is summarized below and documented in the attached appendices.

1. Global Interactions

a. Aerosols

A major research result documenting the role played by Saharan dust in the Amazon rain forest is now published in the journal TELLUS (Swap et al., 1992). The paper is attached in Appendix I. The results of this work are summarized below.

Saharan dust is shown to enter the Central Amazon Basin (CAB) in bursts which accompany major wet season rain systems. Low level horizontal convergence feeding these rain systems draws dust from plumes which have crossed the tropical Atlantic under the large-scale circulation fields. Mass exchange of air between the surface and 4 km over the eastern Amazon basin is calculated using rawinsonde data collected during storm events. Mean concentrations of dust observed by aircraft over the western tropical Atlantic are used to calculate the amount of dust injected into the Basin. Individual storm events inject some 480,000 tons of dust into the northeastern Amazon Basin. Storm and dust climatology suggest that the annual importation of dust is in the order of 13 Mtons. In the northeastern basin, this may amount to as much as 190 kg ha^{-1} yr^{-1}. Deposition of trace species, such as phosphate, associated with this dust ranges from 1-4 kg/ha/yr. Uncertainties in these estimates are not believed to be greater than ± 20%. The deposition fluxes from Saharan dust are essentially identical to the CAB wet deposition fluxes from precipitation in the wet season; a result that implies that the major ionic composition of rain water in the CAB wet season may be strongly influenced by inputs of material originating on the African continent nearly 5000 km away.

The total amount of Saharan dust calculated to enter the Amazon Basin is one half to one third of that estimated to cross 60°W longitude between 10° and 25°N latitude. We conclude that part of the productivity of the Amazon rain forest is dependent upon critical trace elements contained in the soil dust

originating in the Sahara/Sahel. This dependence should be reflected by expansions and contractions of the Amazon rain forest in direct relationship to expansions and contractions of the Sahara/Sahel. Turnover rates for nutrient species deposited with Saharan dust in the Amazon Basin suggest a time scale of 500 to 20,000 years. We believe the dependence of one large ecosystem upon another separated by an ocean and coupled by the atmosphere to be fundamentally important to any view of how the global system functions. Any strategy designed to preserve the Amazonian rain forest or any part thereof should equally concern itself with the interrelationship between the rain forest, global climate and arid zones well removed from Amazonia.

Research has begun during this reporting period to determine the extent to which nutrients contained in aerosols being emitted by continental north Africa contribute to the ocean ecosystem.

b. Energy

The role of the Amazon Basin as a global center of action has been quantified in terms of deep convective transports and the contribution of these transports to the planet's heat balance. Results of this work are contained in a paper now submitted to the MONTHLY WEATHER REVIEW (Appendix II) entitled "Amazon Coastal Squall Lines - Part II: Heat and Moisture Transports".

Mesoscale heat and moisture budgets are presented for three synoptic scale Amazon coastal squall lines (ACSL) over the central Amazon Basin during the 1987 wet season. The budgets are obtained from volumetric analyses of mesoscale rawinsonde data from the second Amazon Boundary Layer Experiment (ABLE IIb). Classification of cloud and rainfall components are based on data from Portable Automated Mesonet (PAM) towers, GOES images, and radar. Satellite estimates of the total active cloud area, coupled with the mesoscale budget calculations, are used to determine the upper level vertical heat transport for an entire ACSL as a function of life cycle.

The instantaneous upper level heat transport in a mature ACSL equals nearly 20% of the theoretical export requirement for the equatorial trough zone. A little more than half of the system-wide transport occurs in the dynamically active anvil cloud. Amazon coastal squall lines are shown to exist over the basin simultaneously in various stages of formation, maturity and decay. When three stages are present, the combined instantaneous production of heat exceeds one third of the requirement to balance the global heat budget.

Work has been started on establishing the above findings on a scale of the basin itself. To achieve this result we are using the large scale cloud fields to identify organized synoptic and

mesoscale features. Once identified, then the rainfall and diabatic heating associated with these systems will be calculated.

2. Local and Regional Interactions

a. Nocturnal wind structure

The paper describing the nocturnal wind fields entitled "Low-level Nocturnal Wind Maximum over the Central Amazon Basin" (Greco et al., 1992, Appendix I) has now been published in the journal of BOUNDARY-LAYER METEOROLOGY.

A low level nocturnal wind maximum is shown to exist over extensive and nearly undisturbed rain forest near the central Amazon city of Manaus. Analysis of meteorological data collected during the 1985 and 1987 Amazon Boundary Layer Experiments (ABLE 2a and 2b) indicate the presence of this nocturnal wind maximum during both the wet and dry seasons of the Central Amazon Basin (CAB). Daytime wind speeds which are characteristically 3-7 m s^{-1} between 300 m and 1000 m increase to 10-15 m s^{-1} shortly after sunset. The wind speed maximum is reached in the early evening, with wind speeds remaining high until several hours after sunrise. The nocturnal wind maximum is closely linked to a strong low-level inversion formed by radiational cooling of the rain forest canopy. The nighttime inversion extends up to 300 m with strong vertical shear of the horizontal wind below the inversion top and uniformly strong horizontal winds above the inversion top. Frictional decoupling of the air above the inversion from the rough forest below, however, is responsible for only part of the observed increase. Surface and low-level pressure gradients between the undisturbed forest and the large Amazon river system and the city of Manaus are shown to be responsible for much of the nocturnal wind increase. The pressure gradients are interpreted as a function of the thermal differences between undisturbed forest and the river/city. The importance of both the frictional decoupling and the horizontal pressure gradient suggest that the nocturnal wind maximum is not uniformly occurring over all Amazonia. We suspect that stronger low-level winds are pervasive under clear skies and strong surface cooling and that, in many places (i.e., near rivers), local pressure gradients enhance the low-level nocturnal winds.

b. Structure and kinematics of Amazon coastal squall lines

A manuscript describing the structure and kinematics of Amazon coastal squall lines has been submitted to the MONTHLY WEATHER REVIEW (Appendix II).

This paper describes the meso-to-synoptic scale lines which form along the northern coast of South America as seabreeze-

induced instability lines and which propagate through the Amazon basin using data collected during the April-May 1987 ABLE 2b.

These systems, termed "Amazon Coastal Squall Lines" (ACSL), have been noted by others, but details of the structure and evolution of the ACSL are limited. The present paper uses analyses of GOES satellite, upper air rawinsonde and surface Portable Automated Mesonet (PAM) data to describe the structure, dynamics and life-cycle evolution of the ACSL. Twelve ACSL were sampled during ABLE 2b and three examples are discussed in detail.

The ACSL are discontinuous lines of organized mesoscale cloud clusters which propagate across the Central Amazon Basin at speeds of 50-60 km h^{-1}. The ACSL undergo six possible life cycle stages: coastal genesis, intensification, maturity, weakening, reintensification and dissipation. Analysis also indicates that the ACSL are composed of three distinct components: pre-storm cumulus (PSC), leading edge convection (LEC) and multiple precipitating cloud layers in the trailing stratiform region (TSR).

Divergence and vertical velocity calculations indicate deep vertical ascent in the LEC and a region of mid-level convergence ($\approx$ 500 mb) inthe TSR. The latter is associated with a weak updraft above and an unsaturated downdraft below. The TSR vertical motions are an order of magnitude smaller than in the LEC.

Substantial shear in the low-level inflow occurred in all 3 case studies and, as suggested by model simulations, may play an important role in the longevity (24-48 h) of the ACSL. Pre- and post-ACSL profiles of Θ_e demonstrate that the ACSL stabilize the troposphere in their wake and erode a pre-storm minimum Θ_e. It is hypothesized that the removal of this minimum is accomplished not only by direct mixing via vertical motions in the LEC ("hot towers"), but also through detrainment in the multiple-layered TSR.

c. Gap formation

Work was begun in this period to document the maximum wind speeds at canopy height and relate these winds to the processes which cause them and to the results following such winds. The creation of gaps or blow-downs in the rain forest is a well known phenomena described by ecologists. They attribute a number of important processes in the rain forest to gap dynamics including diversity and propagation.

APPENDIX I

List of Papers Published in Reviewed Literature

Greco, S., S. Ulanski, M. Garstang and S. Houston, 1992: Low-level nocturnal wind maximum over the central Amazon Basin. Bound.-Layer Meteor., 58, 91-115.

Swap, R., M. Garstang, S. Greco, R. Talbot and P. Kållberg, 1992: Saharan dust in the Amazon Basin. Tellus, 44B, 133-149.

Garstang, M., 1991: Destruction of the rain forest and climate change. In Aspects of Environmental Change, Misc. Ser. No. 91/1, 35-47.

APPENDIX II

FUTURE WORK

Manuscripts Submitted

Garstang, M., H.L. Massie, Jr., J. Halverson, S. Greco and J. Scala, 1992: Amazon coastal squall lines: Part I: Structure and kinematics. Submitted to Mon. Wea. Rev.

Greco, S., H.L. Massie, Jr., M. Garstang, J. Halverson, J. Scala and W.-K. Tao, 1992: Amazon coastal squall lines: Part II: Heat and moisture transports. Submitted to Mon. Wea. Rev.

Papers Under Preparation

Connors, V., M. Garstang and S.R. Nolf, 1992: Structure and texture of satellite observed cloud fields over the Amazon basin.

Connors, V. and M. Garstang, 1992: Organization and implications of the large scale cloud fields over the Amazon basin.

Garstang, M., B. Nelson, J. Halverson and D. Larom, 1992: Formation of gaps in the rain forest of Amazonia.

Tellus (1992), *44B*, 133–149

Saharan dust in the Amazon Basin

By R. SWAP, M. GARSTANG, S. GRECO, *University of Virginia, Department of Environmental Sciences, Charlottesville, VA 22903, USA*, R. TALBOT, *Institute for the Study of Earth, Oceans and Space, University of New Hampshire, Durham, NH 03824, USA* and P. KÅLLBERG, *Swedish Meteorological and Hydrological Institute, Norrköping, Sweden*

(Manuscript received 4 April 1991; in final form 2 October 1991)

ABSTRACT

Saharan dust is shown to enter the Central Amazon Basin (CAB) in bursts which accompany major wet season rain systems. Low-level horizontal convergence feeding these rain systems draws dust from plumes which have crossed the tropical Atlantic under the large-scale circulation fields. Mass exchange of air between the surface and 4 km over the eastern Amazon basin is calculated using rawinsonde data collected during storm events. Mean concentrations of dust observed by aircraft over the western tropical Atlantic are used to calculate the amount of dust injected into the Basin. Individual storm events inject some 480,000 tons of dust into the northeastern Amazon Basin. Storm and dust climatology suggest that the annual importation of dust is in the order of 13 Mtons. In the northeastern basin, this may amount to as much as 190 kg $ha^{-1}\ yr^{-1}$. Deposition of trace species, such as phosphate, associated with this dust ranges from 1–4 kg $ha^{-1}\ yr^{-1}$. Uncertainties in these estimates are not believed to be greater than $\pm 50\%$ and may be as low as $\pm 20\%$. The deposition fluxes from Saharan dust are essentially identical to the CAB wet deposition fluxes from precipitation in the wet season; a result that implies that the major ionic composition of rain water in the CAB wet season may be strongly influenced by inputs of material originating on the African continent nearly 5000 km away. The total amount of Saharan dust calculated to enter the Amazon basin is 1/2 to 1/3 of that estimated to cross 60° W longitude between 10° and 25° N latitude. We conclude that part of the productivity of the Amazon rain forest is dependent upon critical trace elements contained in the soil dust originating in the Sahara/Sahel. This dependence should be reflected by expansions and contractions of the Amazon rain forest in direct relationship to expansions and contractions of the Sahara/Sahel. Turnover rates for nutrient species deposited with Saharan dust in the Amazon Basin suggest a time scale of 500 to 20,000 years. We believe the dependence of one large ecosystem upon another separated by an ocean and coupled by the atmosphere to be fundamentally important to any view of how the global system functions. Any strategy designed to preserve the Amazonian rain forest or any part thereof should equally concern itself with the inter-relationship between the rain forest, global climate and arid zones well removed from Amazonia.

1. Introduction

The tropical rain forests of the world are generally regarded as large ecosystems in relatively delicate nutrient balance. Balance is achieved by efficient cycling in a nutrient-limited environment (Jordan, 1985; Vitousek and Sanford, 1986). In the northeastern and parts of central Amazonia, where nutrient poor oxisols and ultisols are present and nutrient supply by rivers is limited, deposition of airborne soil dust particles is needed to achieve a nutrient balance (Jordan, 1985; Salati and Vose, 1984; Vitousek and Sanford, 1986). The amounts of aeolian influx have been estimated to be relatively high (in the order of millions to tens of millions of tons per year). In the case of some of the critical trace elements, this influx may be crucial to the health of the forest. Jordan (1985) and Vitousek and Sanford (1986), for example, have suggested that phosphorus may be a critical airborne element which could limit annual net primary production of the rain forest.

A substantial body of literature identifies the Sahara and sub-Saharan Sahel as the probable

source region of dust found over a large fraction of the earth's surface. Saharan dust transported over distances of greater than 5000 km has been shown to reach areas in northern Europe (DeAngelis and Gaudichet, 1991; Reiff et al., 1986) and the middle east (Levin et al., 1980). In addition, there is considerable evidence mainly provided by Prospero and colleagues that Saharan dust reaches the eastern Caribbean (Prospero and Carlson, 1972; Talbot et al., 1990), southern North America (Savoie and Prospero, 1977) and the northeastern coast of South America (Parkin et al., 1972; Prospero et al., 1981; Prospero et al., 1987; Talbot et al., 1990).

There is also general agreement that transport of dust to the far western tropical Atlantic and the Caribbean occurs in the northeasterly trades at relatively low altitudes, mostly below 6–7 km (Prospero and Carlson, 1972; Jaenicke and Schütz, 1978; D'Almeida, 1986; Westphal et al., 1988; Bergametti et al., 1989). This layer of air, called the Saharan Air Layer (SAL), is situated most frequently between 850 and 700 mb (1.5 and 3 km) (Prospero and Carlson, 1972; Reiff et al., 1986; Bergametti et al., 1989).

Our results suggest that a considerable amount of the dust found in the Central Amazon Basin (CAB) is of Saharan origin. This Saharan dust is transported across the Atlantic under steady state (undisturbed) conditions in the 850 to 700 mb layer (Prospero and Carlson, 1972). However, we suggest that such steady state transport is not sufficient to bring the dust into the CAB. Synoptic scale weather systems, with associated organized low level convergence, are required to gather the dust into the Basin. Thus, dust events in the CAB are a function of synoptic scale systems coinciding with the existence of a dust plume in the far western tropical Atlantic. The role played by synoptic scale systems in producing pulses of Saharan dust in the CAB may also explain why Prospero et al. (1981) observed the maximum in dust concentrations in Cayenne, French Guiana to occur during the height of the wet season. Similarly, synoptic scale systems provide a mechanism in the far western Atlantic to inject dust across an active Intertropical Convergence Zone (ITCZ). Penetration of Saharan dust across an active ITCZ into the southern hemisphere has been deemed unlikely (Junge, 1979) because of wet removal of the dust.

Prospero and Carlson (1972) and Prospero et al. (1981) have made estimates of the annual amount of dust reaching a particular location. D'Almeida (1986) has also given estimates of the annual amount of particulate matter exported northward, westward and southward from the Sahara/Sahel. Uncertainties, however, remain in the estimates of the total amount of dust reaching such locations. An associated uncertainty also exists in the number and amount of trace elements delivered to a given location.

In the discussion which follows, aircraft sampling of aerosols, mass divergences calculated from rawinsonde stations and rain and dust storm climatology are used to calculate the storm and annual amount of dust brought into the Amazon Basin. A breakdown of the trace species concentrations present in the dust is also attempted. The resulting annual amounts of dust are compatible with those obtained by Prospero and Carlson (1972) across 60° W between 10 and 25° N latitude. The results obtained support the belief that the dust observed during the wet season in the central Amazon Basin is of Saharan origin. The storm convergence mechanism called upon to inject dust into the CAB provides a means to calculate the event, seasonal and annual amounts of dust imported.

If Saharan dust provides a major source of nutrients for the Amazonian rain forests, then a series of most important consequences follow. Reichholf (1986) has suggested that major fluctuations in rainfall over northern Africa during and following the pleistocene should be reflected by parallel expansions and contractions of the Amazon rain forest. Petit et al. (1981) have indeed reported evidence of increased continental aerosol concentrations during the pleistocene, attributed to increased size and activity of sand deserts located between 30° N and 30° S. Short term variations in the amount of particulate matter coming off West Africa have been related to the recent Sahelian droughts (Prospero and Nees, 1977, 1986). The possible response of the Amazon rain forest to variations in the airborne nutrient supply depends upon whether, how, what kind and how much dust is imported into the Amazon basin. The findings we present below to answer some of these questions are based upon a series of National Aeronautics and Space Administration (NASA) experiments carried out under the Division of

Atmospheric Chemistry's Global Tropospheric Experiment (GTE).

2. GTE Atlantic and Amazon Boundary Layer Experiment (ABLE)

The NASA GTE is attempting to document the chemical composition of the global troposphere by selecting and examining the atmosphere over important ecosystems. The Atlantic Boundary Layer Experiment (ABLE 1) (Gregory et al., 1986; Talbot et al., 1986) examined the troposphere over the open western tropical atlantic ocean in June 1984. The two Amazon experiments ABLE 2a and 2b, examined conditions over the relatively undisturbed tropical rain forest of the CAB in the dry, July–August 1985, and wet, April–May 1987, seasons (Harriss et al., 1988; 1990).

Field measurements made in the ABLE 1, 2a and 2b provide information on a range of interacting scales (e.g., space scales from 50 km to 5000 km) which appear essential to the understanding of both the chemistry and the dynamics of this fluid system (Fig. 1). The field experiments, associated observations and results are summarized in two special issues of the JGR devoted to ABLE 2a and 2b (JGR, 1988; 1990). A number of these results are used to present a mechanism to introduce Saharan dust into the CAB and to calculate the total importation of dust and associated trace species.

Sampling of atmospheric aerosols was conducted from the ground (Artaxo et al., 1990) and at various altitudes (0.2 to 6.0 km) from the NASA Electra research aircraft (Talbot et al., 1990). The ground-based sampling network was located on three of the towers shown in Fig. 1b at 45 m, 28 m and 2 m. Sampling duration ranged from 24 to 48 h. Samples were collected continuously from April 8 to May 14, 1987. The concentration of particulates and elements contained in soil dust (e.g., Si, Al, Fe) was determined on a daily basis.

Elemental concentrations were determined using particle induced X-ray emission (PIXE) analysis. Coarse ($>2\ \mu m$) and fine ($<2\ \mu m$) mode particle contributions were determined. Artaxo et al. (1990) found the following 22 elements in the ABLE 2b ground-based aerosol samples: Na, Mg, Al, Si, P, S, Cl, K, Ca, Ti, V, Cr, Mn, Fe, Ni, Cu, Zn, Br, Rb, Sr, Zr, and Pb. Rain water analysis

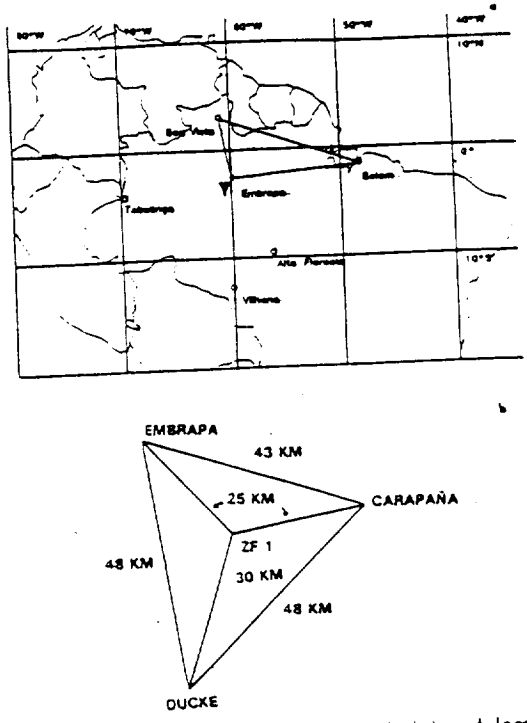

Fig. 1. Basin-scale rawinsonde network (a) and local mesoscale network (b) employed in the Amazon basin during ABLE 2B. Location of the mesoscale network is indicated by the darkened triangle in (a).

was performed on samples collected at 3 of the tower locations shown in Fig. 1b (Andreae et al., 1990). Rain water samples were collected on an event basis at each station.

Airborne (NASA Electra) sampling of aerosols consisted of collection on teflon filters and subsequent analysis of the water-soluble trace species using ion chromatography (Talbot et al., 1990). The constituents observed included Na, NH_4, K, Cl, NO_3, SO_4, C_2O_4, CH_3SO_3, HCOO, and CH_4COO (Talbot et al., 1990).

The European Centre for Medium Range Weather Forecasting (ECMWF) global wind analyses are used for the computation of 10 day backward and forward isobaric trajectories. An overview of the ECMWF data assimilation system may be found in Hollingsworth (1987). The ECMWF analyses are available every 6th h with a horizontal resolution corresponding to 125 km at 19 vertical hybrid levels.

The 2-D trajectory method is a straightforward

Lagrangian following of air parcels in the analyzed wind field with wind components interpolated linearly in time every 6 h. The wind components are further interpolated, both horizontally and vertically (pressure), to the actual position of the parcel. The interpolated wind components are then used to track the parcel forward or backward over 6 h in 15-min increments.

Horizontal wind fields were compiled using ECMWF global data together with commercial aircraft and satellite wind observations (T. Krishnamurti, personal communication). The data at 850, 500, and 200 mb are used to determine the streamline fields over the tropical Atlantic, Africa, and South America during the ABLE 2b experiment.

Satellite imagery from the European Meteosat are used to provide coverage of the tropical Atlantic from northern Africa to the coast of South America including the arid region of northeast Brazil.

Ground-based rawinsonde measurements, obtained 4 times daily, were made in a basin scale network (1000–1500 km apart) shown in Fig. 1a. Local meteorological measurements used in this study include rawinsondes from the three corner stations of the mesoscale network in Fig. 1b (approximately 50-km spacing) together with rainfall measurements made on the towers at 5 m above the canopy.

Aerosol optical thickness values deduced from the Advanced Very High Resolution Radiation (AVHRR) satellite measurements (Rao et al., 1988) were not available during any of the ABLE missions. We refer to post field experiment aerosol optical thickness data to confirm the frequency and geographic extent of Sahara dust outbreaks.

3. Analysis and results

Ground-based measurements of aerosol concentration and composition during ABLE 2b indicate the occurrence of several large pulses containing both terrestrial and marine aerosols (Fig. 2a). Three maxima were centered around April 12–14 (experimental days 12–14), April 29–May 1 (experimental days 29–31) and May 5–8 (experimental days 36–40).

Aerosols associated with these pulses had relatively high concentrations of alkali and alkaline earth elements in the atmospheric mixed layer of the CAB (Talbot et al., 1990). Amazonian soils, however, are highly weathered and exhibit deficits of these elements. This finding suggested a non-local source region for the dust, which Talbot et al. (1990) believe to be the Sahara. Pulses of Saharan dust were also observed at Barbados during ABLE-2b (Talbot et al., 1990). These pulses, with concentrations at the surface reaching 180 $\mu g\ m^{-3}$, appeared at Barbados 1 to 2 days before Saharan dust was seen in the CAB.

The temporal variation of major mineral aerosol

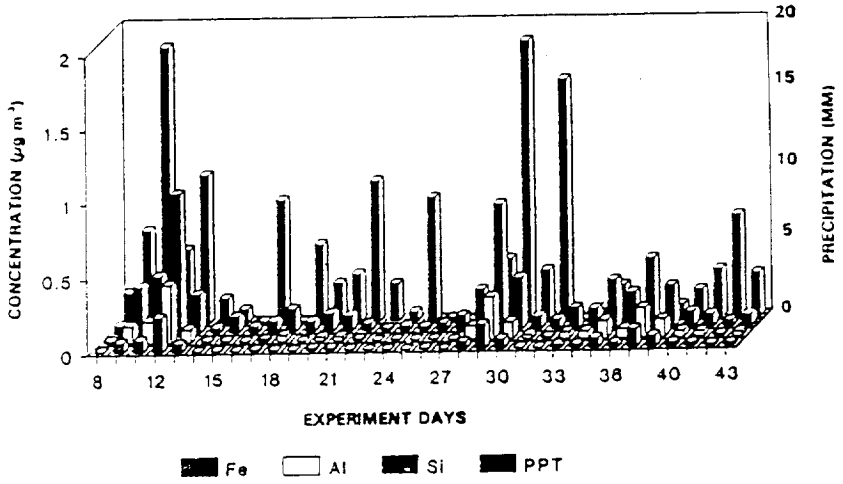

Fig. 2. Time series of ground-based concentrations of terrestrial elements (Fe, Al, Si) measured at Ducke tower with mesoscale network rainfall. (PPT)

constituents (e.g., Fe, Al, Si) shown in Fig. 2, are compared with the mean regional mesoscale (4 station) rainfall in Fig. 2. Both aerosols and rainfall occur in distinct pulses. The two major pulses in Si coincided with the two major rain events. The third, weaker aerosol pulse preceded a weaker rainfall event by about 48 h. Other rain events show little or no association with increases in dust. On days with little or no rain, however, very low concentrations of dust are observed.

Analysis of the rainfall during ABLE 2b (Greco et al., 1990; Garstang et al., 1990; Swap, 1990) showed that more than 80% of the rain was due to large (linear scales of 1000 km or larger) organized synoptic scale systems.

Wet season rainwater chemistry associated with large systems compared to small or local rain systems is different. The highest concentrations of SO_4^{2-} and Cl^- as well as higher pH values occur in large organized rain systems compared to local rain showers (Andreae et al., 1990). The presence of marine constituents (e.g., Na^+ and Cl^-) in these large rain systems suggest that they are ingesting low level air from over the western tropical Atlantic. Higher pH values in rain water, however, have also been found to be associated with Sahara dust (Löye-Pilot et al., 1986). Therefore, marine chemical constituents and continental components from African regions south of the Sahara may contribute to the rainwater composition of large rain systems in the CAB.

High concentrations of mineral aerosols occurring in close association with large rain events requires an explanation because wet removal would suggest the opposite result. We propose below that low level convergence covering a large area and preceding such large rain systems by 24 to 72 h is responsible for increasing the dust concentrations in near coincidence with the production of rain from these weather systems. This explanation requires the presence of a Saharan dust plume in the far western tropical Atlantic at the time that the synoptic scale weather system is organizing on the northeastern South American coast. First, we show from trajectory analysis that Saharan dust can reach the eastern and central Amazon Basin. Secondly, we calculate mass convergence in the low troposphere preceding the weather system and will show that this convergence can concentrate the dust from the preexisting plume residing over the western tropical Atlantic. Finally, we show that measured values of concentrations in the oceanic dust plume allow the calculation of both the total mass of dust and the mass of the associated chemical constituents transported into the Amazon Basin.

3.1. *Streamline and trajectory analysis*

The large subtropical anticyclones are indicators of the nature of the lower tropospheric fields of motion linking western Africa and eastern South America. The position of the West African Subtropical High (WASH) with ridging over the central tropical Atlantic has been shown to influence low level flow across the Atlantic into the Amazon Basin (Talbot et al., 1990). Fig. 3 shows that, with the WASH centered in a prescribed area of West Africa, flow at 500 mb extends across the Atlantic and into the Amazon Basin. Each of the three concentrated pulses of soil dust into the CAB shown in Fig. 2 followed a 4–7 day period of the WASH so established over West Africa (Talbot et al., 1990). Meteosat visible images (not shown) confirm that, during such periods of dominance by the WASH, fair weather extends across the low latitude north Atlantic. Under a slowly changing large-scale anticyclonic field, the streamlines approach trajectories. The absence of deep convection or other forms of strong vertical motion along the path provide conditions which are near optimal for the calculation of trajectories.

Two-dimensional horizontal isobaric trajectories were calculated at 975, 950, 925, 900, 850, 800, 700, and 600 mb based upon the 6 h ECMWF global wind analysis. The 2-D trajectory calculations at multiple levels over 10 days were used to produce an envelope to bound the possible path taken and as an indication of the approximate origin or end point of the air parcels. Visible satellite imagery and the large scale wind fields in the 5–7 day period prior to a soil dust event in the CAB suggest near steady state conditions with little or no deep convection in the region of dust transport (Talbot et al., 1990). In the absence of deep convective clouds, vertical motions in the lower troposphere are confined to large scale subsidence in the order of 400 m day^{-1} (Riehl, 1954; Riehl et al., 1951). Forward trajectories were calculated from two locations:

15° N latitude	10° E longitude in the Sahel, and
20° S latitude	15° E longitude in the Namib.

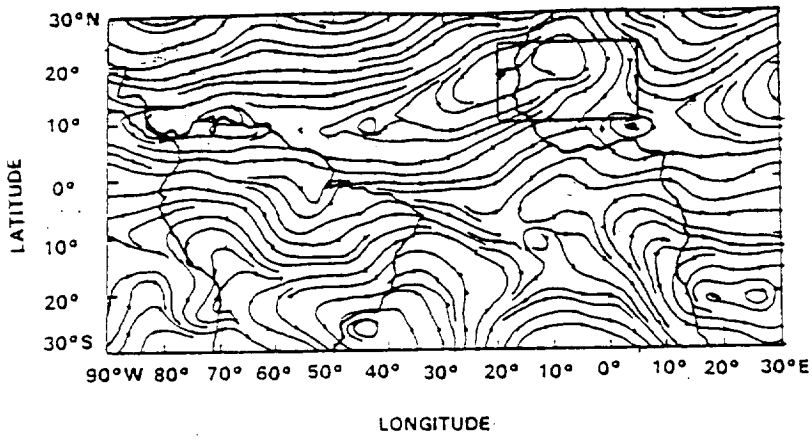

Fig. 3. 500 mb streamlines on 17 April 1987 illustrating the West African Subtropical High and associated wind flow across the Atlantic Ocean and into the Amazon Basin.

Backward trajectories were calculated from

0 latitude 60° W longitude in the CAB.

Three 10-day periods were chosen, two to coincide with the two major dust events seen in the CAB and one to coincide with a period of very low dust concentrations in the CAB (Fig. 2). The results of these calculations are discussed below.

3.1.1. Dust event of 12 April–14 April. Backward trajectories starting on 12 April 1987 (Figs. 4a, b) and 14 April 1987 (Figs. 4c, d) and forward trajectories starting on 4 April 1987 (Fig. 5) suggest that air parcels between 800 and 700 mb (Figs. 4b, 4d and 5b) originate from a region near Lake Chad. Air below 800 mb is traced back to the eastern Atlantic and the West African coast (Figs. 4a, c). Air below 800 mb originating (Fig. 5a) near Lake Chad does not leave the west coast of Africa after 10 days of travel time. Air above 700 mb is either not traced back to Africa (Fig. 4b) or does not reach the Sahel in the backward trajectory calculation. In the 10-day forward calculation (Fig. 5b), air at 600 mb heads towards, but does not reach the mouth of the Amazon.

Backward and forward trajectories were also calculated for the dust event of 29 April–1 May 1987 and for a low dust concentration day, 26 April 1987. We discuss our findings from these trajectory calculations without showing the graphical results. The backward trajectories starting on 29 April 1987 and 1 May 1987 and forward trajectories starting on 21 April 1987 show results similar to the April 12–14 event. Backward trajectories at 800 to 700 mb once again end up near Lake Chad. Above 800 mb and below 700 mb, however, parcels show a diverse set of pathways. Forward trajectories with the calculation beginning on 21 April 1987 just west and north of Lake Chad do not show any connection to the Amazon Basin. Backward trajectory results suggest that the point of origin chosen for the calculation is too far north and east. Trajectories for the low dust case show no connection to the Amazon Basin.

10-day forward trajectories were also calculated for three separate dates: 4, 16 and 21 April 1987 to determine whether dust could be coming from the southern hemisphere deserts of the Namib and Kalahari. No such connection was found.

While the trajectory calculations carried out as part of this paper do not rule out any other source of soil dust, we believe that the results show support for the contention that the Sahara/Sahel is the primary source. We find no evidence in the trajectory calculations that would support a South American location as a source region in the April/May time of year. None of the backward trajectories calculated from the CAB point (0° latitude, 60° W longitude) approach the dry zone of northeastern Brazil. Transport from the Namib/Kalahari, as well as from NE Brazil, into the Amazon basin may well, however, occur during astral spring and summer.

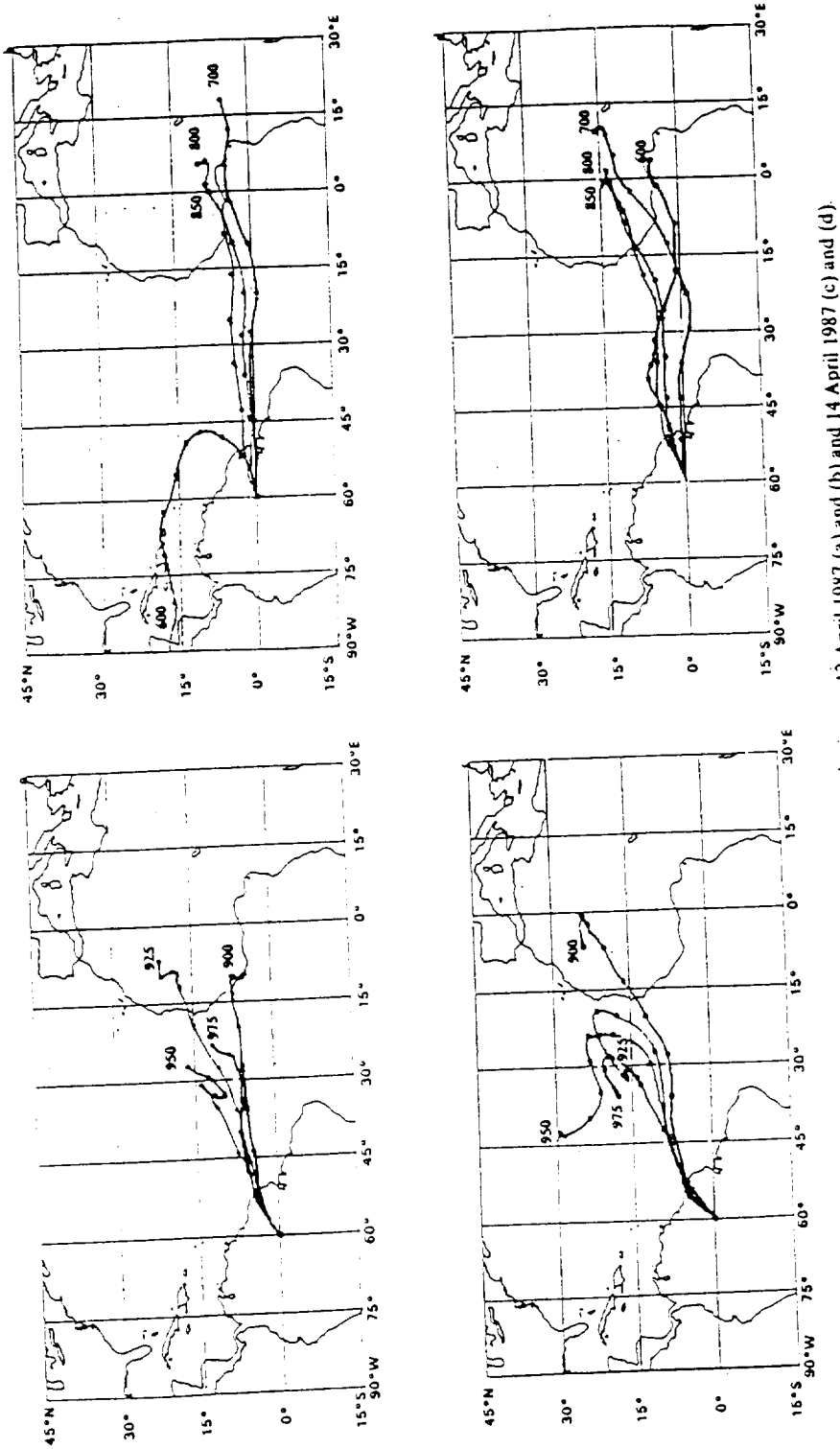

Fig. 4. 10-day backward isobaric trajectories beginning on 12 April 1987 (a) and (b) and 14 April 1987 (c) and (d).

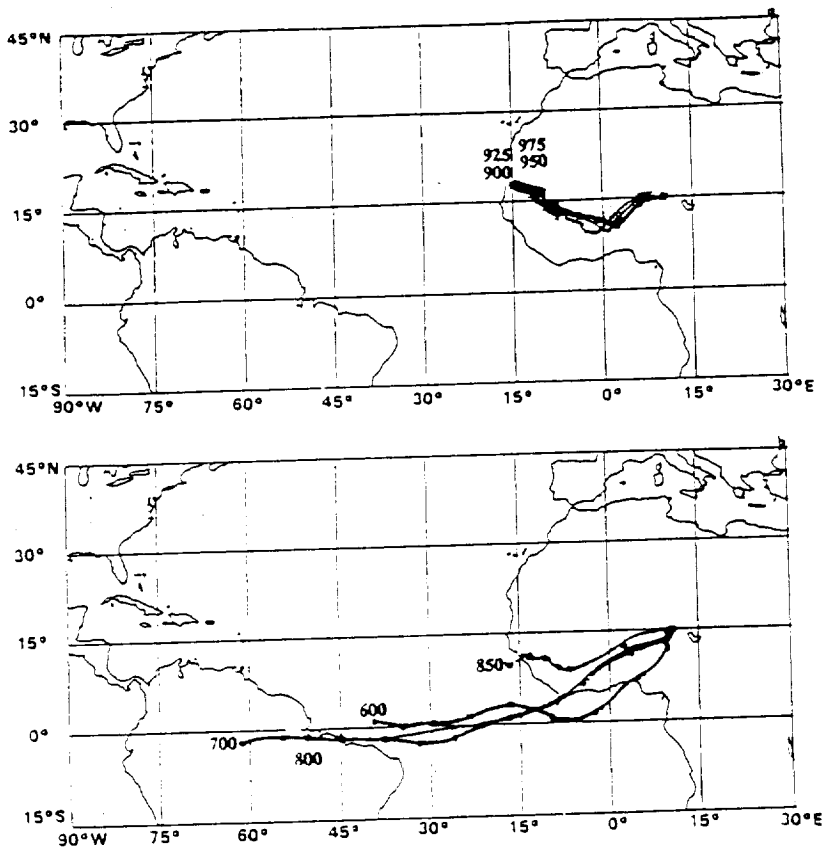

Fig. 5. 10-day forward trajectories beginning on 4 April 1987.

3.2. Horizontal mass divergence calculations

The large triangle in Fig. 1a shows the relative location of three of the six basin scale rawinsonde network stations operated during ABLE 2b and designed to describe large-scale meteorological conditions over the entire Amazon Basin. The line from Boa Vista to Belém is nearly parallel to the northeast coast of South America. This line is also approximately normal to low level inflow into the Amazon Basin under conditions which favor both the transport of dust across the Atlantic and the development of synoptic scale weather systems in the Amazon Basin. The Belém, Boa Vista and Embrapa triangle over the northeastern Amazon Basin is thus positioned to capture any enhanced mass inflow into the Basin, drawing lower tropospheric air from over the western tropical Atlantic.

Rawinsonde data from the basin-scale stations were used to calculate horizontal divergence for the Belém, Boa Vista and Embrapa triangle by employing a line integral method utilizing the wind components normal to each leg of the triangle (Brummer, 1978). The horizontal divergence calculated for the triangle serves to determine the amount of air and, with measured aerosol concentrations, the amount of dust imported into the triangle volume as a function of the circulation of the synoptic scale storm system.

Fig. 6 shows the experiment time series of horizontal divergence at 850 mb and 700 mb. The rawinsonde network was not fully functional until 15 April 1987. The dust event of 29 April–1 May 1987 is captured by this time series and is used below to calculate total mass inflow into the volume above the triangle. The divergence signal in Fig. 6 shows a major perturbation about

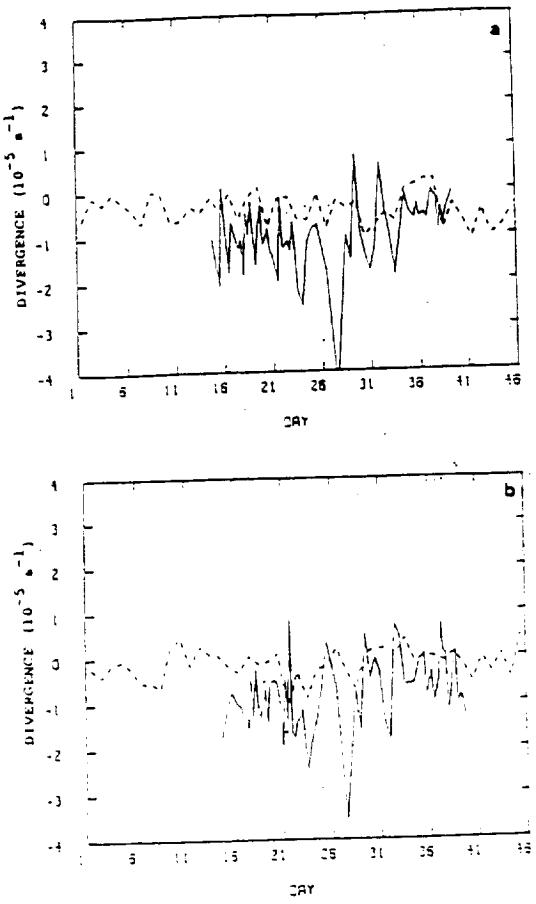

Fig. 6. Time series of horizontal divergence at 850 mb (a) and 700 mb (b) calculated for the Belém-Boa Vista-Embrapa triangle using rawinsonde (solid) and ECMWF (dashed) data.

the 29 April–1 May event. Increasing low level convergence precedes the event, followed by divergence which is coincident with the major rain pulses.

Divergence calculations for the triangle were repeated based solely upon ECMWF data. The results of this calculation are also shown in Fig. 6. While the ECMWF data captures much of the temporal variation in the signal, divergence is an order of magnitude lower than that obtained from the calculations based on the soundings.

Divergence calculated for the smaller mesoscale triangle shown in Fig. 1b (Scala et al., 1990) yield divergence values an order of magnitude higher (10^{-4} s^{-1}) than those obtained from the large scale triangle network soundings. Such a hierarchal increase in divergence (10^{-6}, 10^{-5}, 10^{-4} s^{-1}) proceeding from the large scale flow fields, as represented by the ECMWF, to the synoptic fields large scale triangle (Fig. 1a) to the mesoscale (mesoscale triangle soundings, Fig. 1b) is consistent with other work in the tropical atmosphere (see for example the GARP Atlantic Tropical Experiment results such as Frank, 1978). We, therefore, use a 48-h mean convergence of 2.0×10^{-5} s^{-1} as representative of the mass inflow into the volume bounded by the surface to 4 km and the sides Boa Vista to Belem to Manaus.

3.3. Calculation of mass transports of Saharan dust into the Amazon Basin

The area of the large triangle in Fig. 1a is approximately 4.0×10^{11} m^2. The volume of air from the surface to 4 km over the triangle is 1.6×10^{15} m^3. If the mean divergence over 48 h preceding the dust event is -2.0×10^{-5} s^{-1}, then the amount of air exchanged during this time is $(-2.0 \times 10^{-5}\ \text{s}^{-1})(1.728 \times 10^5\ \text{s}) = 3.5$ times the original volume. In contrast, with large-scale flow in the absence of an organized synoptic scale weather system (divergence $= 10^{-6}$ s^{-1}), the exchange rate would be an order of magnitude less, or only 1/3 of the low level volume would be exchanged in 48 h. Under synoptic scale forcing, the volume of air contained below 4 km over the triangle is exchanged 3.5 times in 48 h equalling $(3.5)(1.6 \times 10^{15}\ \text{m}^3) = 5.6 \times 10^{15}$ m^3 of air.

Under northeasterly inflow into the Amazon Basin, we may assume that all of this exchange occurs across the side of the triangle parallel to the coast. Fig. 7 shows the dust plume laying off the NE coast of South America. Fig. 8 shows a Saharan dust plume immediately east of Barbados (60° W, 13° N) as observed by downward looking airborne lidar (Browell, personal communication). The plume lies between 1.5 and 4.2 km. In the presence of such a dust plume, the air being brought into the basin-scale triangle by the storm system will contain large amounts of dust. Talbot et al. (1986) showed that these dust plumes contained up to 400 μg m^{-3}, with a mean value of 51 μg m^{-3} for the surface to 3.7 km layer. A weighted mean for the layer between 1.5 and 4 km from Prospero and Carlson (1972) gives a value of 45 μg m^{-3}. We take a mean value of 50 μg m^{-3} for the dust concentration in such a plume between

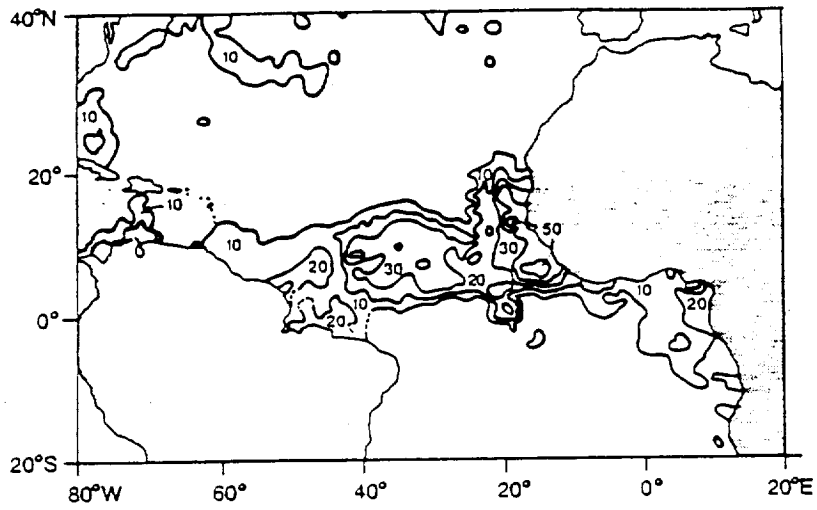

Fig. 7. Aerosol optical depth (τ) on 21 April 1988 showing a dust plume between western Africa and the northeastern coast of Brazil. Values for τ derived at NOAA/NESDIS using satellite radiance values obtained from the AVHRR. Contour intervals are multiplied by 100.

the surface and 4 km over a continuous period of 48 h. Using this mean concentration, we calculate the mass of dust entering the volume in 48 h to be:

(the volume of air exchanged in 48 h)

(mean concentration)

$(5.6 \times 10^{15}\ m^3)(5.0 \times 10^{-5}\ g\ m^{-3})$

$= 2.8 \times 10^{11}$ g or

280,000 tons per storm system.

A given storm may have a convergence field which acts on the dust plume for longer than 48 h. However, this may be counteracted by the fact that a mean concentration of 50 $\mu g\ m^{-3}$ may be high for the entire duration of the inflow. Thus, we feel that 48 h and 50 $\mu g\ m^{-3}$ are representative of the average dust event.

The calculation above assumes the dust enters across the side of the triangle (Fig. 1a) parallel to the coast. In fact, the dust will enter across the entire NE coast of South America. Aerosol optical depth data from the Advanced Very High Resolution Radiometer (AVHRR) presented in (Fig. 7) shows that the length of coastline across which the dust is transported extends from Sao Luis, Brazil (44°30′W longitude, 2°30′S latitude) to the Gulf of Paria (63°0′W longitude, 10°30′N latitude), a total distance of 2500 km. The linear distance of the triangle side to the coastline is 1:1.7. We thus increase our above estimate by 1.7:

$(2.8 \times 10^5)(1.7)$

$= 4.8 \times 10^5$ tons/storm system.

Greco et al. (1990) have shown that 80% of the CAB rainfall during the wet season is produced by organized synoptic scale weather systems. The average amount of rainfall in the CAB during the 6 months (December–May) of the CAB wet season coincident with Saharan dust outbreaks is about 1600 mm (Villa Nova et al., 1976; Marques-Filho et al., 1981). Swap (1990) shows that the average amount of rain per synoptic scale system is 20 mm. Thus, approximately 60 synoptic scale weather systems occur in the 6-month wet season or approximately 10 systems a month. Other evidence (Madden and Julian, 1972) show a 5-day periodicity in the equatorial tropics or 6 systems a month.

The wet season for the eastern Amazon basin (EAB) is approximately 2 months longer than the CAB wet season. The EAB wet season lasts from December to July (Villa Nova et al., 1976), and with approximately 2000 mm of rain falling during this period. If 80% of the EAB rain is also delivered by organized synoptic scale systems, approximately 80 storms occur in the 8-month

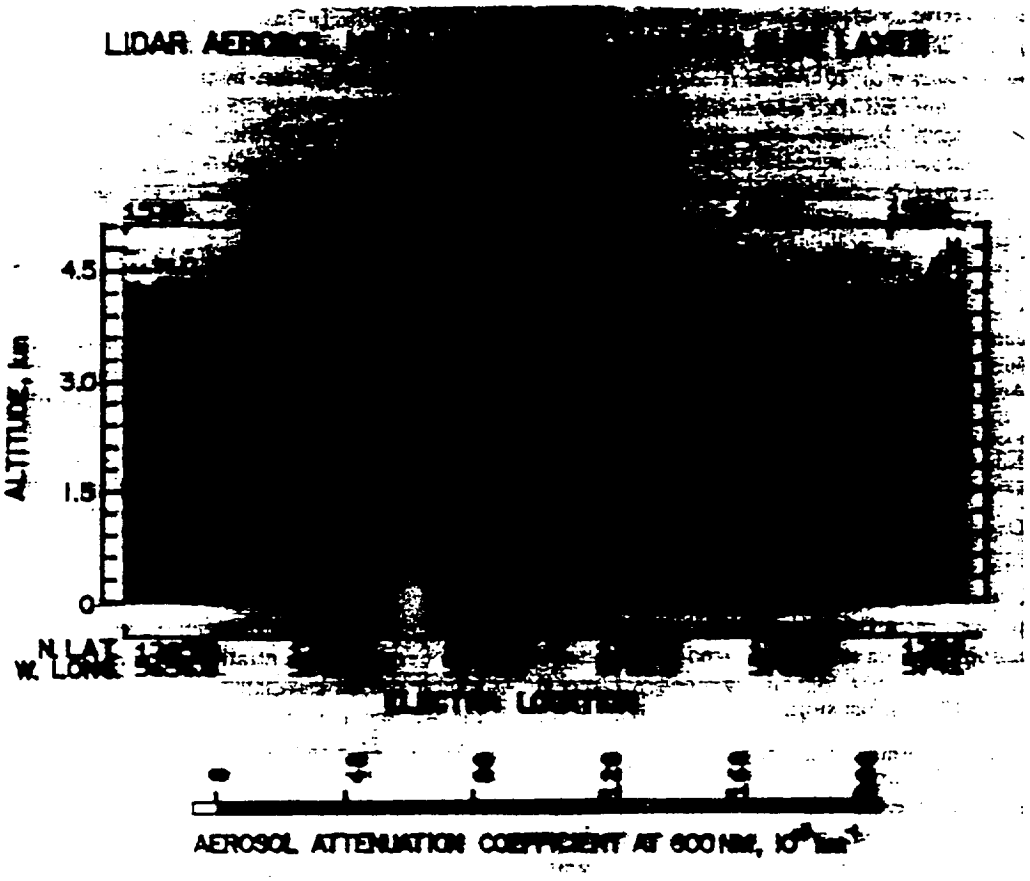

Fig. 8. Lidar-measured aerosol attenuation coefficient near Barbados on 21 July 1984 (courtesy of E. Browell, personal communication). The dust plume is seen between 1.5 km and 4.2 km.

wet season (10 systems a month). These numbers are supported by Cohen (1989) who reported an average annual value of 67.5 synoptic scale instability lines in the EAB during these months between 1979 and 1986. Cohen's numbers are confined to "instability lines" and do not include all synoptic scale systems.

Aerosol optical thickness measurements made from the AVHRR equipped satellite over a 32-month period from 4 June 1987 to 1 March 1990 are used to obtain a measure of the number of weeks in which Saharan dust outbreaks are present off the NE coast of South America. Table 1 shows that 34.1% of the weeks during the 32 months have aerosol optical thickness values of at least 0.3 within the area bounded by 10°N–0°, 60°W–40°W. Values of 0.3 or greater are representative of heavy aerosol outbreaks (Carlson, 1979). Table 1 also shows that heavy dust outbreaks are seen from December to July. This corresponds to the height of the wet season for eastern and northeastern Amazon Basin (Villa Nova et al., 1976) and to the period of increased coastal squall line activity (Cohen, 1989).

Based on the results of rainfall per system and the aerosol optical depth analysis, 34.1% of the 80 or 27.3 synoptic scale systems have the potential to carry dust into the eastern Amazon Basin during the extended wet season of December–July. If we round off the number of dust bearing storms to 27

Table 1. *% of weeks with aerosol optical thickness values of (a) < 0.2, (b) < 0.3 and (c) ≥ 0.3 for the area bounded by 10° N and 0° and 60° W–40° W from 4 June 1987 to 1 March 1990*

	a	*b*	*c*
January	27.2	18.2	54.6
February	0	16.7	83.3
March	9.1	9.1	81.8
April	0	14.3	85.7
May	12.5	37.5	50.0
June	0	53.8	46.2
July	7.7	61.5	30.8
August	66.7	33.3	0
September	83.3	16.7	0
October	83.3	16.7	0
November	64.3	35.7	0
December	58.3	25.0	16.7
Overall	36.2	29.7	34.1

per wet season then the annual amount of Saharan dust introduced into the Amazon Basin is

$(4.8 \times 10^5$ tons per storm)

$\times$ (27 storms/wet season).

If all of the Saharan dust introduced into the Amazon Basin in a year is accomplished in the wet season, then the amount of dust per year is *13.0 Mtons/year*.

Prospero and Carlson (1972) have estimated the annual transport of Saharan dust through a wall extending from 10° N latitude to 25° N latitude along 60° W longitude to range between 25 and 37 Mtons per year. D'Almeida (1986) has estimated annual westward transport immediately off West Africa to lie between 45 and 53 Mtons per year. Estimates of the total annual West African source strength for westward transport vary from 80 Mtons per year (Prospero and Carlson, 1972) to 260 Mtons/year (Jaenicke and Schütz, 1978) with 190 Mtons per year having been reported by D'Almeida (1986).

Our results suggest that the amount of dust that enters the Amazon basin is between one half and one third of the amont of dust found by Prospero et al. (1981) to cross the 60th meridian between 10 and 25° N. The major uncertainties in our calculations are the mean concentration (50 $\mu g\ m^{-3}$) and the number of synoptic scale systems (27) which bring dust into the Amazon Basin. Mean concentrations of dust in the outbreaks coinciding with synoptic scale systems in the Amazon Basin are unlikely to drop below 25 $\mu g\ m^{-3}$ or to rise above 75 $\mu g\ m^{-3}$. Extreme variations in mean wet season rainfall in the CAB reach ±20% (Kousky and Kagano, 1981). The presence or absence of a single synoptic scale system in each of the 8 wet season months can account for such a variation in rainfall. Thus, a maximum or minimum possible variation in dust supply due to a variation in storm systems is ±8 systems. These extremes, if coincident, give a range of 4.4 Mtons/year to 24.4 Mtons/year. We believe that such an extreme range is unrealistic. For example, all storms added or subtracted will not coincide with dust events; nor are concentrations of dust likely to go down in dry years or up in wet years. Both effects reduce the extremes. A more realistic range is half the extreme range or 8.5 to 18.5 Mtons/year.

3.4. Transport of trace species with Saharan dust

The mass concentrations of selected water-soluble species associated with Saharan dust over the western tropical Atlantic and the CAB are given in Table 2. Many of the nutrient species associated with Saharan dust (e.g., K, NH_4, NO_3, PO_4) are believed critical to the physiology of tropical rain forests (Vitousek and Sanford, 1986). The mass % contributions of the various species range from tenths of a percent to several percent.

Mass concentrations of Na and Cl are enhanced over the CAB compared to their levels in the Sahara air layer over the western tropical Atlantic (Table 2). This apparent enrichment is presumably due to entrainment of sea salt into dust-containing air masses that are advected inland from the South American coast. The sea salt concentration over the CAB is on the order of 0.5 $\mu g\ m^{-3}$ during periods influenced by the injection of marine air (Talbot et al., 1990). Besides Na and Cl, NH_4 and SO_4 appear to be enriched 2-fold and NO_3 3-fold over the CAB compared to the Sahara air layer over the western tropical Atlantic. We attribute these differences to inputs of nitrogen-rich biomass burning emissions along coastal Africa (Delmas, 1982). The levels of NH_4, NO_3, and SO_4 associated with Saharan dust over the tropical Atlantic appear to be strongly influenced by African biomass burning products during the winter-to-spring time of the year (Savoie et al.,

Table 2. *Mass concentrations (%) of selected trace species associated with Saharan dust over the Western Tropical Atlantic and the Central Amazon Basin*

Species	Average (%)	Range (%)
(a) *Western tropical Atlantic*[a]		
Na	0.37	0.24 –0.85
K	0.17	0.10 –0.33
NH_4	0.18	0.01 –0.27
Cl	0.32	0.19 –0.50
NO_3	0.51	0.21 –1.5
SO_4	1.29	0.35 –3.0
PO_4	0.037	0.017–0.071
(b) *Central Amazon basin*[b]		
Na	1.1	0.42–1.8
K	0.29	0.12–0.46
NH_4	0.44	0.08–0.91
Cl	1.9	1.3 –2.6
NO_3	1.6	0.20–2.6
SO_4	2.4	0.22–3.7
PO_4	N/A	N/A

[a] From Talbot et al. (1986).
[b] From Talbot et al. (1990).

1989). Our ABLE 1 measurements over the western tropical Atlantic were conducted during summertime and exhibit minimal influence from African biomass combustion products; a dramatic seasonal signal in this source appears in the annual record of aerosol composition at Barbados (Savoie et al., 1989). Thus, Saharan air intrusions into the CAB during the wet season appear to reflect combined chemical inputs from mineral aerosol, sea salt, and possibly biomass burning products.

The annual rates of supply of trace species were estimated assuming that all the dust entering the Boa Vista/Manaus/Belem triangle is deposited within that area. In assessing this assumption, it should be noted that Manaus lies more than 1300 km inland from the NE coast of South America. If all the Saharan dust introduced into the triangle (Fig. 1b) in a year was effectively deposited in that area, its deposition flux would be:

$$\frac{13 \times 10^9 \text{ kg yr}^{-1}}{(1.7)(4.0 \times 10^7 \text{ ha})} = 190 \text{ kg ha}^{-1} \text{ yr}^{-1}.$$

This value, 190 kg ha^{-1} yr^{-1}, is on the high end of other reported Saharan dust depositional rates; 13 kg ha^{-1} yr^{-1} at Miami, Florida (Prospero et al., 1987) and 77 kg ha^{-1} yr^{-1} in the French Alps (DeAngelis and Gaudichet, 1991).

Using the mass concentrations of selected trace species associated with Saharan dust over the CAB (Table 2) and our above estimate of dust deposition to the Amazonian ecosystem, we find that most species are deposited at a rate of 1–4 kg ha^{-1} yr^{-1} (Table 3). These deposition fluxes are essentially identical to the average wet deposition fluxes measured at two stations within the triangle area during the ABLE 2B experiment (Table 3). This result suggests that precipitation scavenging is the principal removal mechanism of Saharan dust associated material from the atmosphere during the CAB wet season. During the CAB wet season, the average residence time of aerosols in boundary layer air relative to precipitation washout is 0.25–1 day (Andreae et al., 1990). Our analysis suggests that the major ionic composition of precipitation (e.g., NH_4, NO_3, SO_4) in the CAB wet season may be strongly influenced by inputs of material originating on the African continent nearly 5000 km away. This transcontinental bio-

Table 3: *Comparison of deposition fluxes (kg ha^{-1} yr^{-1}) of selected trace species associated with intrusions of Saharan dust and precipitation in the Amazonian wet season (December–May)*

Species	Dust Intrusions[a] average	Dust Intrusions[a] range	Precipitation[b] average	Precipitation[b] range[c]
Na	2.1	0.80 –3.4	1.7	0.73–2.9
K	0.55	0.23 –0.87	1.3	0.41–2.3
NH_4	0.84	0.15 –1.7	0.71	0.38–1.4
Cl	3.6	2.5 –4.9	2.9	1.4 –5.1
NO_3	3.0	0.38 –4.9	1.4	0.90–3.7
$SO_4^=$	4.6	0.42 –7.0	1.8	1.2 –3.1
PO_4	0.07[d]	0.032–0.14[d]	0.04[e]	0.01–0.12[e]

[a] Calculated using mass concentrations reported in Table 2.
[b] Based on measurements reported in Table 1 from Andreae et al. (1990).
[c] Based on upper and lower quartile concentrations observed at two sites within the triangle area (Andreae et al., 1990).
[d] Estimated using average mass concentration (see Table 2) reported by Talbot et al. (1986).
[e] Based on unpublished data from ABLE 2b (R. Talbot and M. Andreae, personal communication, 1987).

geochemical link appears to be severed during the dry season when the large-scale meteorological regime which favors transport of Saharan air masses into the CAB migrates to the north. The aerosol and precipitation chemistries in the CAB dry season support such a scenario (Talbot et al., 1988; Andreae et al., 1988). Long-range transport of aerosol-associated species to the CAB appears to explain the higher wet season precipitation fluxes of Na, Cl, and K compared to the dry season. It also seems to be responsible for the similar seasonal precipitation fluxes of NH_4, NO_3, and SO_4 despite a five-fold contrast in rainfall amounts. Our estimate of long-range chemical inputs to the CAB are significantly lower than Reichholf's (1986), who suggests at least 2 orders of magnitude higher dust transport to the western tropical Atlantic atmosphere than any reported estimate.

Table 4 compares our deposition fluxes to reported annual internal fluxes (the amount of nutrients internally recycled) and standing stock values (the total ecosystem amount of a nutrient) for the Amazon Basin. Inputs of K and P associated with Saharan dust aerosols represent from a few tenths to 6% of the annual nutrient turnover due to litterfall, and from a few thousandths to a few tenths of a percent of the total ecosystem standing stock. The nutrient influx of these and other trace elements into the EAB and CAB does not appear important on short time scales (10^1–10^2 years). However, with respect to the long-term geochemical mass balance of the Basin, Saharan dust and associated aerosols are important as an outside source of elements that help replenish those lost from the system. This importance is amplified in a tightly constrained nutrient system such as the EAB and CAB.

The time required for the imported K and P to be equal to the amount of their respective Amazonian standing stocks is estimated using our deposition fluxes to evaluate the potential biogeochemical importance of Saharan dust inputs to the Amazon rainforest. Dividing the standing stock of K in the Amazon oxisol rainforest, ~380 kg ha^{-1} (Jordan, 1985), by our maximum and minimum values of K influx (Table 3), we arrive at values ranging from 440 to 1700 years. The same calculation for P, using a standing stock value of 220 kg ha^{-1} for the CAB (Golley et al., 1975) results in values ranging from 4700 years to 20,000 years. These calculations do not account for losses from the system, such as the Amazon River outflow (Gibbs, 1972). Hydrologic loss values (Franken and Leopoldo, 1984) of P from the CAB vary from an order of magnitude less than our deposition values to the same order of magnitude.

These results suggest that if Saharan dust aerosol is a principal source of these trace species to the EAB and CAB, then the effect on the biogeochemical cycling would be on the long term (10^2–10^3 years). Other possible mechanisms may play additional roles in this seemingly storm event driven system. The accumulation of nutrients in rain water stored in epihytes may be one such mechanism. Increased tree falls in tropical rain forests are noted during the wet season (Oldeman, 1972; Brokaw, 1985). Large trees heavily loaded with epiphytes may therefore be prime candidates to fall during the CAB wet season. Tree fall is most likely to occur in the synoptic scale storms called upon to gather the dust into the Basin. Downdrafts from deep convective clouds in these storm systems reach speeds of 20 to 25 m s^{-1} (45–55 mph). The creation of gaps in the rain forest at the time of maximum soil dust influx may

Table 4. *Range of values for depositional influx of P and K due to Saharan dust and associated aerosols compared to and expressed as %s of annual internal flux from litterfall and total ecosystem nutrient amount*

	Depositional input (kg ha^{-1} yr^{-1})	Internal flux from litterfall (kg ha^{-1} yr^{-1})	Input as % of litterfall (min–max)	Standing stock (kg ha^{-1})	Input as % of standing stock
P	0.011–0.047	1.4– 4.1[a]	0.27–3.4	220[b]	0.005–0.021
K	0.23 –0.87	13 –21[a]	1.1 –6.7	378[c]	0.061–0.23

[a] Proctor (1984).
[b] Klinge (1976).
[c] Golley et al. (1975).

be an important component in the utilization of small amounts of trace elements.

4. Summary and conclusions

We conclude that Saharan dust penetrates the eastern Amazon Basin and is detected in the Central Basin. The dust is delivered in intermittent pulses which occur in association with major pulses in rainfall. Since these large rain events are due to organized storm systems with horizontal scales of up to a few thousand kilometers and time scales of days, we conclude that part of the mechanism driving the storm system is responsible for the accumulation of dust.

Low-level (up to 4 km) horizontal negative divergence associated with the storm system is shown to be sufficient to draw dust into the Amazon Basin. Previous work together with results provided here show that Saharan dust easily reaches the western tropical north Atlantic. Mean flow into the Basin can neither concentrate the dust nor deliver it in the aperiodic fashion observed. Storm systems are shown to be sufficiently frequent to draw upon existing dust plumes. The presence of Saharan dust off the northeast coast of South America is also shown to coincide with the high frequency of storms. Not all rain events in the CAB are accompanied by dust, but all of the dust events we observed occurred in association with rain events.

Observations of the horizontal extent, vertical depth and concentrations of dust permit an estimate of the amount of dust introduced into the Amazon Basin in a given storm event. Storm climatology yields an estimate of 13 Mtons/year of dust introduced into the Amazon Basin. In the northeastern basin, this may amount to as much as 190 kg ha^{-1} yr^{-1} of dust. The amount of trace species supplied with this dust ranges from a few kg ha^{-1} yr^{-1} to less than 1 kg ha^{-1} yr^{-1}.

The total amount of Saharan dust calculated to enter the Amazon Basin is one half to one third of that estimated by others to cross 60° W longitude between 10° and 25° N latitude (Prospero and Carlson, 1972). It is two orders of magnitude less than is implied by Reichholf (1986) who has estimated quantities of trace species needed by the rain forest on nutrient poor soils. This large discrepancy may be due to an underestimate in the total amount of soil dust supplied to the Amazon Basin if, as we have, one confines the calculation to the Sahara as the only source. The discrepancy may also be due to an overestimation of the necessary nutrient influxes and a simultaneous underestimation of the efficiency in recycling nutrients in this ecosystem.

Whatever the resolution of the above paradox is, we conclude that part of the Amazon rain forest is dependent upon soil dust which originates in the Sahara/Sahel region of western Africa. We concur with conclusions drawn by others that such a dependence must be reflected by expansions and contractions of the Amazon rain forest in direct relationship to expansions and contractions of the Sahara/Sahel. We hypothesize that such fluctuations in the size of the rain forest are on time scales which lie between about 500 and 20,000 years. Evidence for such a coupled response must be present in the records of the pleistocene pluvial periods. Such a dependence of one large ecosystem upon another separated by an ocean is of fundamental importance to our view of the role of these ecosystems in the global atmosphere. A view of the role of Amazonian rain forest in the global system must take this coupled process into account. Any strategy designed to preserve the Amazonian rain forest or any part thereof should equally concern itself with the interrelationship between the rain forest, global climate and acid zones well removed from Amazonia.

5. Acknowledgements

We wish to acknowledge the support provided by the Tropospheric Chemistry Program of NASA which has included the three ABLE missions and continued support of analytical work at the University of Virginia. The contributions of many individuals through the field experiments can regretfully only be acknowledged collectively. Similarly, we wish to acknowledge the help of the graduate students and faculty of the Department of Environmental Sciences. Data and computer support for the trajectory analysis by the ECMWF is recognized with appreciation. This paper draws upon Mr. Swap's thesis submitted in partial fulfillment of the Master of Science degree at the University of Virginia.

This paper is dedicated to Robert Harriss in recognition of his wisdom and enthusiasm in creating and carrying out the Atlantic and Amazon Boundary Layer Experiments.

REFERENCES

Andreae, M. O., Browell, E. V., Garstang, M., Gregory, G. L., Harriss, R. C., Hill, G. F., Jacob, D. J., Pereira, M. C., Sachse, G. W., Setzer, A. W., Silva Dias, P. L., Talbot, R. W., Torres, A. L. and Wofsy, S. C. 1988. Biomass-burning emissions and associated haze layers over Amazonia. *J. Geophys. Res. 93*, 1509–1529.

Andreae, M. O., Talbot, R. W., Berresheim, H. and Beecher, K. M. 1990. Precipitation chemistry in Central Amazonia. *J. Geophys. Res. 95*, 16987–16999.

Artaxo, P., Maenhaut, W., Storms, H. and Van Grieken, R. 1990. Aerosol characteristics and sources for the Amazon Basin during the wet season. *J. Geophys. Res. 95*, 16971–16985.

Bergametti, G., Gomes, L., Coude-Gaussen, G., Rognon, P. and Le Coustumer, M. N. 1989. African dust observed over Canary Islands: Source-regions identification and transport pattern for some summer situations. *J. Geophys. Res. 94*, 14855–14864.

Brokaw, N. V. L. 1985. Treefalls regrowth and community structure in tropical forests. In: *The ecology of natural disturbance and patch dynamics* (eds. S. T. A. Pickett and P. S. White). Academic Press, Inc., Orlando, pp. 53–69.

Brummer, B. 1978. Mass and energy budgets of a 1 km high atmospheric box over the GATE C-scale triangle during undisturbed and disturbed weather conditions. *J. Atmos. Sci. 35*, 997–1011.

Carlson, T. N. 1979. Atmospheric turbidity in Saharan dust outbreaks as determined by analyses of satellite brightness data. *Mon. Wea. Rev. 107*, 322–335.

Cohen, J. C. P. 1989. *Um estudo observacional de linhas de instabilidade na Amazônia.* INPE-4865-TDL/376, San Jose dos Campos, Brazil.

D'Almeida, G. A. 1986. A model for Saharan dust transport. *J. Clim. and Appl. Meteor. 25*, 903–916.

DeAngelis, M. and Gaudichet, A. 1991. Saharan dust deposition over Mount Blanc (French Alps) during the last 30 years. *Tellus 43B*, 61–75.

Delmas, R. 1982. On the emission of carbon, nitrogen and sulfur in the atmosphere during brushfires in the inter-tropical savannah zones. *Geophys. Res. Lett. 9*, 761–764.

Frank, W. M. 1978. The life cycles of GATE convective systems. *J. Atmos. Sci. 35*, 1256–1264.

Franken, W. and Leopoldo, P. R. 1984. Hydrology of catchment areas of central-Amazonian forest streams. In: *The Amazon: limnology and landscape ecology of a mighty tropical river and its basin*, (ed. H. Sioli). Junk Pub., Dordrecht, 501–519.

Garstang, M., Ulanski, S., Greco, S., Scala, J., Swap, R., Fitzjarrald, D., Martin, D., Browell, E., Shipham, M., Connors, V., Harriss, R. and Talbot, R. 1990. The Amazon boundary layer experiment (ABLE 2B): a meteorological perspective. *Bull. Amer. Meteor. Soc. 71*, 19–32.

Gibbs, R. J. 1972. Water chemistry of the Amazon River. *Geochim. Cosmochim. Acta 36*, 1061–1066.

Golley, F. B., McGinnis, J. T., Clements, R. G., Child, G. I. and Duever, M. J. 1975. *Mineral cycling in a tropical moist forest ecosystem.* University of Georgia Press, Athens, GA.

Greco, S., Swap, R., Garstang, M., Ulanski, S., Shipham, M., Harriss, R. C., Talbot, R., Andreae, M. O. and Artaxo, P. 1990. Rainfall and surface kinematic conditions over Central Amazonia during ABLE 2B. *J. Geophys. Res. 95*, 17001–17014.

Gregory, G. L., Harriss, R. C., Talbot, R. W., Rasmussen, R. A., Garstang, M., Andreae, M. O., Hinton, R. R., Browell, E. V., Beck, S. M., Sebacher, D. I., Khalil, M. A. K., Ferek, R. J. and Harriss, S. V. 1986. Air chemistry over the tropical forest of Guyana. *J. Geophys. Res. 91*, 8603–8612.

Harriss, R. C., Wofsy, S. C., Garstang, M., Browell, E. V., Molion, L. C. B., McNeal, R. J., Hoell, J. M., Jr., Bendura, R. J., Beck, S. M., Navarro, R. L., Riley, J. T. and Snell, R. L. 1988. The Amazon Boundary Layer Experiment (ABLE 2A): Dry season 1985. *J. Geophys. Res. 93*, 1351–1360.

Harriss, R. C., Garstang, M., Wofsy, S. C., Beck, S. M., Bendura, R. J., Coelho, J. R. B., Drewry, J. W., Hoell, J. M., Jr., Matson, P. A., McNeal, R. J., Molion, L. C. B., Navarro, R. L., Rabine, V. and Snell, R. L. 1990. The Amazon boundary layer experiment: wet season 1987. *J. Geophys. Res. 95*, 16,721–16,736.

Hollingsworth, A. 1987. Objective analysis for numerical weather prediction. *Short- and medium-range numerical weather prediction*, Collection of Papers Presented at the WMO/IUGG NWP Symp., Tokyo, Japan, 4–8 August 1986.

Jaenicke, R. and Schutz, L. 1978. Comprehensive study of physical and chemical properties of the surface aerosols in the Cape Verde Islands region. *J. Geophys. Res. 83*, 3585–3589.

Jordan, C. F. 1985. *Nutrient cycling in tropical forest ecosystems: principles and their application in management and conservation.* John Wiley and Sons, New York, 190 pp.

Junge, C. 1979. The importance of mineral dust as an atmospheric constituent. In: *Saharan dust, mobilization, transport, deposition* (ed. C. Morales). John Wiley and Sons, New York, pp. 49–60.

Klinge, H. 1976. Bilanzierung von Haupt nahrstoffen im Okosystem tropischer regenwald (Manaus)-vovlaufige daten. *Biogeographica 7*, 59–76.

Kousky, V. and Kagano, K. 1981. A climatological study of the tropospheric circulation over the Amazon region. *Acta Amazonica 11*, 743–758.

Levin, Z., Joseph, J. H. and Mekler, Y. 1980. Properties of Saharan (Khamsin) dust-comparison of optical and direct sampling data. *J. Atmos. Sci. 37*, 882–891.

Lõye-Pilot, M. D., Martin, J. M. and Morelli, J. 1986. Influence of Saharan dust on the rain acidity and atmospheric input to the Mediterranean. *Nature 321*, 427–428.

Madden, R. A. and Julian, P. R. 1972. Description of global-scale circulation cells in the tropics with a 40–50 day period. *J. Atmos. Sci. 29*, 1109–1123.

Marques-Filho, Ade O., Ribeiro, M. N. G., dos Santos, H. M. and dos Santos, J. M. 1981. Estudos climatológicos da Reserva Florestal Ducke-Manaus-AM, IV. Precipitacao. *Acta Amazonica 11*, 759–768.

Oldeman, R. A. A. 1972. L'architecture de la végétation ripicole forestiére des flueves et criques guyanais. *Adansonia* N.S., 12, 253–265.

Parkin, D. W., Phillips, D. R., Sullivan, R. A. L. and Johnson, L. R. 1972. Airborne dust collections down the Atlantic. *Quart. J. Roy. Meteor. Soc. 98*, 798–808.

Petit, J. R., Briat, M. and Royer, A. 1981. Ice age aerosol content from East Antartic ice core samples and past wind strength. *Nature 293*, 391–394.

Proctor, J. 1984. Tropical forest litterfall. II. The data set. In: *Tropical rainforest: The Leeds Symposium* (eds. S. L. Sutton and A. C. Chadwick). Leeds: Leeds Philos. Nat. Hist. Soc., pp. 83–113.

Prospero, J. M. and Carlson, T. N. 1972. Vertical and areal distribution of Saharan dust over the Western Equatorial North Atlantic Ocean. *J. Geophys. Res. 77*, 5255–5265.

Prospero, J. M. and Nees, R. T. 1977. Dust concentration in the atmosphere of the Equatorial North Atlantic: Possible relationship to the Sahelian drought. *Science 196*, 1196–1198.

Prospero, J. M. and Nees, R. T. 1986. Impact of the North African drought and El Niño on mineral dust in the Barbados trade winds. *Nature 320*, 735–738.

Prospero, J. M., Glaccum, R. A. and Nees, R. T. 1981. Atmospheric transport of soil dust from Africa to South America. *Nature 289*, 570–572.

Prospero, J. M., Nees, R. T. and Uematsu, M. 1987. Deposition rate of particulate and dissolved aluminum derived from Saharan dust in precipitation at Miami, Florida. *J. Geophys. Res. 92*, 14723–14731.

Rao, C. R. N., Stowe, L. L., McClain, E. P. and Sapper, J. 1988. Development and application of aerosol remote sensing with AVHRR data from the NOAA satellites. In: *Aerosols and climate* (eds. P. V. Hobbs and M. P. McCormick). A Deepak Publishing, Hampton, VA, 69–79.

Reichholf, J. H. 1986. Is Saharan dust a major source of nutrients for the Amazonian rain forest? *Studies on Neotropical Fauna and Environment 21*, 251–255.

Reiff, J., Forbes, G. S., Spieksma, F. TH. M. and Reynders, J. J. 1986. African dust reaching northwestern Europe: A case study to verify trajectory calculations. *J. Clim. and Appl. Meteor. 25*, 1543–1567.

Riehl, H. 1954. *Tropical meteorology*. McGraw-Hill Book Company, New York, 392 pp.

Riehl, H., Yeh, T. C., Malkus, J. S. and LaSeur, N. E. 1951. The north-east trade of the Pacific Ocean. *Quart. J. Roy. Meteor. Soc. 77*, 598–626.

Salati, E. and Vose, P. B. 1984. Amazon Basin: A system in equilibrium. *Science 225*, 129–138.

Savoie, D. L. and Prospero, J. M. 1977. Aerosol concentration statistics for the northern tropical Atlantic. *J. Geophys. Res. 82*, 5954–5964.

Savoie, D. L., Prospero, J. M. and Saltzman, E. S. 1989. Non-sea-salt sulfate and nitrate in trade wind aerosols at Barbados: Evidence for long-range transport. *J. Geophys. Res. 94*, 5069–5080.

Scala, J. R., Garstang, M., Tao, W.-K., Pickering, K. E., Thompson, A. M., Simpson, J., Kirchhoff, V. W. J. H., Browell, E. V., Sachse, G. W., Torres, A. L., Gregory, G. L., Rasmussen, R. A. and Khalil, M. A. K. 1990. Cloud draft structure and trace gas transport. *J. Geophys. Res. 95*, 17015–17030.

Swap, R. J. 1990. *The nature and origin of central Amazonian wet season rainfall*. M. S. Thesis, University of Virginia, 116 pp. (Available University Microfilm, Ann Arbor, MI.)

Talbot, R. W., Harriss, R. C., Browell, E. V., Gregory, G. L., Sebacher, D. I. and Beck, S. M. 1986. Distribution and geochemistry of aerosols in the tropical north Atlantic troposphere: Relationship to Saharan dust. *J. Geophys. Res. 91*, 5173–5182.

Talbot, R. W., Andreae, M. O., Andreae, T. W. and Harriss, R. C. 1988. Regional aerosol chemistry of the Amazon Basin during the dry season. *J. Geophys. Res. 93*, 1499–1508.

Talbot, R. W., Andreae, M. O., Berresheim, H., Artaxo, P., Garstang, M., Harriss, R. C., Beecher, K. M. and Li, S. M. 1990. Aerosol chemistry during the wet season in Central Amazonia: The influence of long range transport. *J. Geophys. Res. 95*, 16955–16969.

Villa Nova, N. A., Salati, E. and Matsui, E. 1976. Estimativa do evapotranspiraçao na Bacia Amazônica. *Acta Amazonica 6*, 215–228.

Vitousek, P. M. and Sanford, R. L., Jr. 1986. Nutrient cycling in moist tropical forest. *Ann. Rev. Ecol. Syst. 17*, 137–167.

Westphal, D. L., Toon, O. B. and Carlson, T. N. 1988. A case study of mobilization and transport of Saharan dust. *J. Atmos. Sci. 45*, 2145–2175.

Aspects of Environmental Change

Edited by
R R Johnston and J R Hardy

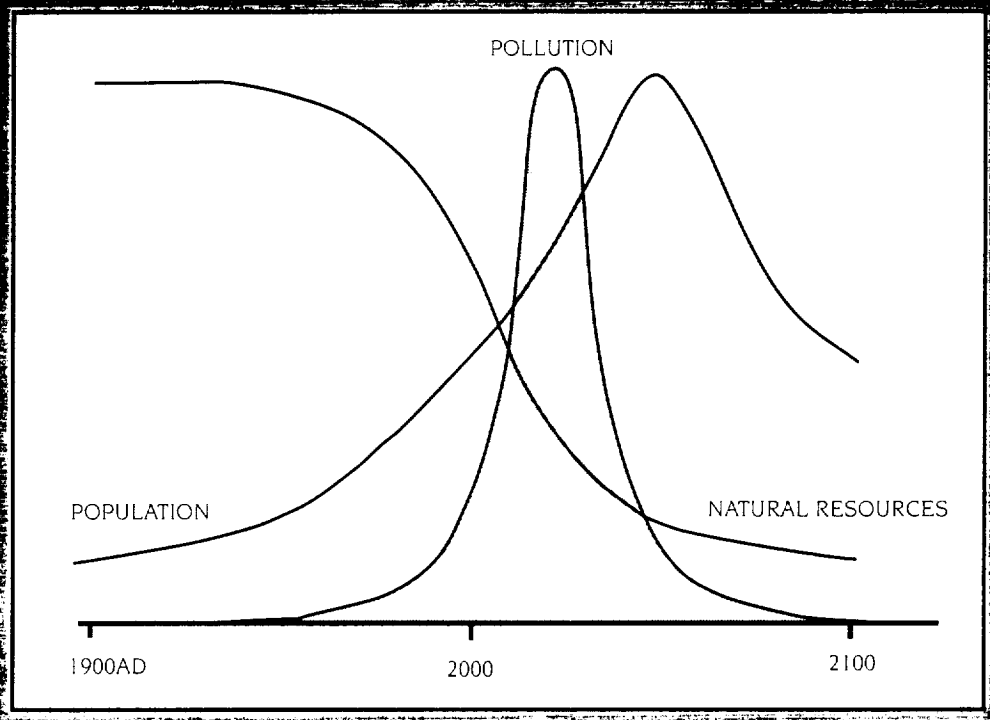

Department of Geography

MISCELLANEOUS SERIES 91/1

DESTRUCTION OF THE RAIN FOREST AND CLIMATE CHANGE

Michael Garstang
Department of Environmental Sciences, University of Virginia, U.S.A.

INTRODUCTION

No *a priori* consequences can be inferred from the possible destruction of the rain forest and the impact of that act upon the global climate. The reason why we cannot project such a response is that we have little or no understanding of how the undisturbed forest influences the global system. If we do not know how the present system works, how can we predict the effect of a changed state of one component on the whole?

Instead the possible effect of the destruction of the rain forest should be posed as a series of questions. Our ability to answer these questions will be a measure of how well we may be able to assess the possible global effect of deforestation.

Three questions will be addressed in this paper. First, are there grounds for assuming that the tropical rain forests play a role in the global atmospheric system? Second, are the tropical rain forests being destroyed and at what rate? Third, depending upon the answers to the first two questions, how do the current rain forests function in the global system? A follow on to this last question is then, how well can we predict a response of global climate to a change in the rain forest?

SOME BASIC FACTS ABOUT THE TROPICAL RAIN FORESTS

While rain forests occur in both temperate and tropical latitudes, the tropical rain forests are by far the most extensive. Tropical rain forests occupy about 7% of the land surface of the Earth. Nearly half of the world's tropical rain forests are in Brazil's Amazon Basin covering some 336 Mha. One's view of the potential effect of an ecosystem occupying only 7% of the earth's surface is greatly changed when it is recognized that that ecosystem contains 60% of the total global biomass. The primary productivity of the tropical rain forest is some 5 Btons of dry material per year, fixing 6.58 tons of carbon per year (Salati, 1987).

The rain forests are the most diverse of all ecosystems on the planet and are thought to contain as many as 30 million species of which only 3 million are known. The rain forests contain 2500 tall tree species compared to a few dozen tall tree species in

temperate zone forests. The abundance of life in the tropical rain forest means that this ecosystem produces 15-20% of trace gases found in the earth's atmosphere (Harriss *et al.*, 1988). Carbon dioxide, carbon monoxide, hydroxyls, heavy and light hydrocarbons, methane and nitrogen species are all produced and are all directly or indirectly involved in capture and emission of terrestrial radiation. Primary and secondary aerosols, mostly organic in composition, influence the transmission (scattering) of solar radiation and the formation of clouds which in turn influence the albedo. Water in these environments is in abundance (precipitation exceeding evaporation). High water vapor content in the equatorial atmosphere implies high latent heat content. High precipitation (in the order of 2 to 3000 mm/year) means that large amounts of latent heat are being converted to sensible and ultimately geopotential energy. Fresh water runoff is high, the Amazon river alone accounting for 25% of the world's river discharge.

THE PHYSICAL SYSTEM

The equatorial regions which contain the bulk of the tropical rain forests are the firebox of the global atmosphere (Riehl and Malkus, 1958). Vertical injection and subsequent poleward transport of heat to achieve global thermal balance does not occur uniformly around the girdle of the planet. "Hot spots" coincident with the large tropical rain forests are found over the Amazon, the Congo (Zaire) and over the warm ocean continent of Indonesia-New Guinea. Hadley and Walker cells represent mean circulations which are fueled by the intermittent action of deep convection coupled to the forest-atmosphere interface at the top of the canopy some 40 m above the ground. The rain forest canopy has an albedo near 10% allowing 90% of incident solar radiation to be absorbed. Solar radiant energy at the surface is used in photosynthesis. Up to 65% of heat may be returned to the atmosphere via evapotranspiration; the remainder returned by evaporation and sensible heat transfer. Some 20% of the rain falling upon the forest is captured, much in unique species such as bromeliads which amount to 10% of the biomass of the Amazon rain forest. It is estimated, but not known accurately, that 50% of the rain falling in the Amazon basin is recycled through the vegetation and surface waters.

The sum total of the physical processes outlined above leads to the conclusion that the tropical rain forest is coupled in an intimate way with the overlying atmosphere. The overlying atmosphere in turn is connected through the larger scale Hadley-Walker circulations to the global atmosphere.

POLITICAL AND ECONOMIC FORCES

The rain forests are subject to large political and economic forces. Forces acting on the Amazon rain forest illustrate the situation. Much, if not all, of the stress imposed upon the rain forest stems from the increase in human population. The population of Brazil

in 1990 is near 150 million. By the year 2050 that population is expected to double. In 1975 it was estimated that 0.56 ha of arable land was required to support each person in the Brazilian population. Increases in population and the need to improve nutrition (upping the amount of arable land to 0.6 ha/person) means that by the year 2050 an additional 180 Mha of arable land will be needed. If such a demand is met by clearing the Amazon rain forest it would mean consuming more than half the current area of rain forest.

Brazil is under serious energy pressure. Energy needs are expected to double in the next decade. Brazil has no reserves of fossil fuel. Hydroelectric power and wood (charcoal) are the most immediate sources of energy in Brazil. The Amazon basin is estimated to contain 1000 GW of hydroelectricity. It is expected that 22 GW will be tapped by 2000. Dams needed to supply these 22 GW of hydroelectricity would inundate 100 Mha of forest.

Projected use of charcoal, primarily to fuel iron ore smelters in the Amazon basin, is estimated to require some 90 Mha of forest over the next 10 years. Unless the efforts to successfully employ tree species that can sustain such a demand, this use will rapidly encroach upon the existing forest.

Global biomass burning is currently estimated to produce 4 Bton C/yr^{-1}. This compares to 5 Btons C yr^{-1} produced by burning fossil fuel. While not all of the biomass burning is due to consuming the tropical rain forests, a large fraction comes from this source. In Brazil it is estimated that only 5% of the rain forest timber is extracted and effectively used. Ninety-five percent is burnt or left to decompose.

Estimates of the rate of deforestation range from 0.5 to 3.0% per year with some estimates as high as 6% per year. Most studies (Logan *et al.*, 1981; Setzer and Pereira, 1986; Salati, 1987; Watson *et al.*, 1990) suggest that deforestation is increasing at an exponential rate. Evidence from satellite imaging suggests that in the Brazilian state of Rondonia this may have been the case from 1982 to 1987. There is now some possibility that the rate of destruction has slowed.

The above suggests that the first two questions posed are both answered in the affirmative. There is substantial basis to argue that the tropical rain forests are coupled to the global atmospheric system and that the tropical rain forests themselves are undergoing rapid change.

The remainder of the paper will address the third question: how do the tropical rain forests function in the global system?

Trace gases like carbon dioxide (CO_2), carbon monoxide (CO), methane (CH_4), isoprene (C_5 H_8) and nitrous oxide (N_2O) are injected into the atmospheric boundary layer immediately above the forest canopy under undisturbed and disturbed (burning) conditions.

In the undisturbed state, trace gases generated in the rain forest are well mixed vertically by active moist convection. Figure 1 shows the vertical distribution of a trace gas (CO) with its source at the surface (forest) under undisturbed conditions and in the wake of widespread biomass burning. When burning is taking place, the background concentrations of CO are seen to treble and marked layers of trace gas are formed in the lower troposphere.

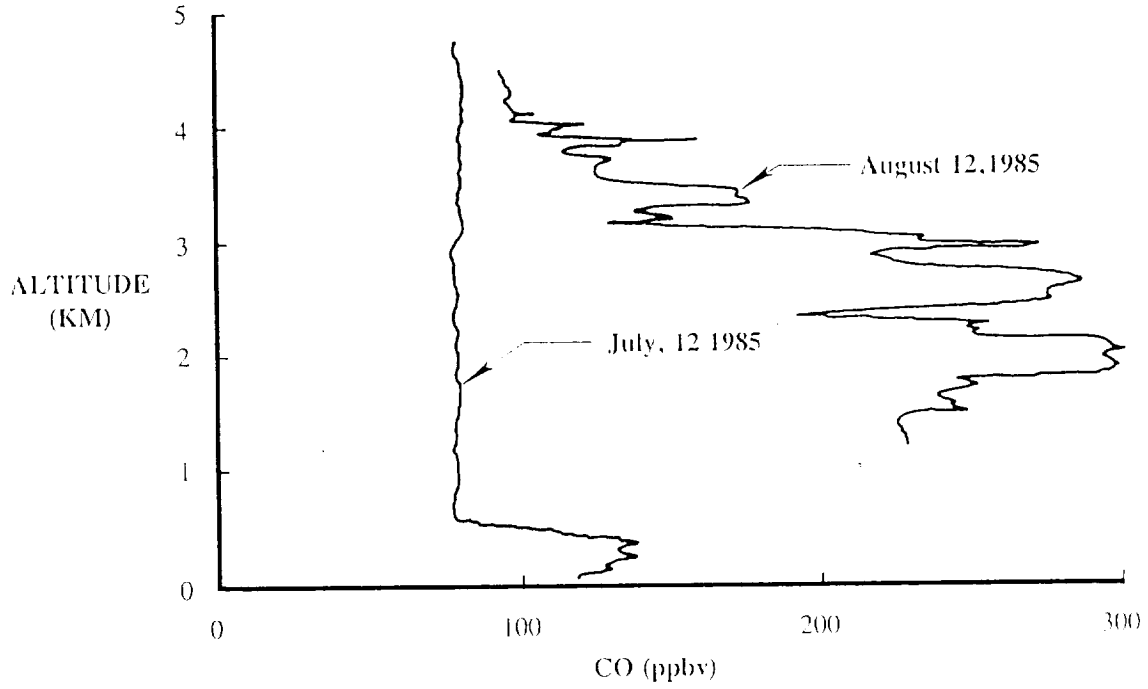

Fig. 1. *Vertical distribution of carbon monoxide in the central Amazon basin under wet (July 12, 1985) and dry (August 12, 1985) conditions. Biomass burning is responsible for the enhanced concentrations observed on August 12.*

Horizontal distributions of the trace gases under undisturbed and disturbed conditions have been shown to be large (JGR, 1990). Measurements in the dry season (burning season) show that products of biomass burning extend over the entire Amazon basin over linear distances of up to 2500 km.

The presence of soil dust was also noted in the Central Amazon Basin (CAB) (Talbot *et al.*, 1990). Figure 2 shows pulses of soil dust elements (Fe, Al, Si) occurring at or nearly at the same time that major rain events are detected in the CAB.

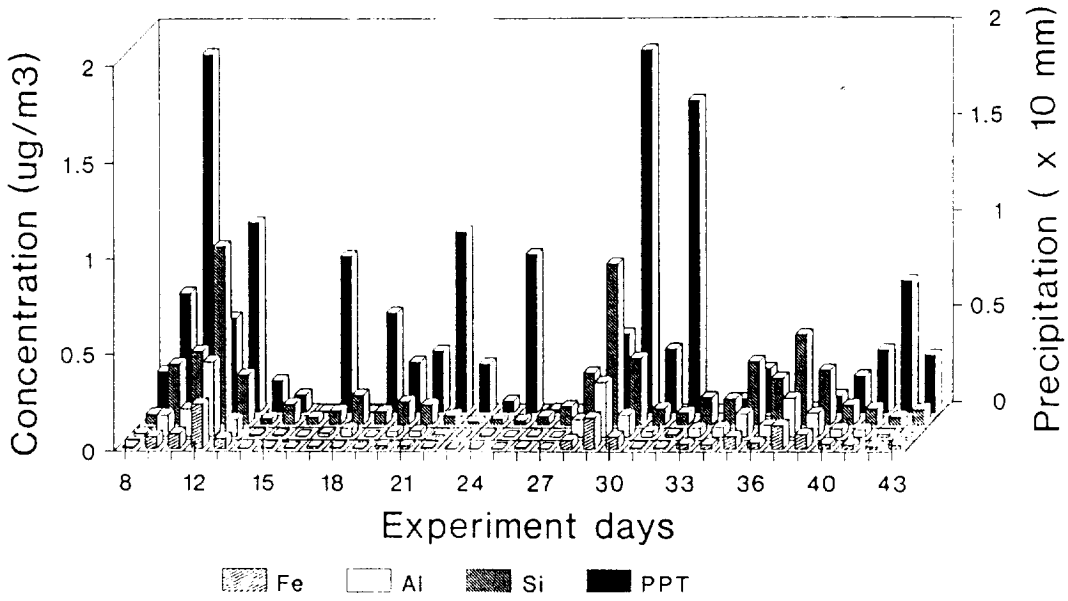

Fig. 2. *Time-series over approximately 6 weeks in the central Amazon basin of ground-based concentrations of terrestrial elements (Fe, Al, Si) together with rainfall.*

PHYSICAL PROCESSES

The chemical measurements show that gases and particles originating in the forest canopy are injected into the atmosphere. The sections below will examine aspects of the vertical transport through three atmospheric layers:

* the canopy-atmosphere interface (100 m deep);
* the atmospheric boundary layer (2 km deep); and
* the cloud layer (15 km deep).

CANOPY-ATMOSPHERE INTERFACE

Figure 3 shows the diurnal flux across the canopy of sensible heat (w'T'), latent heat (w'q'), solar radiation (Rs) and the net radiation (Rn = Rs - outgoing longwave radiation). Air temperature (T) and specific humidity (q) are also shown.

Strong diurnal forcing is noted with latent heat flux reaching 400 W m^{-2} and sensible heat flux 100 W m^{-2} soon after midday. Latent heat fluxes decrease to very small values at night while sensible heat flux reverses direction with heat being lost by the atmosphere to the forest.

The maximum latent heat flux over the forest is twice the amount exchanged by the tropical ocean to the atmosphere. The corresponding sensible heat flux of the forest is six times that occurring over the open tropical ocean. The combined latent and sensible heat input equals the net radiation and approaches the total solar input.

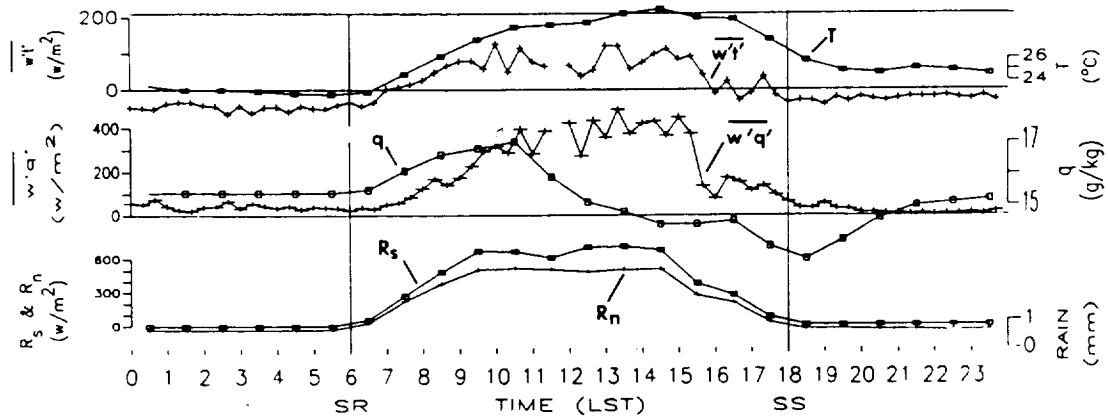

Fig. 3. *Time series under fair weather conditions in the central Amazon basin at 5 m above the forest canopy of heat flux w'T', temperature (T), moisture flux w'q', specific humidity (q), incoming solar radiation flux Rs, net radiational flux Rn, and rainfall. SR and SS are approximate sunrise and sunset.*

The flux of latent heat during the day is such that water vapor divergence occurs at the top of the canopy with specific humidities dropping 2 to 3 g/kg. This "draw-down" of the canopy water vapor must be compensated for by nighttime and early morning recharge.

Other measurements suggest that the greater fraction of the latent energy input is by evapotranspiration (65%) as compared to evaporation from water surfaces (35%). The large energy injection via water vapor during the central hours of the day is clearly an important characteristic of the rain forest. It is likely to trigger a significant buoyant response in the lower atmosphere leading to convective cloud development and further and deeper vertical transport of quantities out of the canopy.

ATMOSPHERIC BOUNDARY LAYER

Figure 4 shows the growth of the mixed layer over the rain forest. For a 5-hour period beginning 1 hour after sunrise, the mixed layer grows at a rate of 8-10 cm s^{-1}. Entrainment across the top of the mixed layer approaches 600 W m^{-2} which is a contributing factor to the drying observed in the surface layer above the canopy in Figure 3 above.

Mixed layer growth ceases at about 1600 LST decaying rapidly to a shallow (< 300 m) night-time mixed layer. A fossil mixed layer (well mixed but no longer actively mixing) remains. In the absence of cloud convection (particularly precipitating), the fossil mixed layer builds concentrations of species on a day-to-day basis. Moist convection acts as a siphon drawing down these concentrations.

The vertical transport of quantities out of the forest canopy depends not only upon the fluxes across the top of the canopy but upon the depth and rate of growth of the mixed layer.

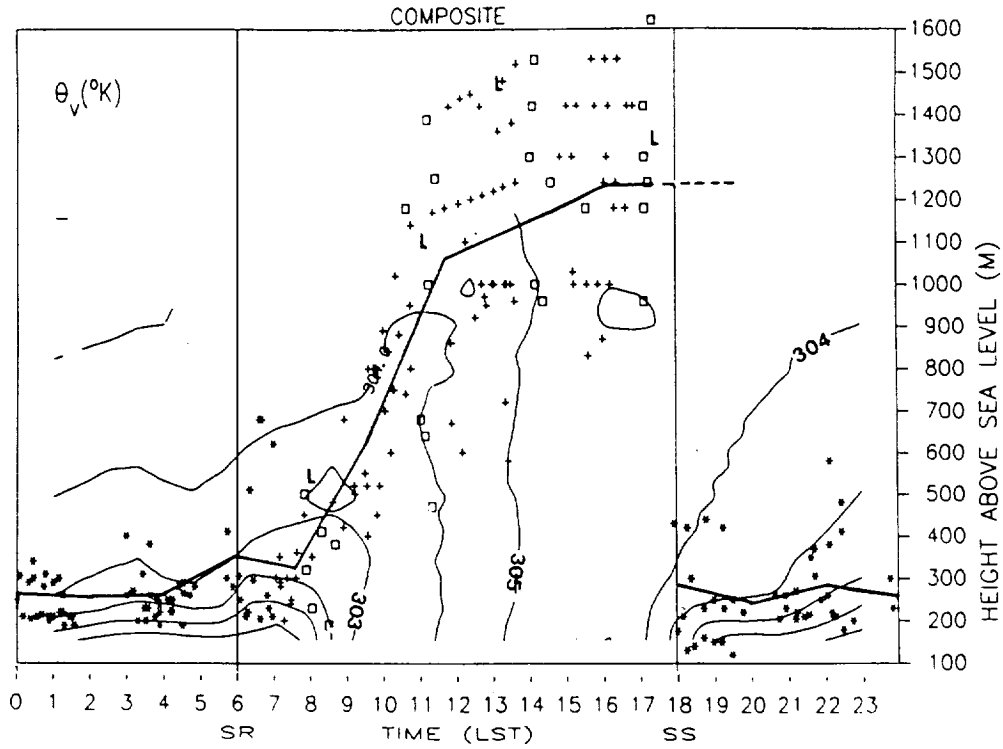

Fig. 4. *A composite of 7 fair days in the CAB showing the mean mixed layer height (solid line) and individual daytime mixed layer heights (crosses and squares). The nocturnal mixed layer heights are marked with an asterisk. Contours are virtual potential temperature v in °K.*

Mixed layer growth rates as predicted by models (Tennekes, 1973; Betts, 1973; Lilly, 1968; Fitzjarrald, 1982) show a good agreement in the early hours of growth after which model produced mixed layer heights are too large. Adjustment to the excessive model heights can be achieved by calling upon convective cloud induced subsidence in the order of 2 to 3 cm s^{-1}. Thus, cloud transports which take over from the mixed layer transports are both upward and downward.

CLOUD LAYER

Cloud transports are calculated using observations of clouds captured within an observational triangle (Figure 5). Rawinsonde measurements were made at the corners of a triangle 50 km on a side. Convergence into the triangle was calculated and vertical motions in the cloud cells deduced from the fraction of active cloud (10% of total area) present. It was assumed that the calculated upward motion in the triangle in the presence of clouds occurred within the cloud cores. Vertical motions of up to 5 m s^{-1} were obtained in the clouds.

The observations of cloud transports were then used to help verify cloud model calculations of transports. A two-dimensional moist cloud model was used (Garstang *et al.*, 1988; Scala *et al.*, 1990). Figure 6 shows the cloud model results. Figure 6 (a) shows a single cell cloud which was found to develop in the very moist environment of

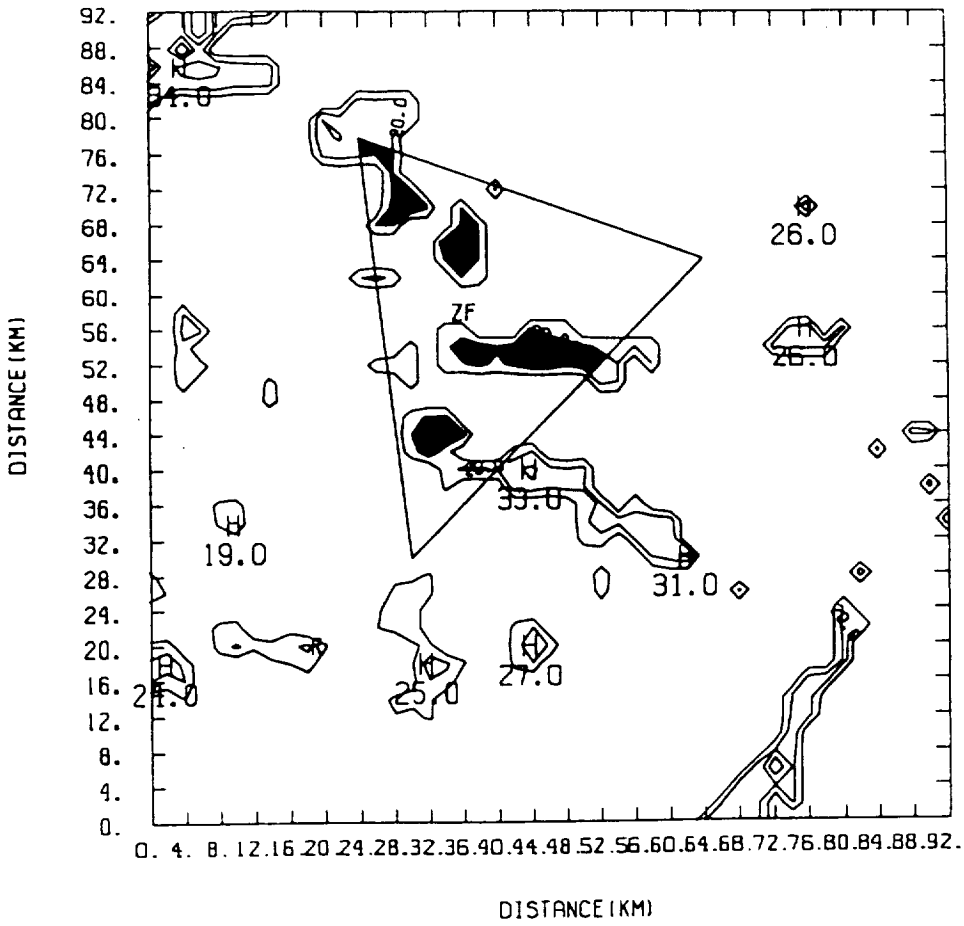

Fig. 5. *Observational triangle 50 km on a side in the central Amazon basin with vertical soundings of wind, temperature and humidity on the corners and radar coverage. Radar echoes are shown with the cores of the echoes shaded.*

the wet season. Figure 6 (b) shows a multicell cloud which occurred in the dry season and intermittently in the wet season. Significantly different vertical transport is achieved by the single and multiple cell clouds. Backward trajectories from 12 km elevation in the single cell cloud (Figure 7 (a)) show that 73% of the air reaching 12 km originates above 6 km. Only 15% of the air reaching 12 km originates in the mixed layer. The single cell wet clouds do not effectively couple the deeper atmosphere to the surface and mixed layers. These clouds, however, are very effective mixers of the middle and upper troposphere.

The multicell cloud occurring in drier conditions (Figure 7 (b)) however, forms a very different link between the surface and deeper atmosphere. Ninety-two percent of the air reaching 12 km originates below 4 km, 60% below 2 km in the multicell cloud.

Dogma which has persisted for 30 years since the first formulation of the "hot tower" concept (Riehl and Malkus, 1958) has held that all deep vertical transport in the equatorial trough region is performed by the multicell clouds. We believe from our findings that the single cell clouds which predominate in wet season conditions create a condition that permits mean circulations such as the Hadley and Walker, to perform deep vertical transport.

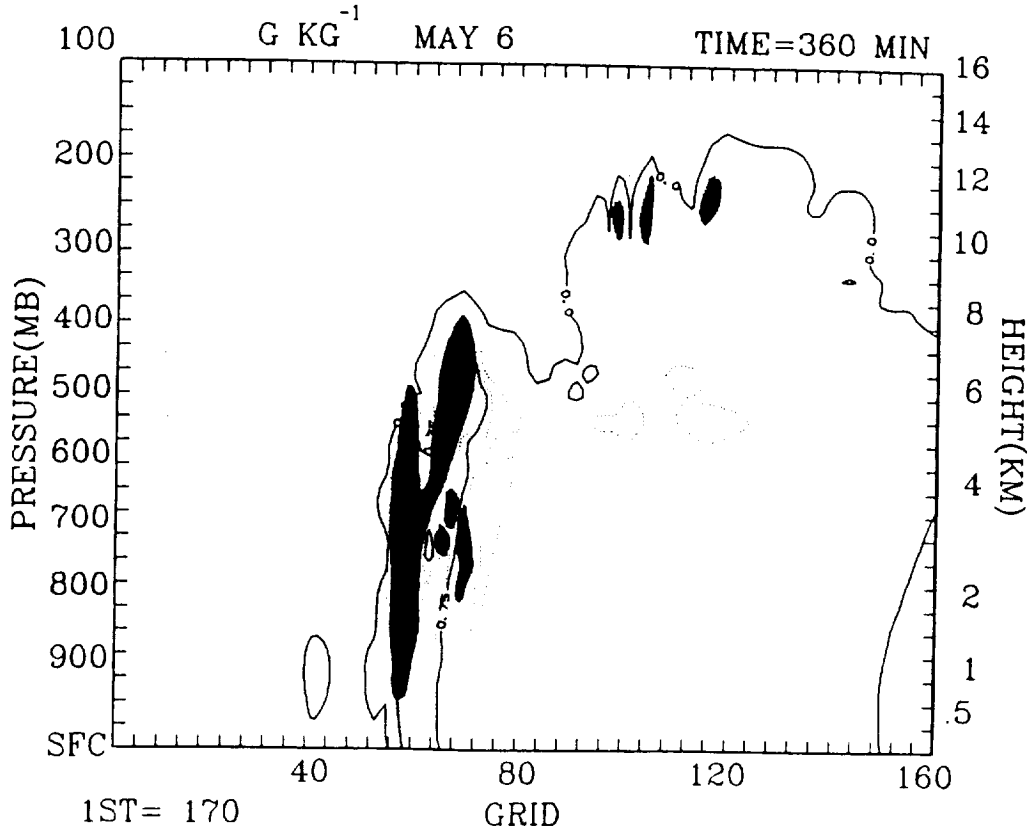

Fig. 6a. *Model generated single cell cloud showing the boundary of the cloud in terms of zero specific humidity (g/kg). Areas of upward and downward motion are shown by light and dark stippling respectively. Model grid units (abscissa) equal .05 km.*

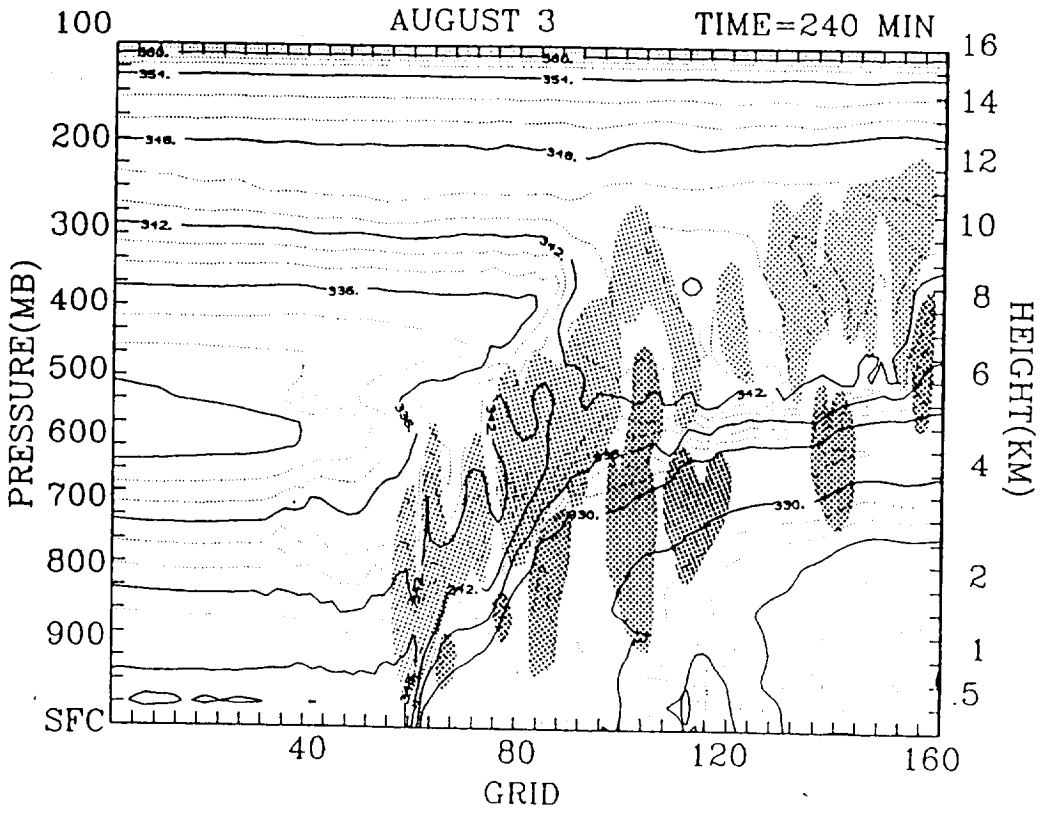

Fig. 6b. *As for Fig. 6a except for a multicell cloud with potential temperature (oK) instead of specific humidity.*

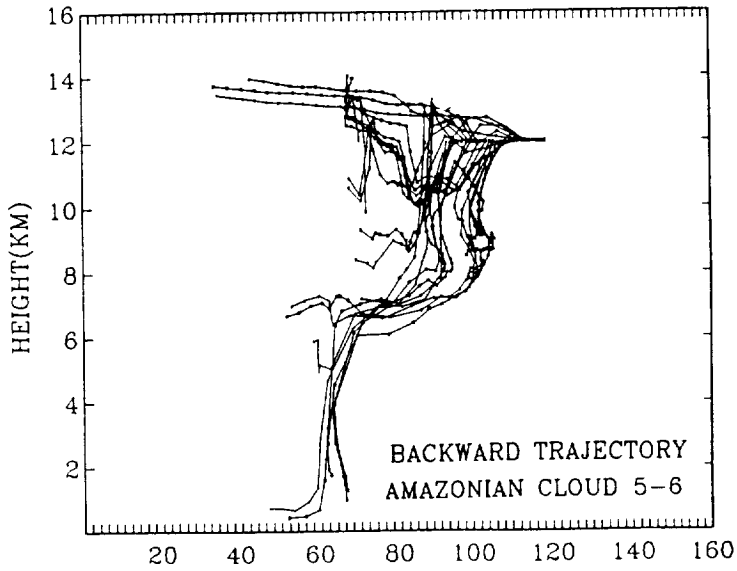

Fig. 7a. *Model generated backward trajectories from 12 km for the single cell cloud.*

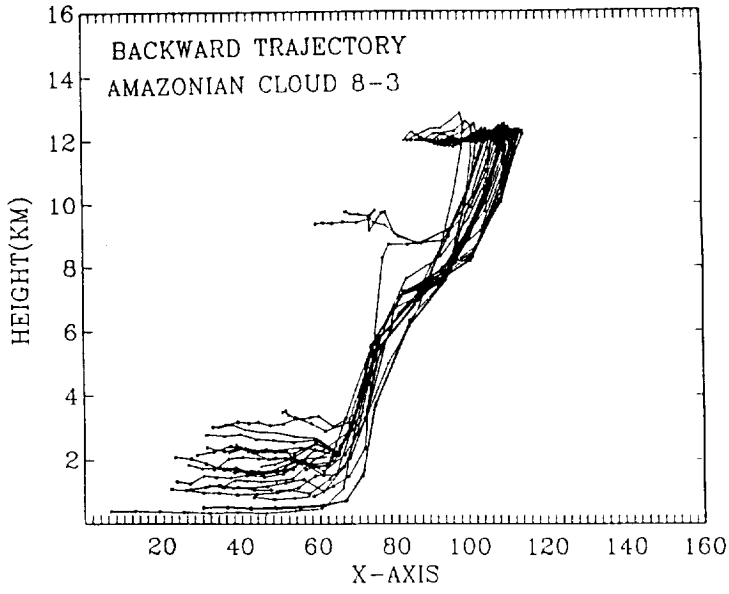

Fig. 7b. *Model generated backward trajectories from 12 km for the multicell cloud.*

Thus, over the rain forest at least two mechanisms exist for deep vertical transport:

* multicell clouds occurring in drier unstable atmospheres, and
* single cell clouds occurring in wetter more stable atmospheres.

When the latter exists, mean circulations can transport surface species through the depth of the troposphere.

HORIZONTAL TRANSPORTS

The physical processes described above have concentrated on vertical transports in the atmosphere over the rain forest. Our results suggest that at least one long range horizontal transport phenomenon is of importance. Figure 2 showed pulses of soil dust coinciding with the major rain events in the Amazon basin. The occurrence of high dust concentrations under the rainiest conditions would appear to be a paradox in the sense that rain cleanses the atmosphere of aerosols. We explain this paradox by showing that the large rain systems of the Amazon basin draw dust into the basin from dust plumes that have originated in the Sahara-Sahel and spread across the Atlantic (Swap *et al.*, 1991).

Synoptic scale (~ 1000 km) convergence between the surface and 4 km is needed to draw the dust into the basin. Calculations show that some 460,000 tons of Saharan dust are injected into the basin by a single synoptic scale storm system. Storm and dust climatology suggest that more than 12 Mtons of Saharan dust are introduced to the basin each year. In the northeastern basin this may amount to as much as 180 kg/ha/yr. The amount of trace elements, such as phosphate, supplied in this dust range from a few kg/ha/yr to less than a kg/ha/yr. The delicate energy balance existing in the rain forests which have developed on nutrient poor soils suggests that the critical trace elements supplied by Sahara dust may be a limiting factor in the survival of the rain forest. Dependence of one ecosystem upon an ecosystem on another continent separated by an ocean and linked by the atmosphere is a real possibility.

CONCLUSIONS

The rain forests inject significant amounts of trace gases into the atmosphere. These gases are detected through much of the troposphere and over the region of the rain forest. Major regional enhancements of certain gases are noted as a product of biomass burning.

Local, regional and large scale circulations suggest that the rain forests are coupled to the global atmosphere. The only clear linkage that has been documented by our research is an effect that has originated outside of the rain forest and impinged upon the forest. We are yet to document effects of the rain forest upon the global atmosphere. We believe that we are in a better position now than before undertaking field measurements to speculate upon the potential effect of changes in the rain forest upon the global atmosphere. Further research is necessary before we can move from speculation to well-founded conclusions about the links and consequences between the rain forest and global system.

ACKNOWLEDGEMENTS

The research reported on in this paper has been conducted with the support of the Tropospheric Chemistry Program of the National Aeronautics and Space Administration and is based upon the Amazon Boundary Layer Experiments (ABLE) conducted by NASA and the Brazilian Space Agency (INPE). Results of the ABLE II(a) and II(b) have been reported on in special issues of the *Journal of Geophysical Research*. Many scientists and technicians are involved in such research. Their contributions are recognized and acknowledged.

REFERENCES

Betts, A.K. (1973): Non-precipitating cumulus convection and its parameterization. *Quarterly Journal of the Royal Meteorological Society*, 99: 178-196.

Fitzjarrald, D. (1982): New applications of a simple mixed layer model. *Boundary-Layer Meteorology*, 22: 431-453.

Garstang, M., J. Scala, S. Greco, R. Harriss, S. Beck, E. Browell, G. Sachse, G. Gregory, G. Hill, J. Simpson, W.-K. Tao and A. Torres (1988): Trace gas exchanges and convective transports over the Amazonian rain forest. *Journal of Geophysical Research*, 93: 1528-1550.

Harriss, R.C., S.C. Wofsy, M. Garstang, E.V. Browell, L.C.B. Molion, R.J. McNeal, J.M. Hoell, Jr., R.J. Bendura, S.M. Beck, R.L. Navarro, J.T. Riley and R.L. Snell (1988): The Amazon Boundary Layer Experiment (ABLE 2A): Dry season 1985. *Journal of Geophysical Research*, 93: 1351-1360.

Journal of Geophysical Research, ABLE 2B: Amazon Boundary Layer Experiment 2B, 95: No. D10, 16721-17050.

Lilly, D.K. (1968): Models of cloud-topped mixed layers under a strong inversion. *Quarterly Journal of the Royal Meteorological Society*, 94, 292-309.

Logan, J.A., M.J. Prather, S.C. Wofsy and M.B. McElroy (1981): Tropospheric chemistry: a global perspective. *Journal of Geophysical Research*, 86: 7210-7254.

Riehl, H. and J.S. Malkus (1958): On the heat balance in the equatorial trough. *Geophysica*, 6: 503-538.

Salati, E. (1987): 'The forest and the hydrological cycle', In *The Geophysiology of Amazonia: Vegetation and Climate Interactions*, R. Dickerson (ed.), pp. 273-296, John Wiley and Sons, New York.

Scala, J., M. Garstang, W.-K. Tao, K. Pickering, A. Thompson, J. Simpson, V.W.J.H. Kirchhoff, E. Browell, G. Sachse, A. Torres, G. Gregory, R.A. Rasmussen and M.A.K. Khalil, (1990): Cloud draft structure and trace gas transport. *Journal of Geophysical Research*, 95: 17015-17030.

Setzer, A.W. and M.C. Pereira (1986): Detection of large biomass burning in the Amazon with satellite images. *EOS Transactions, AGU*, 67: 247.

Swap, R., M. Garstang, S. Greco and P. Kållberg (1991): Long-range transport of Saharan dust into the Central Amazon Basin over 10-14 days. *Proceedings AMS 71st Annual Meeting, 7th Joint Conference on Applications of Air Pollution Meteorology*, January, New Orleans, LA, pp 20-23.

Talbot, R.W., M.O. Andreae, H. Beresheim, P. Artaxo, M. Garstang, R.C. Harriss, K.M. Beecher and S.M. Li (1990): Aerosol chemistry during the wet season in Central Amazonia: The influence of long-range transport. *Journal of Geophysical Research*, 95: 16955-16969.

Tennekes, H. (1973): A model for the dynamics of the inversion above a convective boundary layer. *Journal of Atmospheric Science*, 30: 558-567.

Watson, C.E., J. Fishman and H.G. Reichle, Jr. (1990): Significance of biomass burning as a source of CO and ozone in the southern hemisphere tropics: Satellite analysis. *Journal of Geophysical Research*, 95: 16443-16450.

AMAZON COASTAL SQUALL LINES: PART I: STRUCTURE AND KINEMATICS

Michael Garstang, Harold L. Massie, Jr.[1], Jeffrey Halverson, Steven Greco and John Scala[2]

Department of Environmental Sciences
University of Virginia
Charlottesville, VA 22903

---

[1]Air Weather Service Headquarters, Scott Air Force Base, IL 62225.

[2]Severe Storms Branch, NASA/Goddard Space Flight Center, Greenbelt, MD 20771.

Abstract

Meso- to synoptic-scale lines which form along the northern coast of South America as seabreeze-induced instability lines and propagate through the Amazon Basin are investigated using data collected during the April-May 1987 Amazon Boundary Layer Experiment (ABLE 2B).

These systems, termed "Amazon Coastal Squall Lines" (ACSL), have been noted by others, but details of the structure and evolution of the ACSL are limited. The present paper uses analyses of GOES satellite, upper air rawinsonde and surface Portable Automated Mesonet (PAM) data to describe the structure, dynamics and life-cycle evolution of the ACSL. Twelve ACSL were sampled during ABLE 2B and three examples are discussed in detail.

The ACSL are discontinuous lines of organized mesoscale cloud clusters which propagate across the Central Amazon Basin at speeds of 50-60 km h^{-1}. The ACSL undergo six possible life cycle stages: coastal genesis, intensification, maturity, weakening, reintensification and dissipation. Analysis also indicates that the ACSL are composed of three distinct components: pre-storm cumulus (PSC), leading edge convection (LEC) and multiple precipitating cloud layers in the trailing stratiform region (TSR).

Divergence and vertical velocity calculations indicate deep vertical ascent in the LEC and a region of mid-level convergence ($\approx$ 500 mb) in the TSR. The latter is associated with a weak updraft above and an unsaturated downdraft below. The TSR

vertical motions are an order of magnitude smaller than in the LEC.

Substantial shear in the low-level inflow occurred in all 3 case studies and, as suggested by model simulations, may play an important role in the longevity (24-48 h) of the ACSL. Pre- and post-ACSL profiles of Θ_e demonstrate that the ACSL stabilize the troposphere in their wake and erode a pre-storm minimum Θ_e. It is hypothesized that the removal of this minimum is accomplished not only by direct mixing via vertical motions in the LEC ("hot towers"), but also through detrainment in the multiple-layered TSR. Part I describes the structure and kinematics of the Amazon Coastal Squall Lines (ACSL) while Part II deals with the heat and moisture transports of these systems.

1. Introduction

Among the most important rain producers in the rain forests of the Central Amazon Basin (CAB) of Brazil are meso- to synoptic-scale squall lines of coastal origin. These systems, which we will term the Amazon Coastal Squall Lines (ACSL), form along the northeastern coast of South America as a result of sea breeze-induced convection. The ACSL often propagate away from the coast, reaching as far inland as Manaus in the CAB and, in some instances, reaching the Andes 48 h after genesis (Kousky, 1980; Molion, 1987).

Both Kousky (1980) and Molion (1987) have presented sequences of satellite images which illustrate the coastal genesis and inland propagation of a squall line in the Amazon basin. Molion (1987) found that these lines of instability, or squall lines, may be over 1000 km long and propagate across the Amazon basin with average speeds of 10° longitude per day or 45-55 km h^{-1}. Kousky and Molion (1981) and Molion (1987) have suggested that the diurnal cycle and propagation characteristics associated with these squall lines may explain the relatively smaller precipitation values in the lower Amazon and the precipitation maximum in the central and western Amazon.

More recently, Greco et al. (1990) used data collected during the wet season Amazon Boundary Layer Experiment (ABLE 2B) in April-May 1987 to investigate the ACSL, termed Coastal Occurring Systems (COS) in their work. Greco et al. (1990) found that these COS are generally 1000-2000 km long, but may attain a

length of 3500 km. In addition, they estimated that the COS propagated across the Basin at speeds of 50-60 km h^{-1}, and were observed to last 24-48 h. Similar results were reported by Cohen et al. (1989) in a study of "propagating squall lines" which utilized hourly satellite imagery data between 1979 and 1986. An important finding of Greco et al. (1990) was that 12 COS occurred during the ABLE 2B experiment (1 April-15 May 1987) and were responsible for 40% of the total measured rainfall. Cohen et al. (1989) found that these types of squall lines are most common in the CAB between April and August.

The studies cited above provide only a qualitative description of the ACSL. Detailed investigations of the structure, flow field and energetics of the ACSL have been very limited (Scala et al., 1990) due mainly to the lack of data collected in the relatively harsh environment of the Amazon rain forest. The main goal of this paper is to use data collected from satellites and a mesoscale network of surface and upper air stations employed in the CAB during ABLE 2B to investigate the structure and kinematics of the ACSL on the meso- and convective scales. An additional goal is the comparison of the ACSL with other tropical and non-tropical squall lines. Although satellite imagery and preliminary analyses suggest similarities with the West African (Chalon et al., 1988; Chong et al., 1987), tropical Atlantic (Barnes and Sieckman, 1984), Venezuelan (Betts et al., 1976), and even the United States mid-latitude (Ogura and Liou, 1980) squall lines, a more quantitative assessment is needed and

will be presented in this work.

This paper, which is the first of a two part study on the ACSL, will document the life cycle and cloud components (section 3), and both the thermodynamic and kinematic structure (section 4) of the ACSL as they propagate through the CAB. Important similarities and differences between the structure of the ACSL and other tropical and non-tropical squall lines will be discussed in Sections 4 and 5. Section 5 will also detail the important effects of the ACSL on the larger scale environments of the CAB. Part II of this study will deal with the heat transports associated with the ACSL in the Amazon Basin. In particular, the focus will be upon the contributions of the ACSL heat transports to the total heat export from the tropics, and the relative importance of the heat transport produced by the stratiform regions of the ACSL.

2. Data

The National Aeronautics and Space Administration (NASA), in cooperation with the Brazilian Instituto Nacional de Pesquisas Espaciases (INPE) and Instituto Nacional de Pesquisas da Amazonia (INPA), conducted the wet season Amazon Boundary Layer Experiment (ABLE 2B) during 1 April-15 May 1987. A detailed description of the ABLE 2B can be found in Harriss et al. (1990) and Garstang et al. (1990). ABLE 2B, as part of NASA's Global Tropospheric Experiment (GTE), was primarily an atmospheric chemistry experiment. However, ABLE 2B also included an extensive meteorological component which enabled the study of atmospheric

motions ranging from the turbulent to the planetary scale.

The ABLE 2B meteorological networks provided the focus for meso- through synoptic-scale sampling which was necessary for the study of convective systems over the vast, relatively inaccessible Amazon rain forests. The measurement systems operated during ABLE 2B included both ground and space-based platforms.

Rawinsondes were released nearly simultaneously every 3 h at the three corner stations of a 1000 km^2 mesoscale triangle network located in the CAB (Fig. 1). Procedures for reducing and adjusting these data are described below. After data reduction, the soundings provided horizontal wind velocity, temperature, and mixing ratio from the surface to 100 mb.

Portable Automated Mesonet (PAM) stations, the Geostationary Observational Environmental Satellite (GOES) platform and a 3-cm radar acquisition system continuously monitored the atmosphere in the network triangle and the CAB. These measurements provided the data used to define and partition the ACSL systems into distinct cloud components. Four single level PAM stations (Fig. 1), located 5 m above the rain forest canopy on 40 m towers, measured horizontal wind velocity, temperature, humidity, pressure and precipitation within the mesoscale network. The PAM measurements, obtained at a frequency of 1 Hz and stored as 1 min averages, were transmitted via satellite to the National Center for Atmospheric Research (NCAR) for processing and storage.

The GOES data consisted of visible and infrared (IR) images obtained via a Digital Weather Image Processing System (DWIPS) operated at the ABLE 2B operations center at Eduardo Gomes Airport (EGA) in Manaus, Brazil. The GOES images were used to analyze cloud conditions over the mesoscale triangle and to document the movement of synoptic disturbances. An ACSL life-cycle taxonomy is derived from images obtained over the entire experiment.

A 3 cm radar located at EGA provided Constant Altitude Planned Position Indicator (CAPPI) scans of the mesoscale triangle at 5 min intervals. Signal attenuation severely degraded the CAPPI data during heavy precipitation, thereby limiting the radar's usefulness for making accurate estimates of rainfall rates.

The mesoscale rawinsonde data used in this study were checked against climatology and rawinsonde profiles measured coincidently by a 6-station basin-scale network (Fig. 1) which was also part of the ABLE 2B experiment. This comparison revealed pronounced pressure offset problems in the mesoscale triangle sounding which were ultimately traced to bad instrument calibrations by the rawinsonde manufacturer.

A least squares procedure based on the mean basin scale temperature profile was used to develop a procedure for adjusting and editing the mesoscale soundings. After the pressure offset was determined, temperatures were reassigned to adjusted pressure levels. Geopotential, mixing ratio, and wind velocity were then

recalculated at 25 mb intervals from the surface to 100 mb. The wind calculations employed a smoothed azimuth, elevation, and balloon ascent rate derived from a three-point moving average (Davis, 1986) to reduce noise introduced by antenna errors.

Some soundings launched during thunderstorms reflected data losses due to icing problems. Usually these soundings terminated near the freezing level. These weather-related problems prevented budget calculations for several strong ACSL which passed through the mesoscale network. The cases selected for study either had no problems or contained data deficiencies which were easily handled by the above procedures.

Divergence for the mesoscale triangle was computed from the line integral of the wind components normal to each leg (Gamache and Houze, 1982). Divergence was calculated from 1000 to 100 mb in 25 mb intervals. The vertical velocity at each pressure level was determined first from the vertically integrated divergence, and then adjusted by O'Brien's (1970) method which forces the vertical velocity to zero at the surface and at the highest level (100 mb).

This procedure gives results that compare well with physically realistic estimates of vertical motion from adiabatic and isentropic methods (Haltiner and Martin, 1957). O'Brien's method assumes vertical velocity errors result from linear divergence errors which increase uniformly from a surface minimum to a maximum at the highest level reached by the sonde. Gamache and Houze (1982) obtained acceptable results by applying these

procedures to tropical squall lines.

3. Results

a. Definition of the ACSL Life Cycle

Analysis of both GOES imagery and PAM surface data have shown that 12 ACSL were detected in the CAB during the ABLE 2B wet season (Greco et al., 1990). These large and generally linear meso- to synoptic scale systems form along the northern coast of South America in mid-afternoon and move across the Amazon Basin, usually from NE to SW, at an average speed of 50-60 km h^{-1}. The ACSL often last between 24 and 48 h, reaching the ABLE 2B experiment region in the central Amazon Basin 20-24 h after formation along the coast. Figure 2, taken from Greco et al. (1990), shows the composite hourly cloud cover percentages from the GOES-W brightness temperatures less than -33°C for the 12 ACSL days. The development of the squall or cloud line along the coast by 2200 UTC (1800 LST) is clearly shown. The existence, at the same time, of another cloud line in the CAB should be noted. This is the previous day's ACSL. The propagation of the cloud line or ACSL from near the coast at 2000 UTC to the CAB 18 h later (1600 UTC) is graphically shown.

At maturation, ACSL are usually 1000-2000 km long and 100-300 km wide, but can reach a total length of over 3000 km and are often a dominant synoptic scale cloud feature over the third of the tropics appearing on GOES full-disk images (Molion, 1987). This is illustrated by Fig. 3 which shows the ACSL of 26 April 1987 as it approaches the mesoscale network. This ACSL was

approximately 3500 km long at the time of strongest intensity, although only 1000 km may have contained active convection. The ACSL is not a continuous line of single cells, but rather a highly discontinuous arc or line of discrete clusters of cells. Although organized on the mesoscale, the clusters vary in their dimensions within the line. Each mesoscale cluster is composed of deep cumulonimbus along the leading edge with a shield of anvil cloud that surrounds the convective cells and extends far to the rear.

Greco et al. (1990) showed that these massive, long-lived convective systems accounted for at least 40% of the total rainfall in the mesoscale network during ABLE 2B. Their importance to the water budget of the Amazon Basin makes it necessary to undertake a detailed study of their life cycle and the evolution of the flow field and kinematic structure.

The GOES visible and IR images collected during ABLE 2B indicate that patterns, sizes, intensities of clouds and rainfall can change dramatically during the lifetime of a ACSL. The GOES images from April and May 1987 have been studied to define a ACSL life cycle of six possible stages. These stages are:

1) COASTAL GENESIS

During coastal genesis, the first thunderstorm cells form during the afternoon in the seabreeze convergence zone along the northern coast of South America. The number and size of the cells increases with time, followed by selective merging into thunderstorm clusters with shared anvils.

2) INTENSIFICATION

During late afternoon and evening, merging continues as small clusters of thunderstorms merge to form larger clusters, generally oriented from northwest to southeast in a quasi-linear pattern parallel to the coastline of NE Brazil. Figure 4a illustrates the intensification of clustering of the sea breeze forced convection on the evening of 25 April 1987. The strongest clusters containing intensifying convective elements and anvils are resolved by segment number 7 (black) on GOES images using the Mb enhancement technique (Carlson, 1981). The strong clusters have sharp boundaries and cloud-top temperatures colder than -59.2°C, indicating a height of approximately 13-14 km.

3) MATURATION

During this stage, the entire system achieves maximum length and width and propagates at average speeds of 45-55 km h^{-1}. Individual clusters also reach their largest size and strongest intensity, as seen on the enhanced IR images. A mature ACSL may cover a total length of 2000-3000 km with 30-40% of the leading edge consisting of active deep convection. The width of a mature ACSL is typically 200-300 km. Patches of white (Mb segment 9) in the mesoscale clusters indicate cumulonimbi with cloud top temperatures less than -80.2°C and heights of 16-17 km. The merging clouds between individual clusters give the ACSL distinctive synoptic scale features on the GOES full disk images. This is illustrated in Fig. 4b, which shows an ACSL that formed on 25 April and had already reached maturity over the CAB by

early afternoon of 26 April. The formation of a possible new ACSL is also evident along the coast at this time.

4) WEAKENING

The clusters diminish in size and their outer definition becomes ragged on the Mb enhanced images. Areas previously shown in black on the Mb images change to dark and light gray (segment numbers 6 and 5, respectively), indicating warmer cloud-top temperatures and weaker thunderstorms. The width of the ACSL decreases to 100-200 km.

5) REGENERATION

During the following afternoon, ACSL regeneration resulting from increased daytime surface heating, may follow weakening which occurred at night. During regeneration, an enlargement of the black areas (segment 7) with a sharp outer definition on the Mb images indicates thunderstorm clusters that are growing and intensifying. The system's synoptic-scale features become better defined on the full disk IR images. Figure 4c shows the ACSL of 25-26 April as it regenerates in the western Amazon Basin at 0300 UTC 27 April.

6) DISSIPATION

After a period of weakening, the individual clusters become more ragged and ultimately disappear. The system loses its synoptic scale definition as shown on the full disk images.

The above definition of the ACSL life cycle is similar to taxonomies developed for tropical squall line-type mesoscale convective systems (e.g., Houze, 1977; Frank, 1978; Leary and

Houze, 1979). This present taxonomy, however, defines the life cycle of a meso- to synoptic-scale convective disturbance. Utilizing this life cycle taxonomy, we have classified three ACSL as they passed through the mesoscale network; the ACSL on 26 April 1987 was classified as weakening, the one on 1 May 1987 as mature, and the one on 6 May 1987 as a regenerating system.

b. ACSL Cloud and Rainfall Components

The ACSL have a convective and stratiform structure similar to the design of Gamache and Houze (1982) and satisfy Zipser's (1977) criteria for a tropical squall system. Figure 5, taken from Garstang et al. (1990), shows a schematic representation of a typical mature ACSL. The three primary cloud components comprising ACSL are: pre-storm cumulus (PSC) ahead of the squall front, leading edge convection (LEC), and widespread layers of anvil clouds in the trailing stratiform region (TSR).

The three cloud components of each ACSL were discerned through subjective analysis of both half-hourly GOES images with a 2 km resolution and 5 min CAPPI radar scans also with a 2 km resolution. Most importantly, however, was an analysis of the high frequency PAM data which was used to delineate the three ACSL components. The 1 min averaged values of T, q, Θ_e and wind speed clearly identified the passing of the squall front. Rainfall rates measured by the tipping bucket raingauge mounted on the PAM platform were employed to determine the transition from deep convection stage to anvil stage using .25 mm min^{-1} as a cutoff from convective to stratiform rain. The .25 mm min^{-1}

cutoff was necessitated by the .25 mm resolution of the tipping bucket raingauge.

Figure 6 shows the time series of PAM observations recorded at Embrapa on 26 April 1987. The arrival of the gust front is clearly noted between 1630 and 1700 UTC. The marked response of selected surface variables (as measured by the PAM network) to the passage of the gust front at Ducke, Embrapa, Carapaña and ZF-1 on 26 April 1987 and 6 May 1987 are summarized in Table 1. Results for 1 May 1987 are not shown because lightning disrupted the PAM network during ACSL passage. There are large differences among the four PAM stations in rainfall rate and changes of T, q, P and Θ_e with the gust front passage, especially on 6 May 1987. These differences reflect the spatially discontinuous nature of the ACSL.

4. Squall Line Kinematics and Dynamics

In this section, analysis of the mesoscale network PAM and rawinsonde data is used to reveal the cross-sectional (normal to direction of storm propagation) structure and characteristics of the 1 May 1987 ACSL. We have chosen to emphasize details of the 1 May case because it was the only one of the three for which rawinsonde coverage existed for both the LEC and TSR components. Observations taken from the mesoscale triangle, however, did capture the TSR components of the 26 April and 6 May systems, and we compare the general kinematic structure of this region for the three squall systems. Model simulations of the 6 May and 26 April squall lines have been presented by Scala et al. (1990,

1991).

The 1 May ACSL formed during the mid-afternoon of 30 April 1987 as a line of numerous small convective clusters located along the northeast coast of Brazil. By late afternoon, the clusters had grown rapidly and merged to form a synoptic arc-shaped ACSL. By early evening, the arc acquired a more linear appearance as it propagated toward the southwest at 33 km h^{-1} (Fig. 7). A group of smaller mesoscale clusters formed 250 km ahead of the ACSL leading edge. These clusters produced heavy rain in the northern part of the mesoscale triangle six hours prior to the arrival of the ACSL at 1200 UTC, 1 May.

Mass divergence was calculated over the mesoscale network volume using the near-simultaneous rawinsonde launches at the triangle vertices (Ducke, Embrapa, Carapaña) and by employing a simple line integral method. Vertical profiles of the divergence values calculated for the LEC (1200 UTC) and TSR (1800 UTC) components of the 1 May ACSL are shown in Fig. 8. The LEC profile is characterized by a pronounced vertical couplet of convergence (-1.6×10^{-4} s^{-1}) between 600-700 mb and divergence (1.8×10^{-4} s^{-1}) located between 300-500 mb within the deep convective region. Vertical profiles of vertical p-velocity for the LEC and TSR components are presented in Fig. 9. The divergence couplet is associated with deep upward motion in the LEC with a peak of 40 μbs^{-1} near 550 mb. Figure 10 shows the pre-storm (1200 UTC) and post-storm (1800 UTC) composite vertical profiles of temperature and dewpoint for the triangle. Note that

the deep convective ascent coincides with saturated conditions to a level of 500 mb. It is likely that the 1200 UTC sounding ascended through and directly sampled a portion of the deep convective towers of the squall disturbance.

Six hours following the storm passage, the divergence profile of the TSR is relatively weak throughout the depth of the troposphere and includes a divergent layer that extends from 800 mb to the surface. Peak downward motion is indicated at 800 mb in the TSR, accompanied by progressive warming and drying of the layer (see Figs. 9 and 10). Higher in the atmosphere, weak ascent (5-10 μbs^{-1}) is found between 600 mb and the tropopause. The peak in the upward motion coincides with the upper portion of a mid-level saturated (cloud) layer seen at 1800 UTC in the thermodynamic profiles. While the 1800 UTC sounding indicated that the boundary layer was recovering from the convective disturbance (note the surface layer warming and moistening between 1200 and 1800 UTC), the formation of a warm, dry subsidence-induced inversion in the low levels combined with a distinct region of warming above 500 mb was sufficient to suppress deep convective activity in the wake of the squall line.

The vertical p-velocity values are consistent with the findings of Gamache and Houze (1982) who have shown that upward vertical motion is an order of magnitude larger in the convective region than in the stratiform region. The updraft structure comprised of a concentrated core of rising motion in the leading convective elements and weaker ascent in the trailing stratiform

cloud region is a feature that characterizes many mesoscale convective systems in the tropics, including systems observed during COPT81 (Chalon et al., 1988), AMEX (Frank and McBride, 1989), GATE (Gamache and Houze, 1982), WMONEX (Johnson and Priegnitz, 1981); and in the midlatitudes (Gallus and Johnson, 1991).

Figure 11 presents a comparison of vertical p-velocity calculations for each of the three TSR components on 26 April, 1 May and 6 May. In general, weak ascent occupies the upper portion of the troposphere (above 500 mb) in each of the three TSR components, with descending motion in the lower layers. The weakest motions are those associated with the 6 May regenerating case. It should be noted that the upward motion in the weakening 26 April system occupies nearly the entire tropopause (except for a shallow subsidence layer below 850 mb), and the magnitude of the motions in this deep layer are nearly the same as that for the mature system. These findings may suggest that ascent in the trailing anvil plays a more dominant role in the late stages of the ACSL life cycle. However, since our analysis compares the life cycle stages of individual systems on different days, the observed differences in velocity structure might also reflect variability in the large scale tropospheric conditions which influence the intensity and organization of the squall line circulations.

The pre-storm line-normal component of the relative flow for each of the three ACSL was also calculated. These calculations

utilize a storm coordinate system defined by an x′ axis oriented orthogonal to the orientation of the leading edge of each squall line (Fig. 12). The angle alpha between the storm coordinate x′ axis and the x axis in the standard meteorological reference frame is used to derive a u-wind component normal to the squall orientation (u′-wind component). The u′ wind component was taken from pre-storm triangle composite profiles of wind speed. These profiles are shown in Fig. 13. The storm forward speed was then subtracted from this u′-wind component to obtain the line-normal relative flow. For the three cases of 26 April, 1 May and 6 May we have defined alpha as 50°, 60° and 45°, and used storm speeds of 6 m s^{-1}, 9 m s^{-1} and 10 m s^{-1}, respectively.

The pre-storm relative flow profiles for all three cases are presented in Fig. 14. All three cases show a pronounced shear in the lowest levels. This rear to front low level inflow is mainly a result of the easterly jet that characterizes the lower wet season troposphere over the Central Amazon Basin (located at 2.5 km in Fig. 13). A similar low-level jet structure, the African easterly jet, is associated with West African squall lines investigated during COPT 81 (Chong et al., 1987). The observed relative flow profiles from COPT 81 are very similar to those identified for Amazon systems.

The low-level shear associated with the three ACSL also suggests a mechanism for their observed longevity. Rotunno et al. (1988) have demonstrated that the vigorous, sustained lifting along the squall leading edge is maintained by a balance between

counter-rotating circulations generated by the shear in the outflow cold pools and the opposing low-level relative inflow. Thorpe et al. (1982) have proposed that strong low-level shear relative to the storm prevents the outflow boundary from propagating away from the storm leading edge and thus cutting off the storm's available supply of moist boundary layer air. The 2-D version of the Goddard Cumulus Ensemble (GCE) model (Tao et al., 1991) has been used to simulate the Amazon systems (Scala et al., 1990, 1991).

The results of efforts to simulate the 26 April and 6 May convective events also indicated the potential for convective demise when the updraft and downdraft interface sloped too far upshear. This action initiated a propagating outflow boundary that terminated the influx of high Θ_e air to the developing cells. A convective balance between the low-level shear and storm-induced outflows is likely required for the long-lived storms observed over the Amazon basin.

The distinct minimum in relative flow seen at 2.5 km for the three Amazon systems is a direct consequence of the easterly jet and, in at least two cases (26 April and 6 May), indicates the presence of weak inflow into the rear of the convective region. This inflow can provide a source of momentum and potentially low Θ_e air for convective-scale downdrafts. Low Θ_e air also enters the front of the three squall cases at mid-levels between 4 and 8 km. The trajectory of this air within the storm system is uncertain, although model results (Scala et al., 1990, 1991,

1992) suggest parcels can be entrained in the updraft cores or pass through them to the rear where they may be incorporated in convective scale downdrafts. Houze (1977) suggests that this type of inflow may in fact pass around updraft cores and contribute to the production of convective downdrafts on the trailing sides of the system. The mid-level inflow may also transport hydrometeors that are generated in the convective towers into the trailing portions of the system. These horizontal transports have been found to account for a substantial portion of the condensate that comprises the trailing stratiform clouds of squall lines (Tao et al., 1991; Chong and Hauser, 1989).

Differences in the strength of the mid-level inflow between the three Amazon systems may be a consequence of the variation in the larger-scale tropospheric flow regime, either as variations of the day-to-day flow, or from a modification of the basic state flow produced by passage of a large squall line during the previous day.

The relative flow profiles also demonstrate somewhat different characteristics in the uppermost levels. Studies with the two-dimensional cloud model (Scala et al., 1991, 1992) show that modification of updraft cores by the environmental wind field produces one of two types of anvil circulation; either an overturning or a trailing type of structure. On the one extreme, the environmental flow found at 15-16 km on 1 May promotes development of an overturning anvil, while the strong upper level

westerlies on 6 May favor development of a trailing anvil structure.

As the different features observed in the relative flow fields for the 26 April, 1 May and 6 May squall systems demonstrate, the gross structure and behavior of convective systems in the ACSL classification may be similar, but variations in the finer aspects of the storm flow do occur. These variations reflect both differences in the large scale flow regime and sampling of the particular stage of the storm life cycle.

5. Effects on the Larger Scale Environment

Pre- and post-storm vertical profiles of Θ_e for the 26 April, 1 May and 6 May ACSL are shown in Fig. 15. The pre-storm profiles on 26 April, 1 May and 6 May were taken at 1-2 hours before the passage of the ACSL. The three pre-storm profiles all display a minimum in Θ_e of about 339°K. Differences in the overall shape of the pre-storm profiles in the lower troposphere are due primarily to the time of day and the amount of associated surface heating, although the isothermal structure of the lower portion of the 1 May profile may reflect the actual ascent of the rawinsonde through the core of deep convective towers.

Comparison of the pre-storm and post-storm profiles reveals that the Amazon systems have a pronounced effect on their tropospheric environment. These systems effectively reduce the mid-level pre-storm minimum in Θ_e. This is accomplished by the upward transport of surface air containing high Θ_e values and the

release of latent heat in mid-levels, and the compensating downward transport of cool, dry mid-tropospheric air. Evidence for mid-level warming is seen in the soundings shown in Fig. 10. The troposphere in the wake of the 1 May system has been warmed nearly 2°K between 525 and 250 mb. An accompanying moistening of nearly 1 g kg^{-1} has also occurred. Compensating downward transport of dry (relatively low Θ_e) air is also noted through the formation of a pronounced dry inversion between 700 and 950 mb. This stabilization of the vertical column in the wake of the system is noted in the Θ_e profiles for each of the three Amazon cases.

The profiles of Θ_e suggest that the troposphere is well-mixed by the ACSL. This finding, also concluded by Scala et al. (1990), implies that the Riehl and Simpson (1979) "hot tower" requirement for vertical transport may not be operating within these systems over the Amazon Basin. Transport through protected hot tower conduits, if operating, would preserve the Θ_e minimum in the wake of the squall line. Instead, erosion of the Θ_e minimum and low level decreases in Θ_e imply that vertical motions in the ACSL directly overturn the troposphere. Vertical transports of heat under these circumstances can be accomplished by mean upward and downward circulations ranging in scale from that of the ACSL to an integrated Hadley transport. The cores of the deep convective elements may in fact "leak" or actively detrain latent and sensible heats into the surrounding environment. Evidence for this process was seen during aircraft

flights which revealed multiple layers of cloud that formed in the rear of the deep convective towers. The entrainment of relatively dry mid-tropospheric air into the updraft cores and subsequent dilution and detrainment to the rear of the system provides a possible mechanism for the "leaking" process.

The Θ_e profiles for 1 May also reveal that upper-tropospheric cooling occurred in the wake of this system. This is reflected in the post-storm sounding by a temperature reduction of over 3°K above 175 mb. As indicated by the profiles of Θ_e, the combination of mid-tropospheric warming and this observed upper-level cooling renders the middle and upper troposphere less stable in the wake of the storm. The origin of the cooling is uncertain (perhaps due to ice sublimation), but we note that cooler conditions occurred aloft in the tropospheric environment ahead of the squall line. The 1 May Θ_e profile is up to 2°K cooler than the 6 May profile and 4°K cooler than the 26 April profile. The reduction in stability shown in the Θ_e profiles may help sustain the observed upward motions in the TSR.

5. Summary and Conclusions

In this paper, we have examined the structure and dynamics of a distinct type of synoptic-scale convective system over the equatorial continental tropics, the Amazon Coastal Squall Line (ACSL). ACSL are discontinuous lines of organized mesoscale cloud clusters that form along the northern coast of South America as seabreeze-induced instability lines. The lines then propagate across the Central Amazon Basin at speeds of 50-60 km

h^{-1} with some maintaining enough coherence to arrive at the westernmost boundaries of the Amazon Basin 24-48 h later.

Analysis of satellite and rawinsonde data have shown that the ACSL undergo six possible stages in their life cycle: genesis, intensification, maturity, weakening, reintensification and dissipation. Detailed analyses of surface PAM, satellite and aircraft observations also reveal that ACSL are composed of three distinct components: pre-storm cumulus (PSC), leading edge convection (LEC), and multiple, precipitating layers of cloud in the trailing stratiform region (TSR).

Calculations of divergence and vertical velocity for a mature ACSL indicate deep vertical ascent in the LEC and a region of mid-level convergence in the TSR. This convergence is associated with a weak updraft above 500 mb and unsaturated downdraft below. The vertical motions in the TSR are an order of magnitude smaller than those in the LEC. These findings are similar to the structure and dynamics of squall lines and other types of mesoscale convective system in the tropics and midlatitudes (Houze, 1989).

Substantial shear in the low-level inflow was found to occur with the 26 April, 1 May and 6 May squall lines. The shear is a consequence of an easterly wind maximum located at 2.5 km, and simulations using a two-dimensional cloud model (Scala et al., 1990, 1992) suggest that the shear may play an important role in the longevity of the storm system. Mid-level inflow of air into the leading convective elements was found to vary widely between

the three systems, and may act to dilute the updraft cores as well as advect appreciable quantities of condensate into the trailing portions of the squall system.

Profiles of pre-storm and post-storm Θ_e demonstrate the effect of ACSL on their larger-scale tropospheric environment. The ACSL generally stabilize the troposphere in their wake and erode the pre-storm minimum in Θ_e. We hypothesize that the removal of this minimum is accomplished through direct mixing via vertical motions in the storm, and also through detrainment in multiple layers in the wake of the squall system. The evidence supports the contention that energy transport through protected "hot towers" is not the preferred mechanism that accomplishes the required vertical transports over the Amazon Basin during the wet season. Energy budgets and transports associated with the ACSL will be the main focus for Part II of our study.

Acknowledgements

We gratefully acknowledge the sustained support provided by the Tropospheric Chemistry Program of NASA. This support, following the field work in ABLE 2a and 2b, has made analysis of extensive and unique data sets possible.

A large part of this paper is drawn from Harold L. Massie's doctoral dissertation and from the doctoral research of Jeffrey Halverson.

References

Barnes, G.M., and K. Sieckman, 1984: The environment of fast- and slow-moving tropical mesoscale convective cloud lines. Mon. Wea. Rev., 112, 1782-1794.

Betts, A.K., R.W. Grover, and M.W. Moncrieff, 1976: Structure and motion of tropical squall-lines over Venezuela. Quart. J. Roy. Meteor. Soc., 102, 395-404.

Carlson, D.C., 1981: Weather satellite interpretation - Introduction to Satellite Imagery. NOAA Tech. Memo. NWS SR-103, 47 pp.

Chalon, J.P., G. Jaubert, F. Roux, and J.P. Lafore, 1988: The West African squall line observed on 23 June 1981 during COPT81: Mesoscale structure and transports. J. Atmos. Sci., 45, 2744-2763.

Chong, M., and D. Hauser, 1989: A tropical squall line observed during the COPT81 experiment in West Africa. Part II: Water budget. Mon. Wea. Rev., 117, 728-744.

Chong, M., P. Amayenc, G. Scialom, and J. Testud, 1987: A tropical squall line observed during the COPT81 experiment in West Africa. Part I: Kinematic structure inferred from dual Doppler radar data. Mon. Wea. Rev., 115, 671-694.

Cohen, J.C.P., C.A. Nobre, and M.A.F. da Silva Dias, 1989: Mean distribution and characteristics of the squall lines observed over the Amazon Basin. Third Internat. Conf. Southern Hemisphere Meteor. and Oceanogr., Buenos Aires, Argentina, 205-207.

Davis, J.C., 1986: Statistics and Data Analysis in Geology. John Wiley and Sons, New York, 646 pp.

Frank, W.M., 1978: The life cycles of GATE convective systems. J. Atmos. Sci., 35, 1256-1264.

Frank, W.M., and J.L. McBride, 1989: The vertical distribution of heating in AMEX and GATE cloud clusters. J. Atmos. Sci., 46, 3464-3478.

Gallus, W.A., Jr., and R.H. Johnson, 1991: Heat and moisture budgets of an intense mid-latitude squall line. J. Atmos. Sci., 48, 122-146.

Gamache, J.F., and R.A. Houze, Jr., 1982: Mesoscale air motions associated with a tropical squall line. J. Atmos. Sci., 110, 118-135.

Garstang, M., S. Ulanski, S. Greco, J. Scala, R. Swap, D. Fitzjarrald, D. Martin, E. Browell, M. Shipham, V. Connors, R. Harriss, and R. Talbot, 1990: The Amazon Boundary Layer Experiment (ABLE 2B): A meteorological perspective. Bull. Amer. Meteor. Soc., 71, 19-32.

Greco, S., R. Swap, M. Garstang, S. Ulanski, M. Shipham, R.C. Harriss, R. Talbot, M.O. Andreae, and P. Artaxo, 1990: Rainfall and surface kinematic conditions over central Amazonia during ABLE 2B. J. Geophys. Res., 93, 17001-17014.

Haltiner, G.J., and F.L. Martin, 1957: Dynamical and Physical Meteorology. McGraw-Hill, New York, 470 pp.

Harriss, R.C., M. Garstang, S.C. Wofsy, S.M. Beck, R.J. Bendura, J.R.B. Coelho, J.W. Drewry, J.M. Hoell, P.A. Matson, R.J.

McNeal, L.C.B. Molion, R.L. Navarro, V. Rabine, and R.L. Snell, 1990: The Amazon Boundary Layer Experiment: Wet season 1987. J. Geophys. Res., 93, 16721-16736.

Houze, R.A., 1977: Structure and dynamics of a tropical squall-line system. Mon. Wea. Rev., 105, 1540-1567.

_____, 1989: Observed structure of mesoscale convective systems and implications for large-scale heating. Quart. J. Roy. Meteor. Soc., 115, 425-461.

Johnson, R.H., and D.L. Priegnitz, 1981: Winter monsoon convection in the vicinity of North Borneo. Part II: Effects on large-scale fields. Mon. Wea. Rev., 109, 1615-1628.

Kousky, V.E., 1980: Diurnal rainfall variation in northeast Brazil. Mon. Wea. Rev., 108, 488-498.

Kousky, V.E., and L.C.B. Molion, 1981: Una contribucao a climatologia dinamica da troposfera sobre a Amazônia, INPE-2030-RPI/050, Sao Jose dos Campos, S.P. Brazil.

Leary, C.A., and R.A. Houze, Jr., 1979: The structure and evolution of convection in a tropical cloud cluster. J. Atmos. Sci., 36, 437-457.

Molion, L.C.B., 1987: On the dynamic climatology of the Amazon Basin and associated rain-producing mechanisms. In The Geophysiology of Amazonia: Vegetation and Climate Interactions, R. Dickerson (ed.), Wiley Intersciences, New York, 391-407.

O'Brien, J.J., 1970: Alternative solutions to the classical vertical velocity problem. J. Appl. Meteor., 9, 197-203.

Ogura, Y., and M.-T. Liou, 1980: The structure of a midlatitude squall line: A case study. J. Atmos. Sci., 37, 553-567.

Riehl, H., and J. Simpson, 1979: The heat balance in the equatorial trough zone, revisited. Contrib. Atmos. Phys., 52, 287-305.

Rotunno, R., J.B. Klemp, and M.L. Weisman, 1988: A theory for strong, long-lived squall lines. J. Atmos. Sci., 45, 463-484.

Scala, J.R., M. Garstang, W.-K. Tao, K.F. Pickering, A.M. Thompson, J. Simpson, V.W.J.H. Kirchhoff, E.V. Browell, G.W. Sachse, A.L. Torres, G.L. Gregory, R.A. Rasmussen, and M.A.K. Khalil, 1990: Cloud draft structure and trace gas transport. J. Geophys. Res., 95, 17015-17030.

_____, W.-K. Tao, K. Pickering, A. Thompson, J. Simpson, and M. Garstang, 1991: The effect of tropical squall-type convection on the vertical transport and redistribution of trace gases. Proc. AMS Seventh Joint Conf. on Appl. Air Poll. Meteor. with AWMA, New Orleans, LA, January, 228-231.

_____, _____, and J. Simpson, 1992: Transport dynamics in the convective and stratiform regions of a tropical squall line: Results of a two-dimensional numerical investigation. Proc. AMS 5th Conf. on Mesoscale Processes, Atlanta, GA, 303-306.

Tao, W.-K., J. Simpson, and S.-T. Soong, 1991: Numerical simulation of a subtropical squall line over Taiwan Strait. Mon. Wea. Rev., 119, 2699-2723.

Thorpe, A.J., M.J. Miller, and M.W. Moncrieff, 1982: Two-dimensional convection in nonconstant shear: a model of midlatitude squall lines. Quart. J. Roy. Meteor. Soc., 108, 739-762.

Zipser, E.J., 1977: Mesoscale and convective-scale downdrafts as distinct components of squall-line structure. Mon. Wea. Rev., 105, 1568-1589.

List of Figures

wind gust in m s^{-1}, (c) u-wind component in m s^{-1}, (d) v-wind component in m s^{-1}, (e) pressure in hPa, (f) temperature in degrees (C), (g) mixing ratio in g kg^{-1} and θ_e in K.

Fig. 7. GOES Mb-enhanced infrared image of the 1 May 1987 ACSL at 0230 UTC as it propagated westward across the mesoscale triangle (marked by the +). The letters G and B denote the location of, respectively, Georgetown, Guyana and Belém, Brazil.

Fig. 8. Vertical profiles of mass divergence on 1 May 1987. Solid curve depicts the squall line LEC component at 1200 UTC. Dashed curve is the TSR component at 1800 UTC. Values are in units of 10^{-5} s^{-1}.

Fig.9. Vertical profiles of vertical p-velocity for the 1 May 1987 ACSL. Solid curve depicts the squall line LEC component at 1200 UTC; dashed curve is the TSR component at 1800 UTC. Values are in units of μb s^{-1}.

Fig. 10. Vertical profiles of sounding-derived temperature and dewpoint for the 1 May 1987 ACSL in standard skew-T/ log P format. Mesoscale triangle composite soundings are used for pre-squall (1200 UTC, solid curve) and post-squall (1800 UTC, dashed curve) observations.

Fig. 11. Vertical profiles of vertical p-velocity for the TSR of three squall lines taken at 1800 UTC. TSR divergence values correspond to 26 April (solid curve), 1 May (dashed curve) and 6 May (dash-dot curve) 1987

squall lines.

Fig. 12. Coordinate system used to derive the relative flow line-normal component for the 1 May 1987 ACSL.

Fig. 13. Profiles of rawinsonde-derived wind velocity for three ACSL pre-storm environments: 26 April 1987 (1500 UTC), 1 May 1987 (1200 UTC) and 6 May 1987 (1500 UTC). Wind direction is according to standard compass. A half-barb equals 2.5 m s^{-1}; a full barb equals 5 m s^{-1}.

Fig. 14. Horizontal storm relative flow calculated for the pre-storm components of the 26 April, 1 May and 6 May ACSL. Wind speed is shown in m s^{-1}.

Fig. 15. Profiles of pre-storm and post-storm Θ_e derived for the triangle composite soundings for three ACSL: 26 April 1987 (1500 and 1800 UTC), 1 May 1987 (1200 and 1800 UTC), and 6 May 1987 (1500 and 1800 UTC).

TABLE 1. Summary of changes in surface values of temperature, humidity, Θ_e and pressure observed at the 4 PAM locations with the passage of the squall line on (a) 26 April and (b) 6 May. Also presented are peak wind gusts, maximum rain rate and both total amount and duration of rainfall.

a) **26 April 1987**

	Ducke	Carapaña	Embrapa	ZF1
ΔT	-6°C	-6.5°C	-7.0°C	-6.0°C
Δq	-3.7 g kg-1	-2.1 g kg^{-1}	-2.5 g kg^{-1}	-2.6 g kg^{-1}
$\Delta\Theta_e$	-17.0 K	-11.0 K	-16.0 K	---
ΔP	+0.7 hPa	+0.8 hPa	+0.9 hPa	+0.9 hPa
Peak Gust	13 m s^{-1}	9 m s^{-1}	12 m s^{-1}	13 m s^{-1}
Maximum Rain Rate	0.25 mm min^{-1}	1.5 mm min^{-1}	1.7 mm min^{-1}	1 mm min^{-1}
Total Rainfall	1 mm	34 mm	33 mm	16 mm
Total Duration of Rainfall	0.25 h	2.5 h	3.0 h	2.0 h

b) **6 May 1987**

	Ducke	Carapaña	Embrapa	ZF1
ΔT	-7.0°C	-3.5°C	-5.5°C	-4.0°C
Δq	-1.5 g kg^{-1}	no change	-1.5 g hg^{-1}	no change
$\Delta\Theta_e$	-7.0 K	-5.5 K	-9.0 K	---
ΔP	+0.6 hPa	no change	+0.4 hPa	no change
Peak Gust	7.5 m s^{-1}	6.5 m s^{-1}	15.0 m s^{-1}	8 m s^{-1}
Maximum Rain Rate	1.3 mm min^{-1}	0.8 mm min^{-1}	0.5 mm min-1	-0.3 mm min^{-1}
Total Rainfall	6 mm	15 mm	2 mm	1 mm
Total Duration of Rainfall	1.5 h	8.0 h	6.0 h	1.0 h

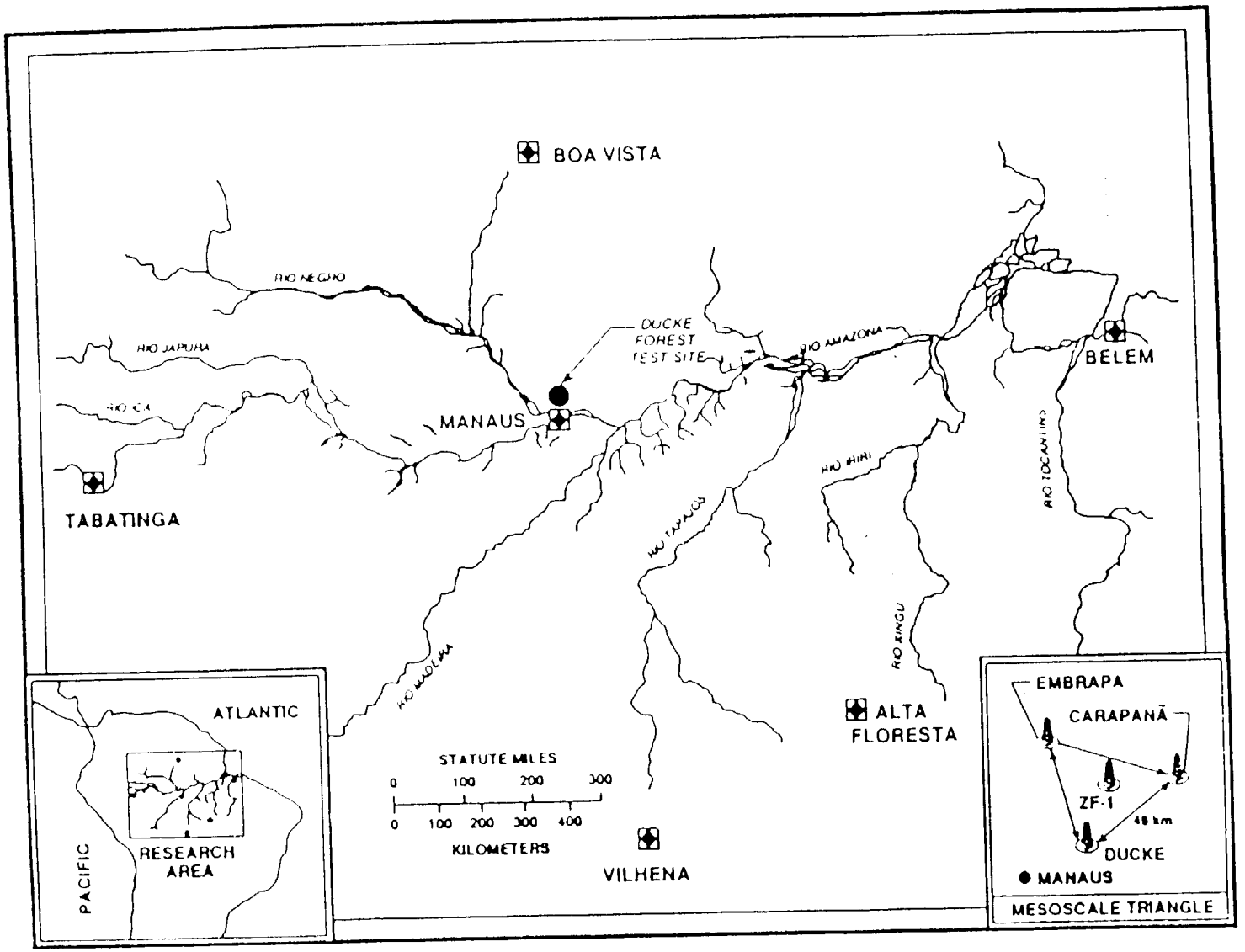
BOA VISTA
RIO NEGRO
RIO JAPURA
RIO IÇA
TABATINGA
MANAUS
DUCKE FOREST TEST SITE
RIO AMAZONAS
BELEM
RIO TAPAJOS
RIO XINGU
RIO TOCANTINS
ALTA FLORESTA
VILHENA
STATUTE MILES
0 100 200 300
0 100 200 300 400
KILOMETERS
ATLANTIC
PACIFIC
RESEARCH AREA
EMBRAPA
CARAPANÃ
ZF-1
48 km
DUCKE
MANAUS
MESOSCALE TRIANGLE

Fig 1

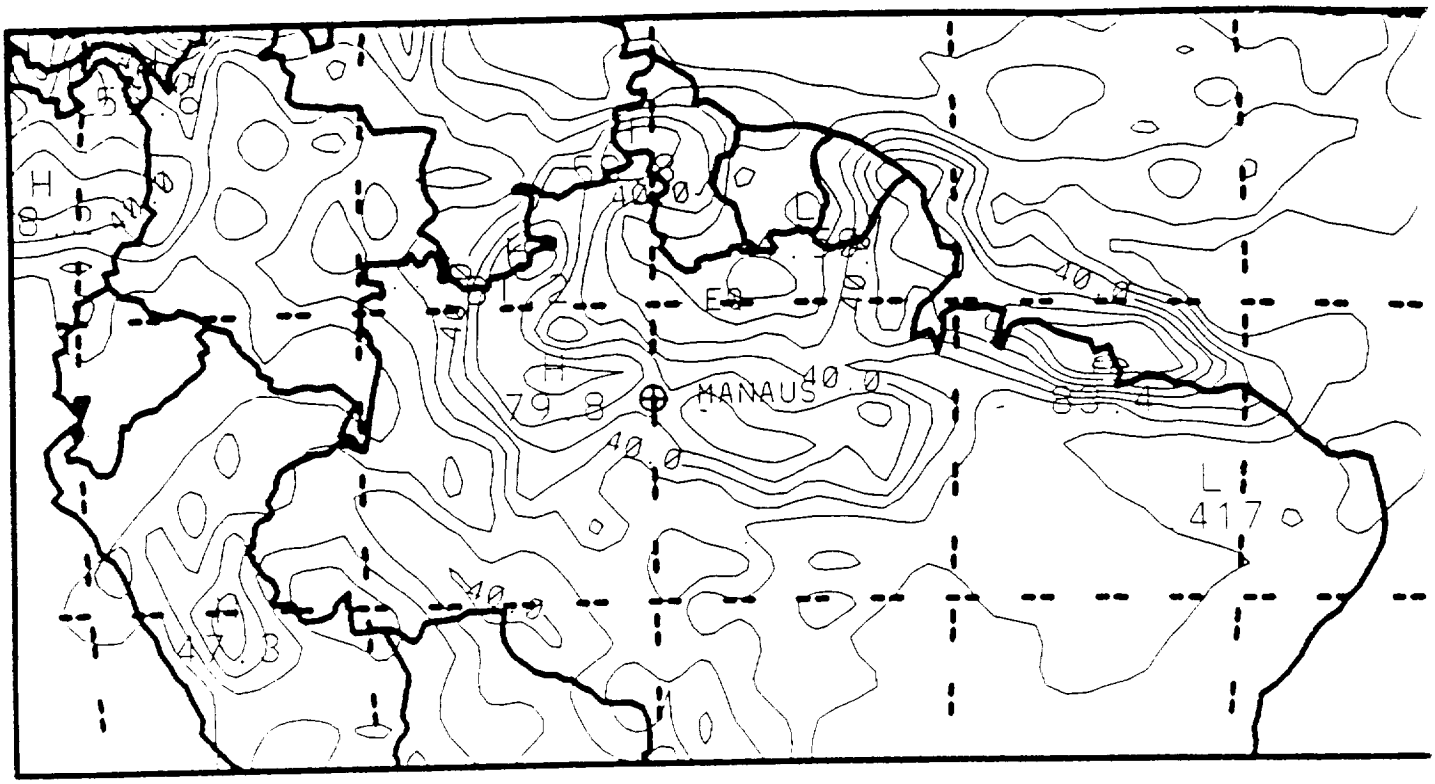
MANAUS
40.0
79.8
L
417
47.3

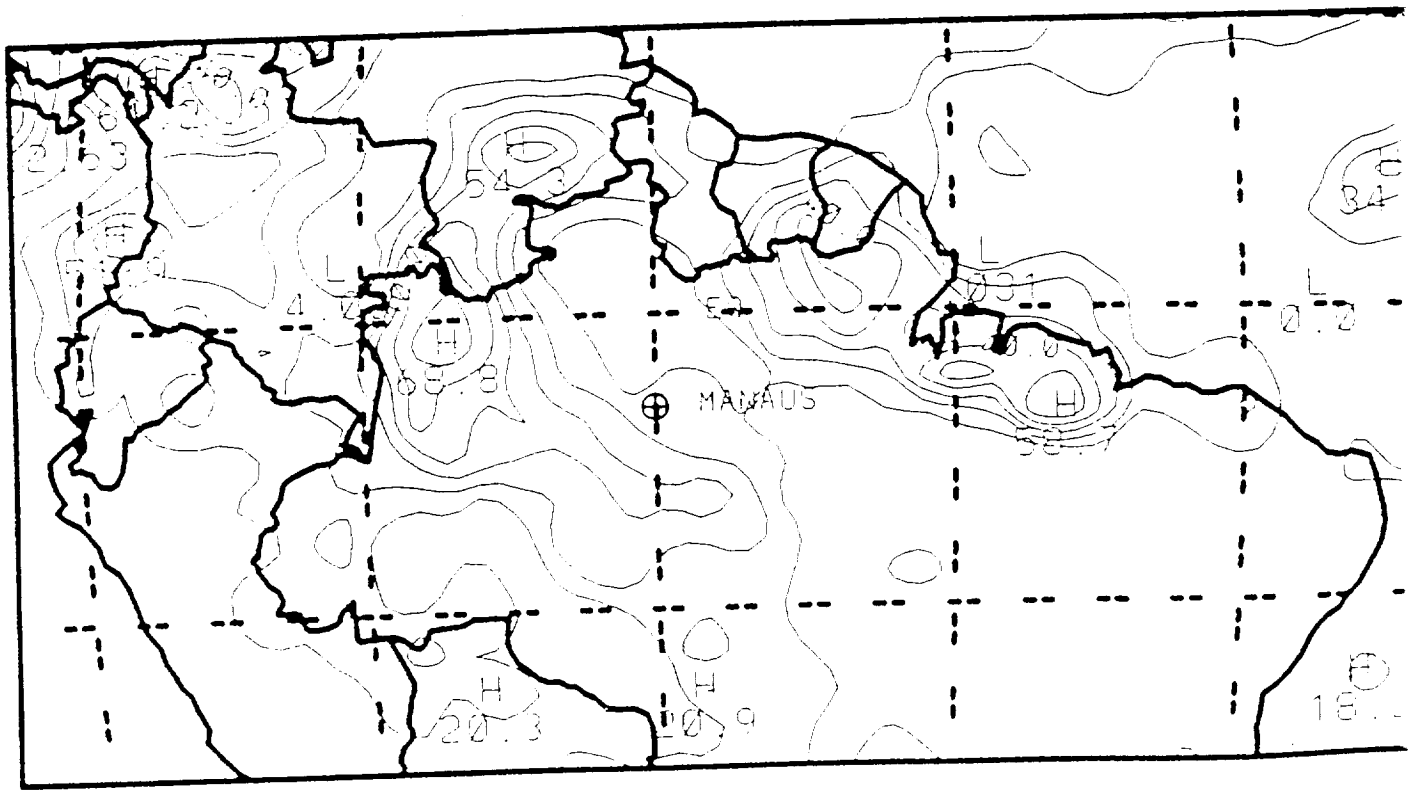
MANAUS
54.3
L
H
20.3
10.9

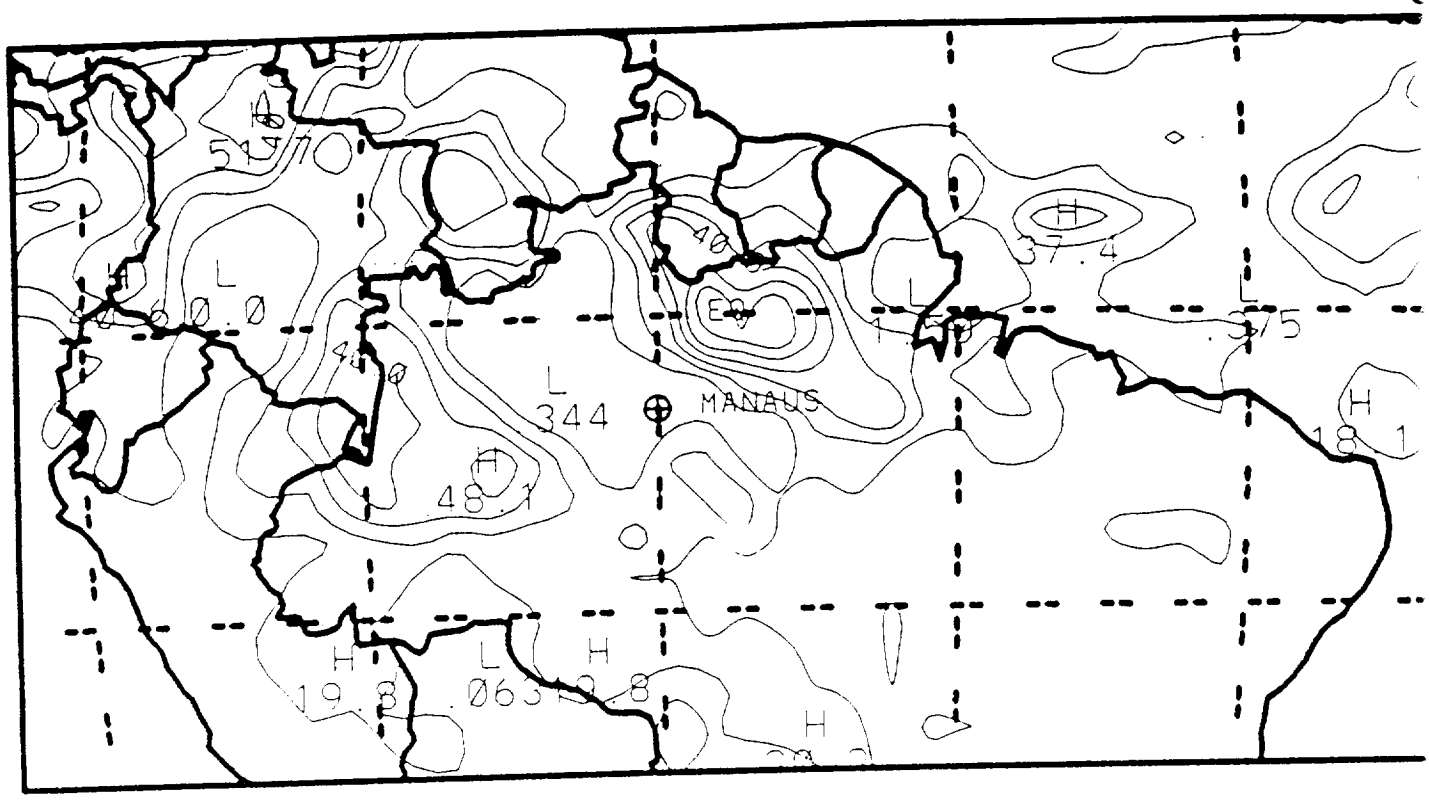
MANAUS
MANAUS

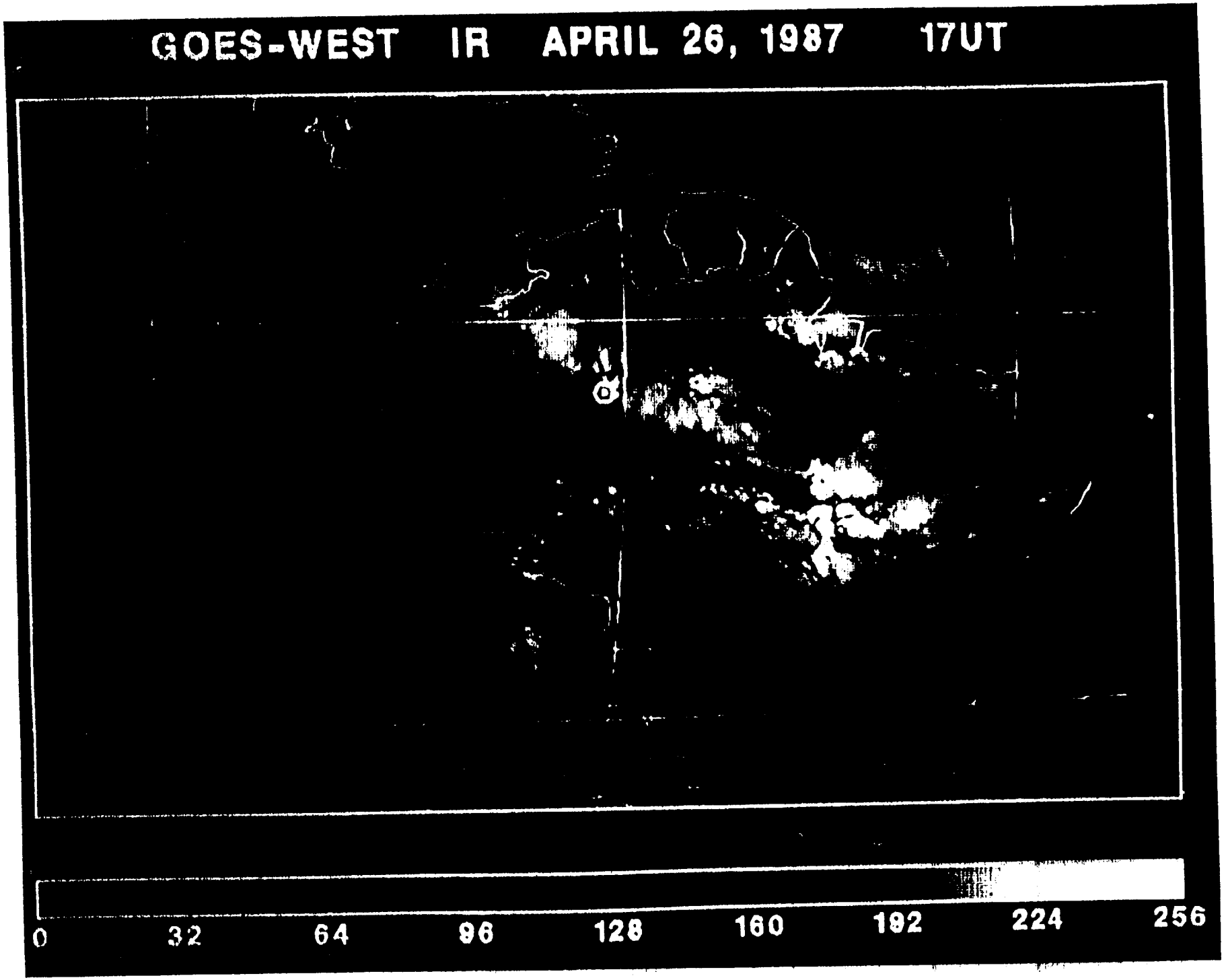

Fig 3

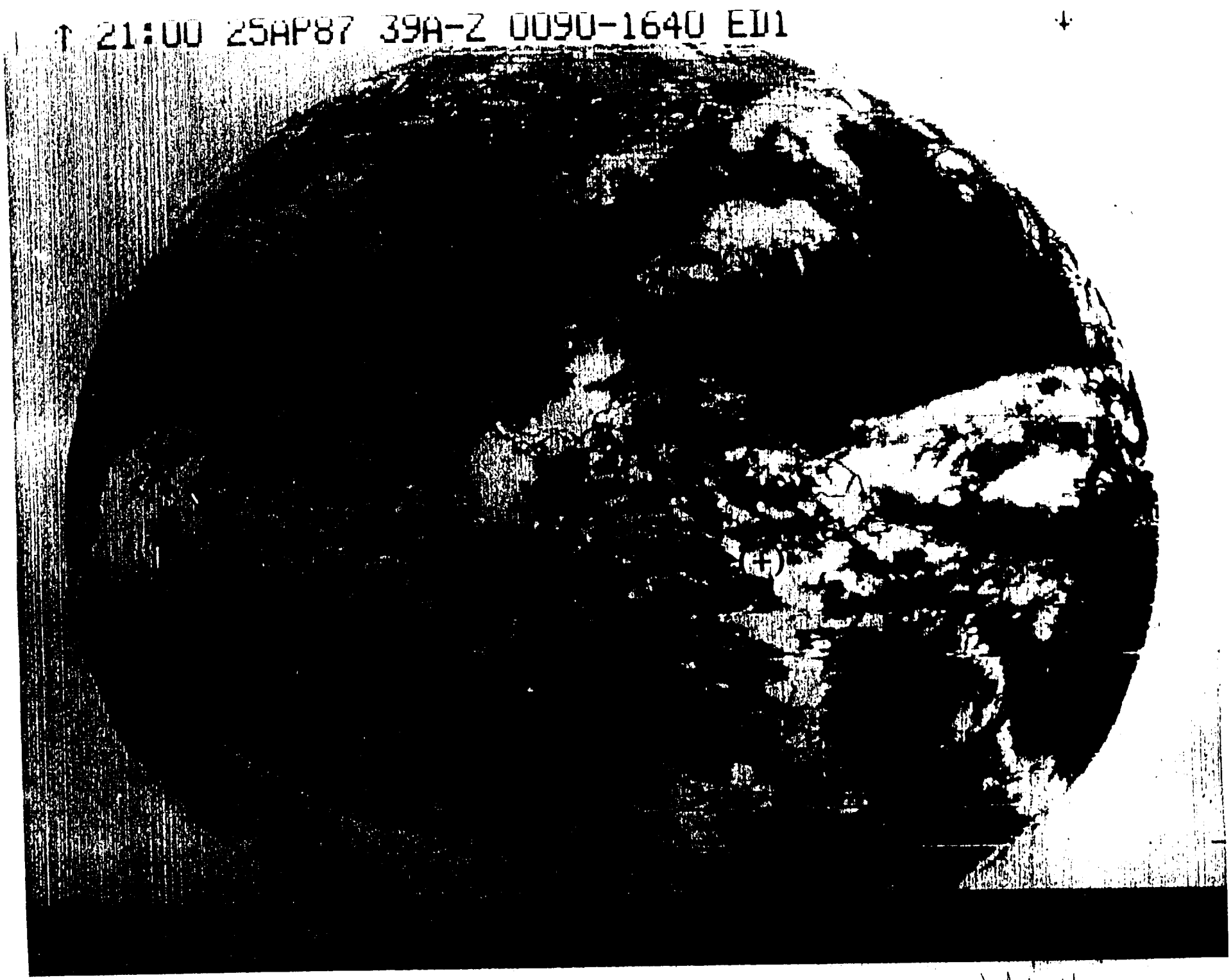
21:00 25APR87 39A-2 0090-1640 EDI

Fig 16

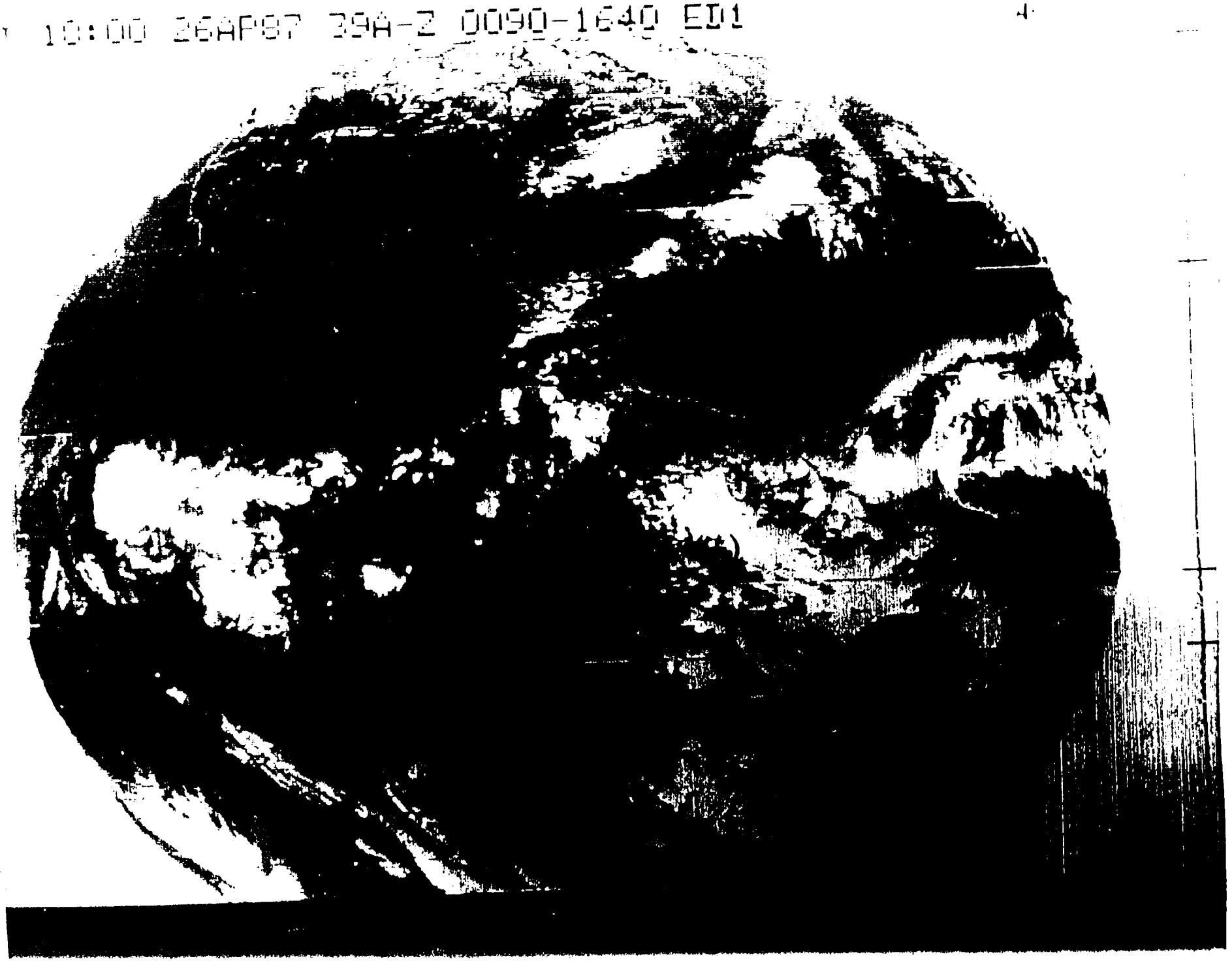

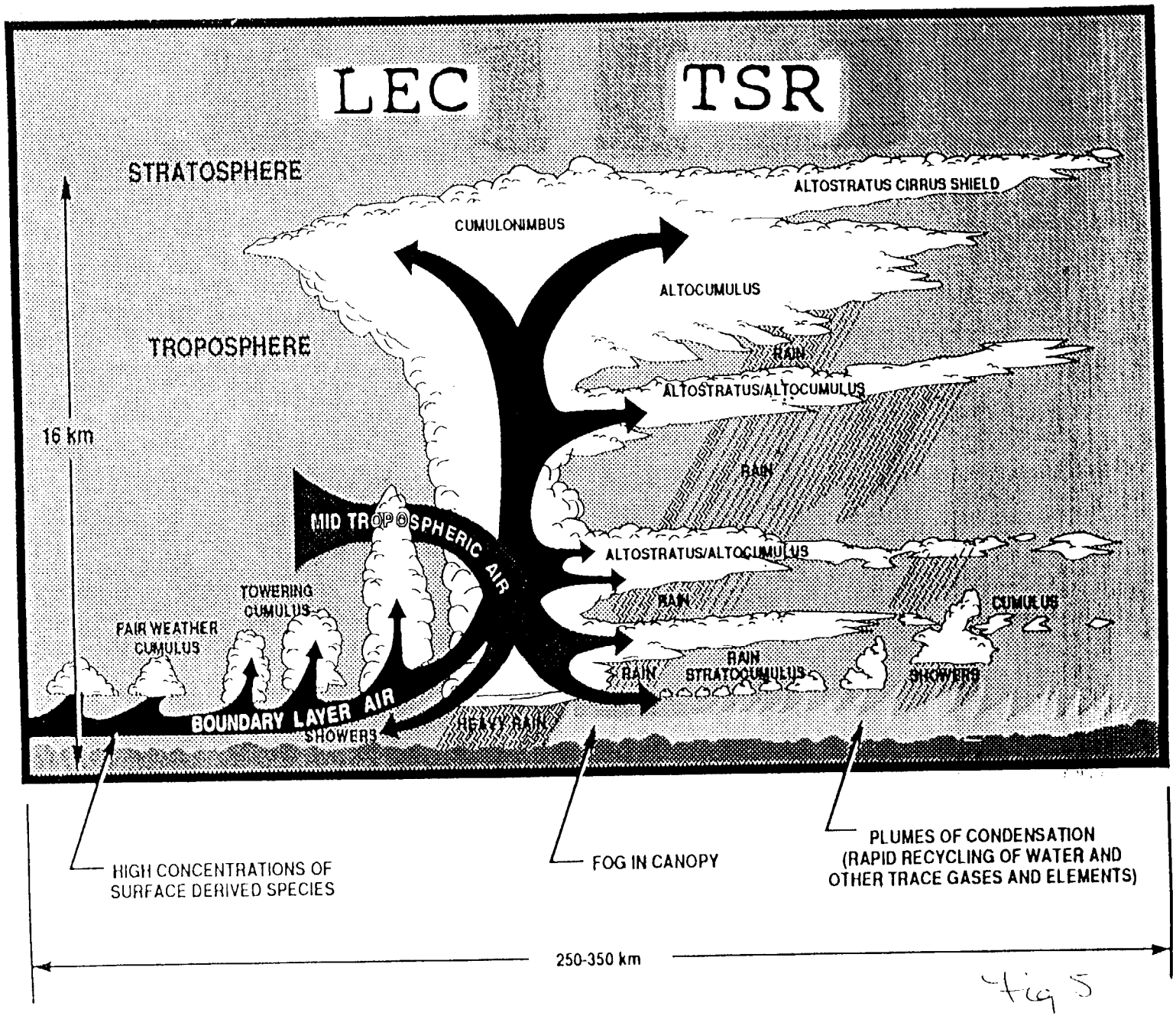
LEC
TSR
STRATOSPHERE
TROPOSPHERE
16 km
CUMULONIMBUS
ALTOSTRATUS CIRRUS SHIELD
ALTOCUMULUS
RAIN
ALTOSTRATUS/ALTOCUMULUS
RAIN
MID TROPOSPHERIC AIR
ALTOSTRATUS/ALTOCUMULUS
TOWERING CUMULUS
FAIR WEATHER CUMULUS
RAIN
CUMULUS
RAIN
RAIN STRATOCUMULUS
SHOWERS
BOUNDARY LAYER AIR
SHOWERS
HEAVY RAIN
HIGH CONCENTRATIONS OF SURFACE DERIVED SPECIES
FOG IN CANOPY
PLUMES OF CONDENSATION (RAPID RECYCLING OF WATER AND OTHER TRACE GASES AND ELEMENTS)
250-350 km

fig 5

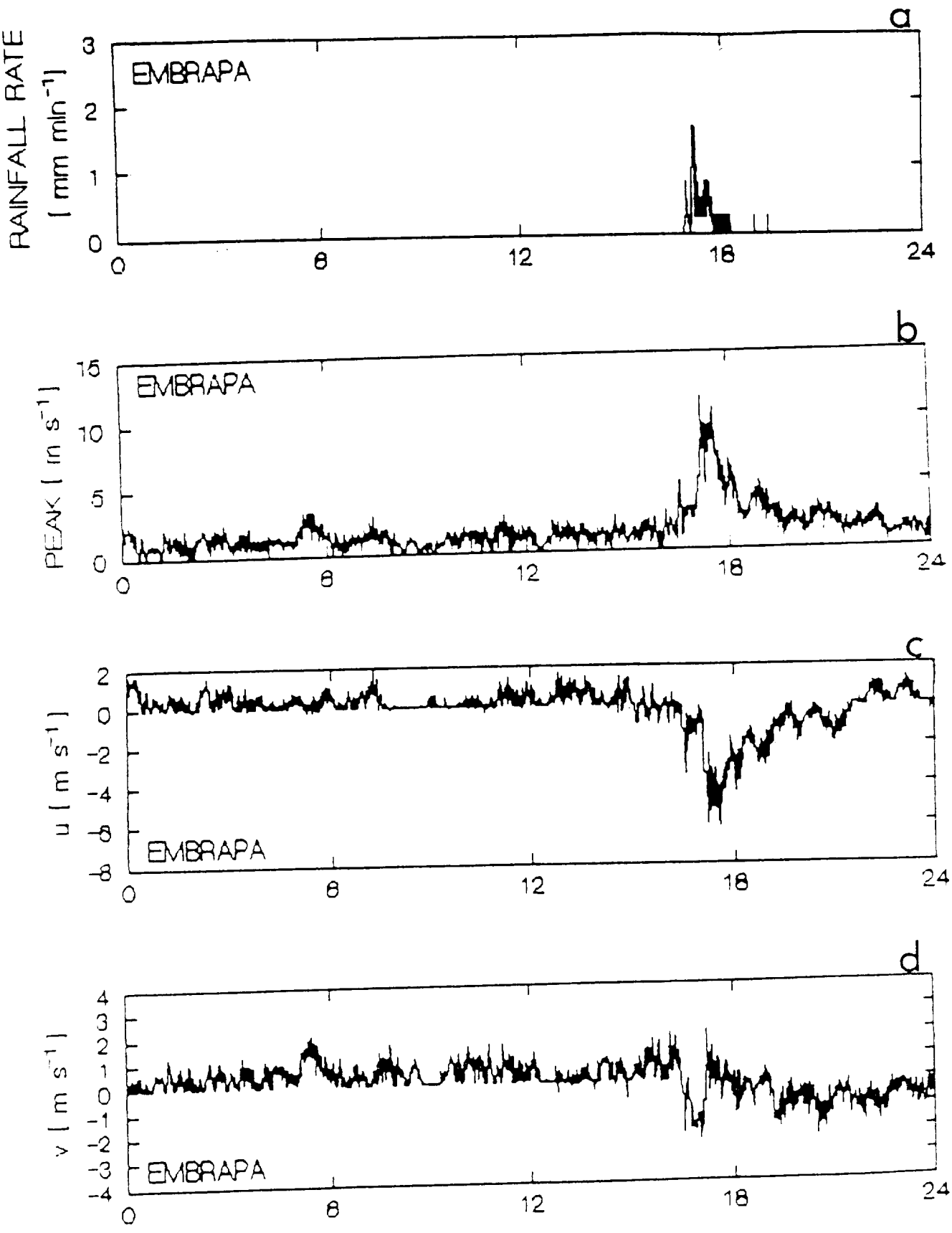
a
RAINFALL RATE [mm min^{-1}]
EMBRAPA
b
PEAK [m s^{-1}]
EMBRAPA
c
u [m s^{-1}]
EMBRAPA
d
v [m s^{-1}]
EMBRAPA
HOUR [UTC], 26 APRIL 1987

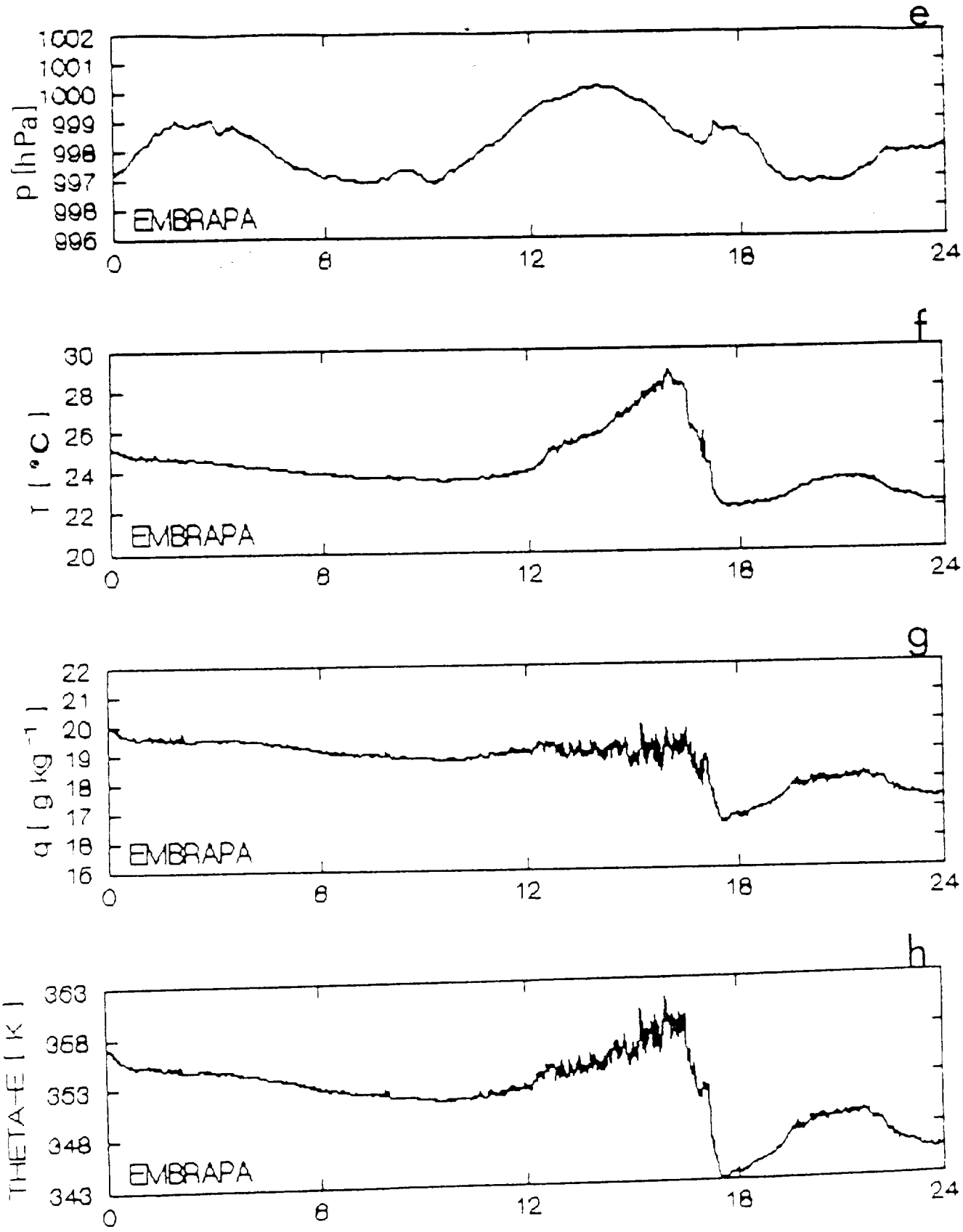
e
p [hPa]
1002
1001
1000
999
998
997
996
EMBRAPA
0
6
12
18
24
f
T [°C]
30
28
26
24
22
20
EMBRAPA
g
q [g kg⁻¹]
22
21
20
19
18
17
16
EMBRAPA
h
THETA-E [K]
363
358
353
348
343
EMBRAPA
HOUR [UTC], 26 APRIL 1987

Fig 7

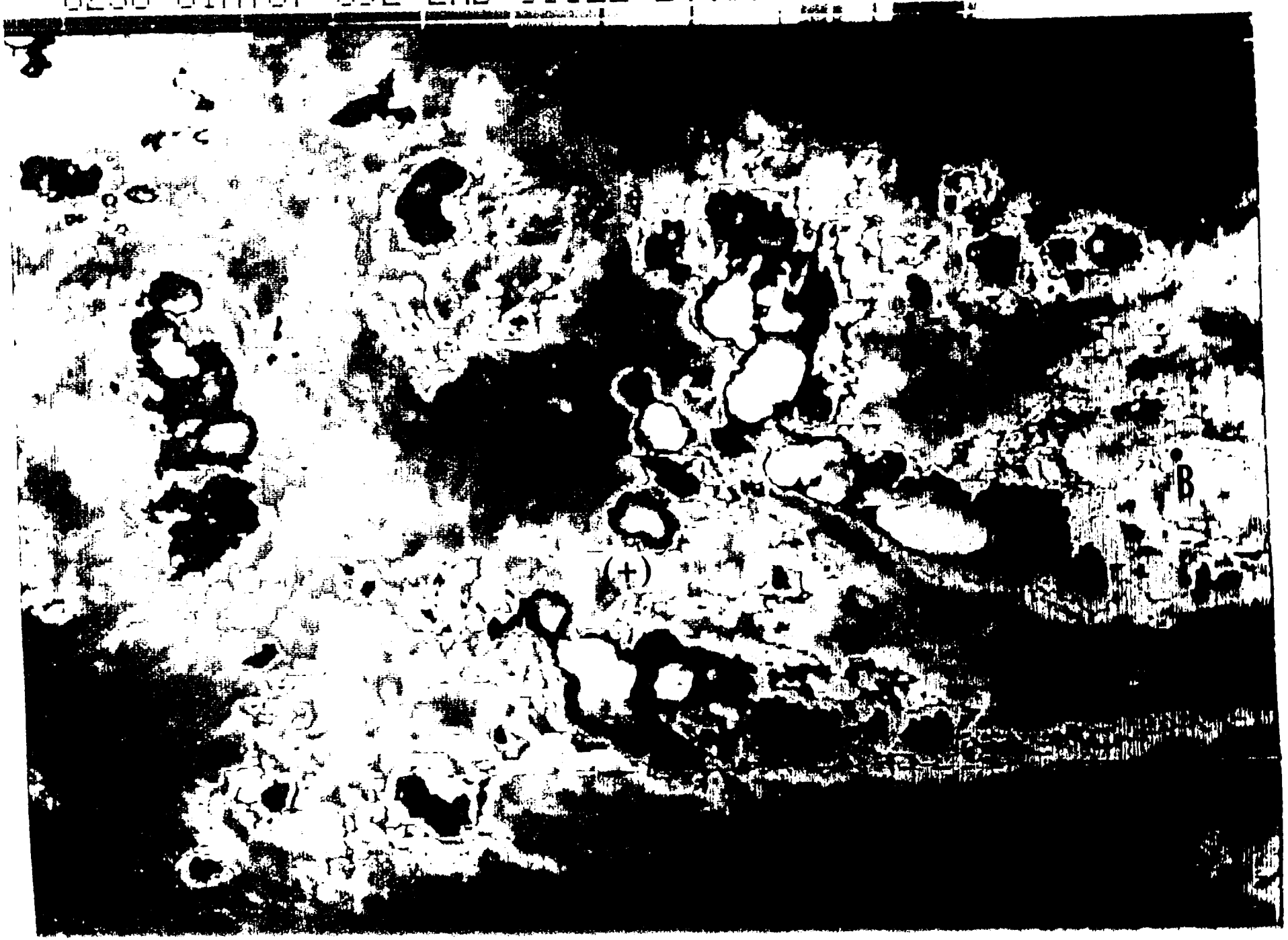

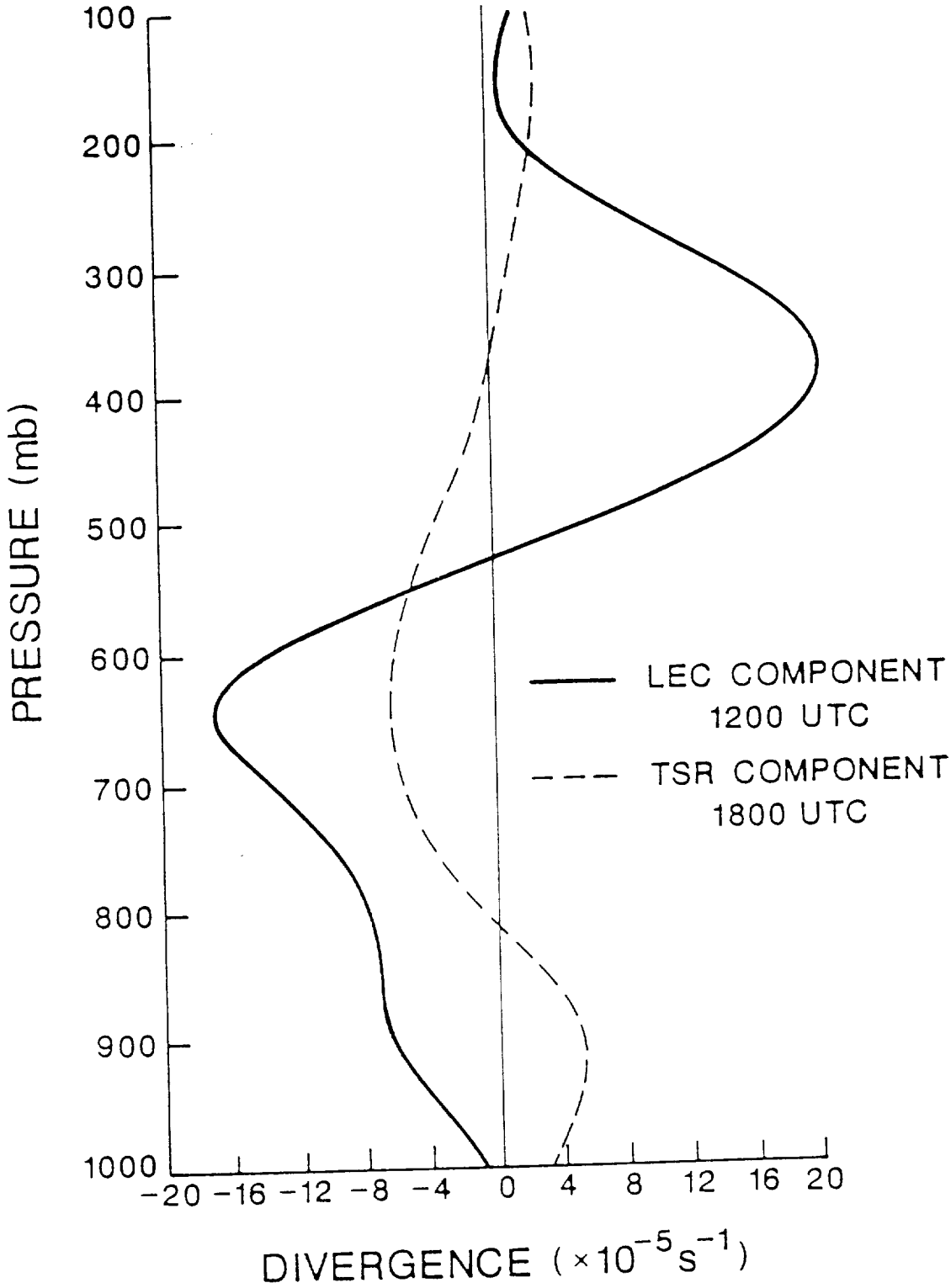
100
200
300
400
500
600
700
800
900
1000
PRESSURE (mb)
−20 −16 −12 −8 −4 0 4 8 12 16 20
DIVERGENCE (×10⁻⁵s⁻¹)
LEC COMPONENT
1200 UTC
TSR COMPONENT
1800 UTC

4 of 8

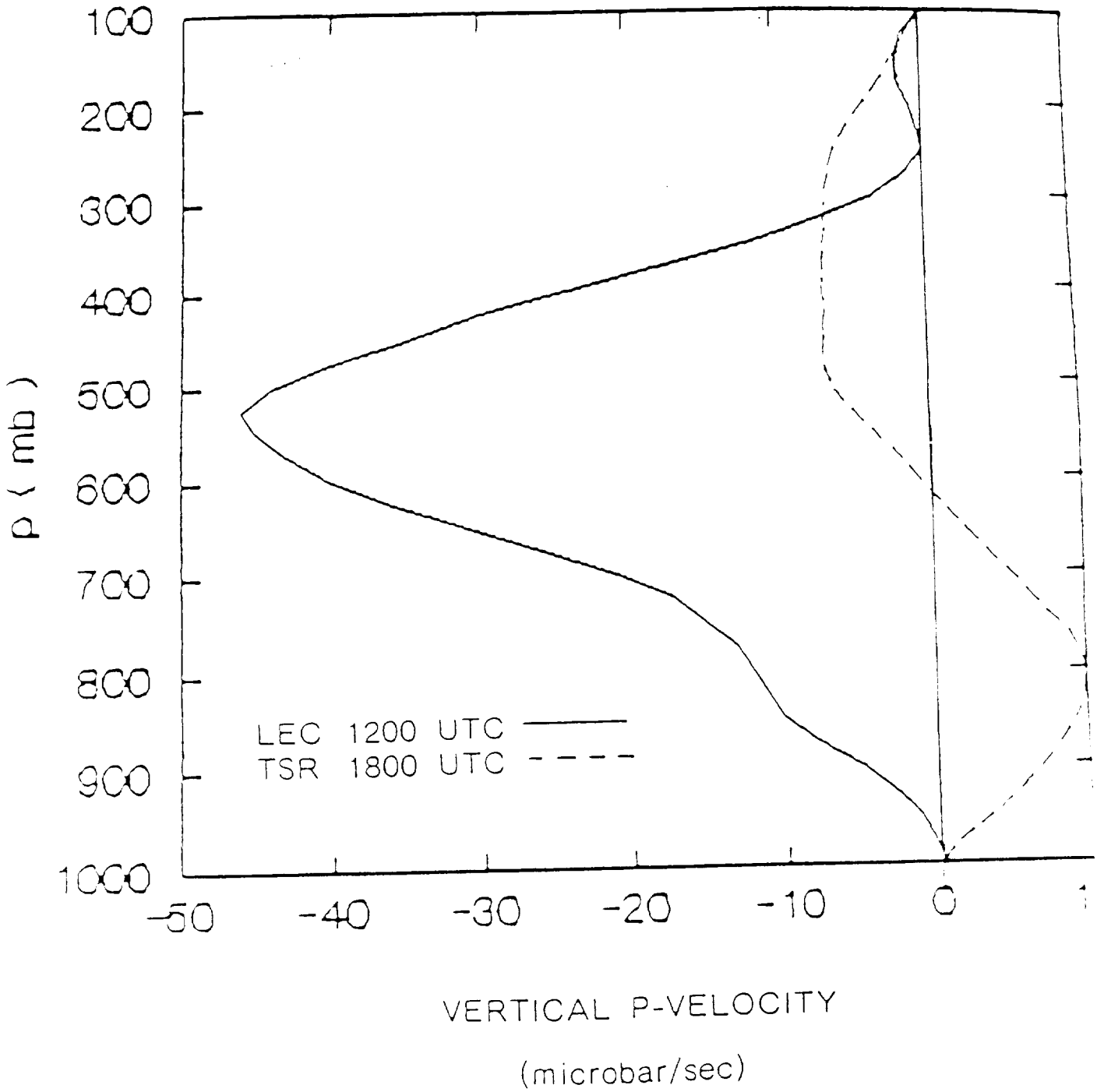
100
200
300
400
500
600
700
800
900
1000
p (mb)
-50
-40
-30
-20
-10
0
LEC 1200 UTC
TSR 1800 UTC
VERTICAL P-VELOCITY
(microbar/sec)

Fig 4

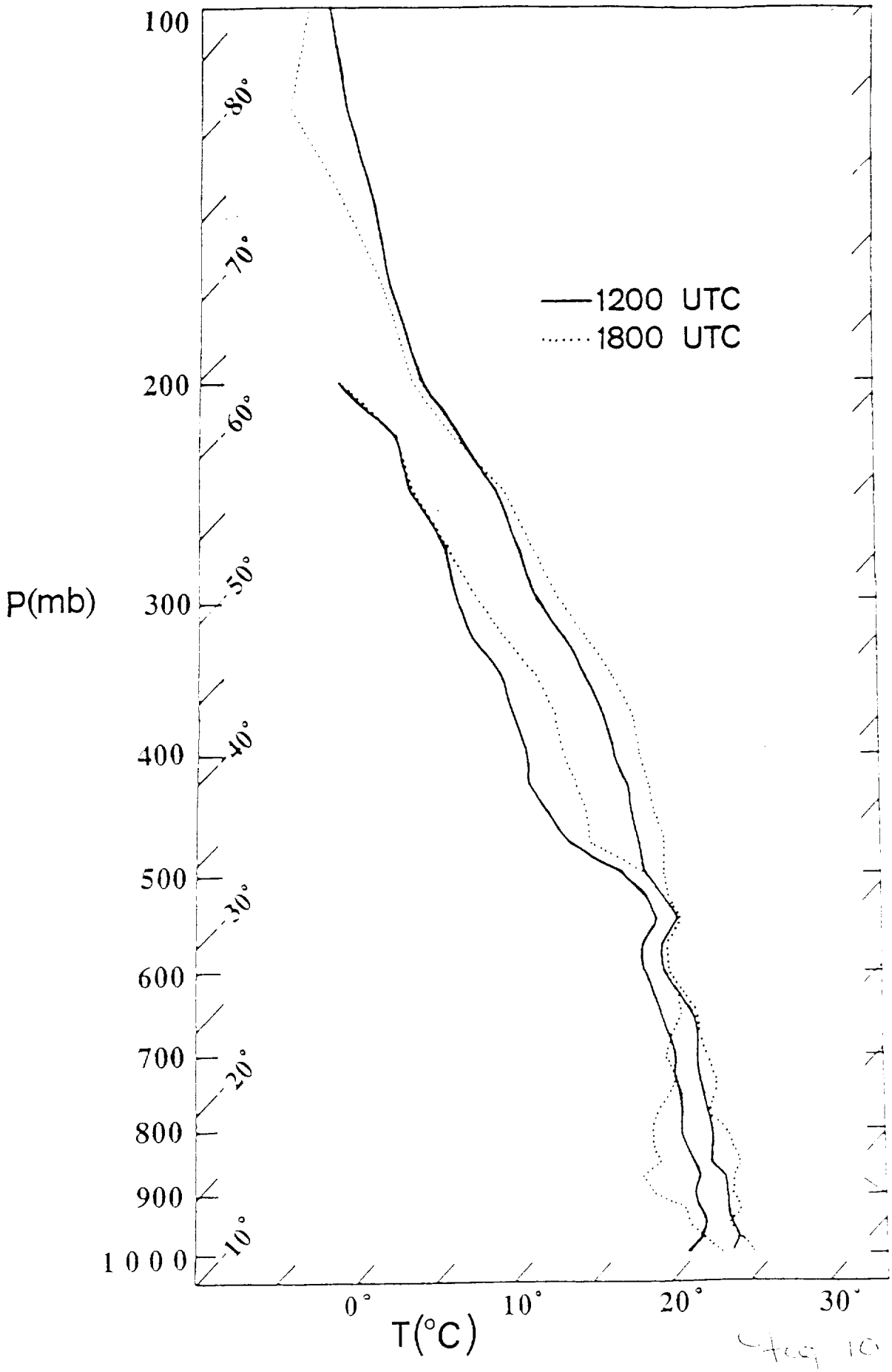
100
200
300
400
500
600
700
800
900
1000
P(mb)
-80°
-70°
-60°
-50°
-40°
-30°
-20°
-10°
0°
10°
20°
30°
T(°C)
1200 UTC
1800 UTC

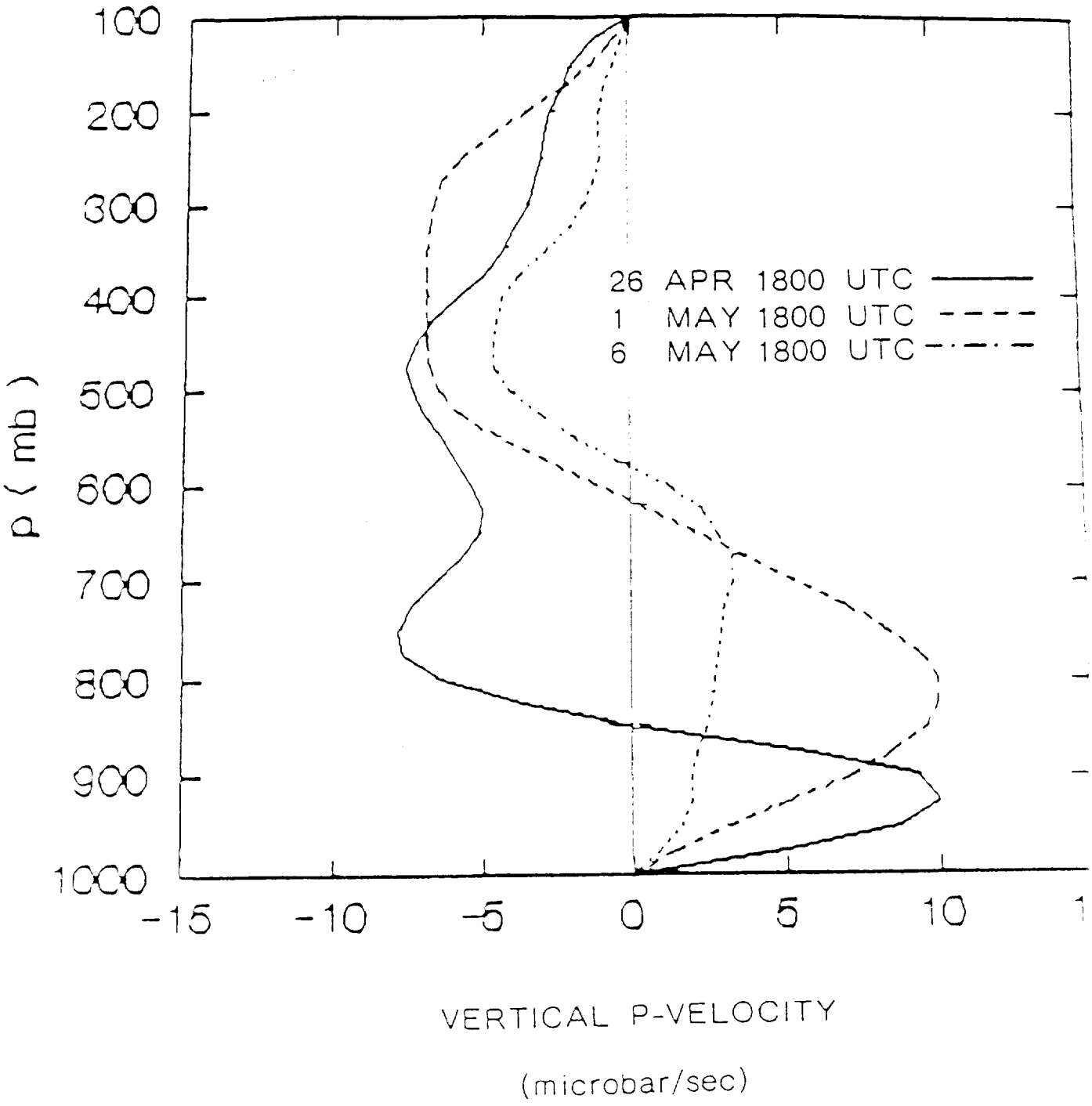
100
200
300
400
500
600
700
800
900
1000
p (mb)
-15
-10
-5
0
5
10
26 APR 1800 UTC
1 MAY 1800 UTC
6 MAY 1800 UTC
VERTICAL P-VELOCITY
(microbar/sec)

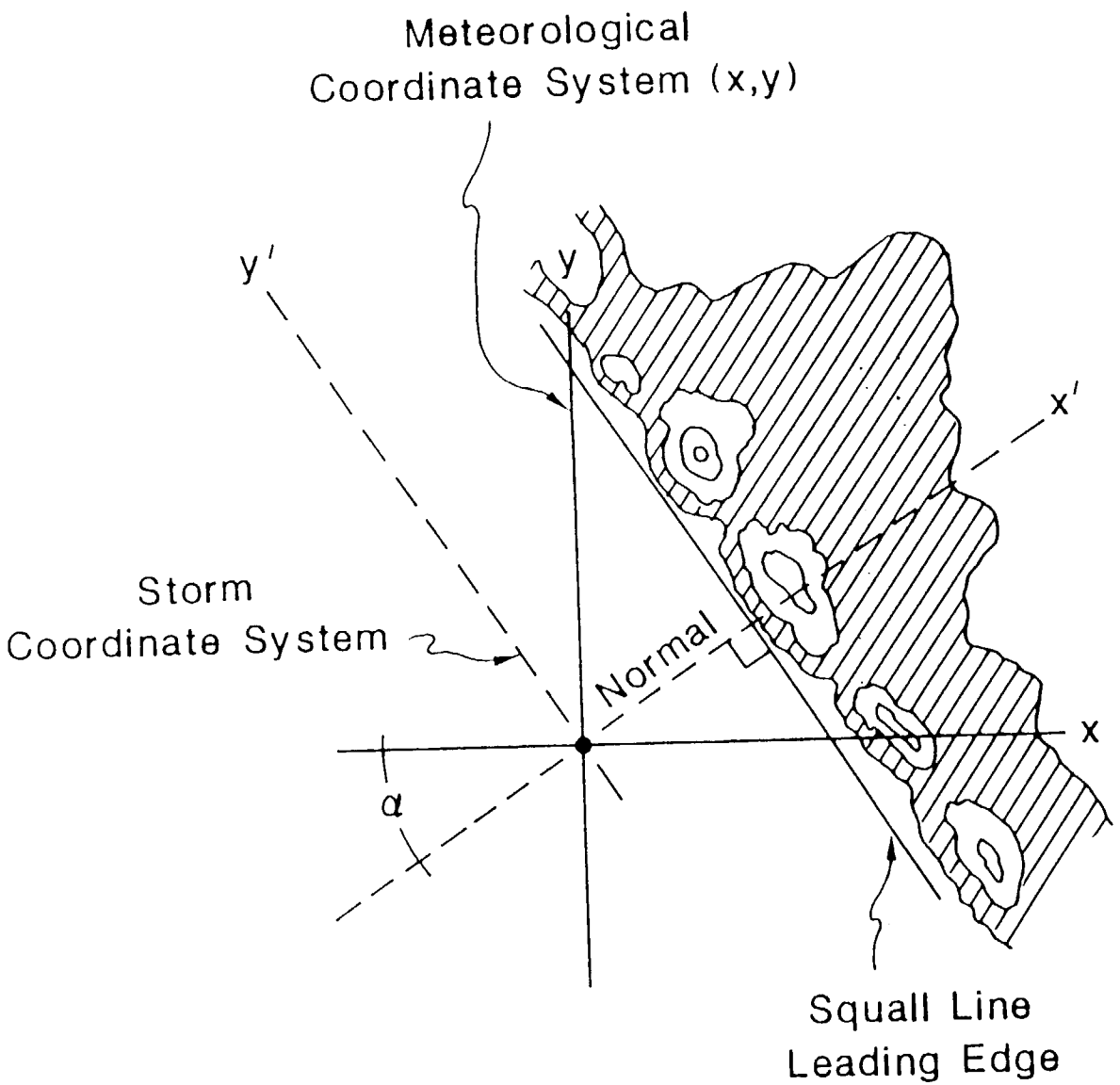
Meteorological
Coordinate System (x,y)
y'
y
x'
Storm
Coordinate System
Normal
x
α
Squall Line
Leading Edge

Fig 12

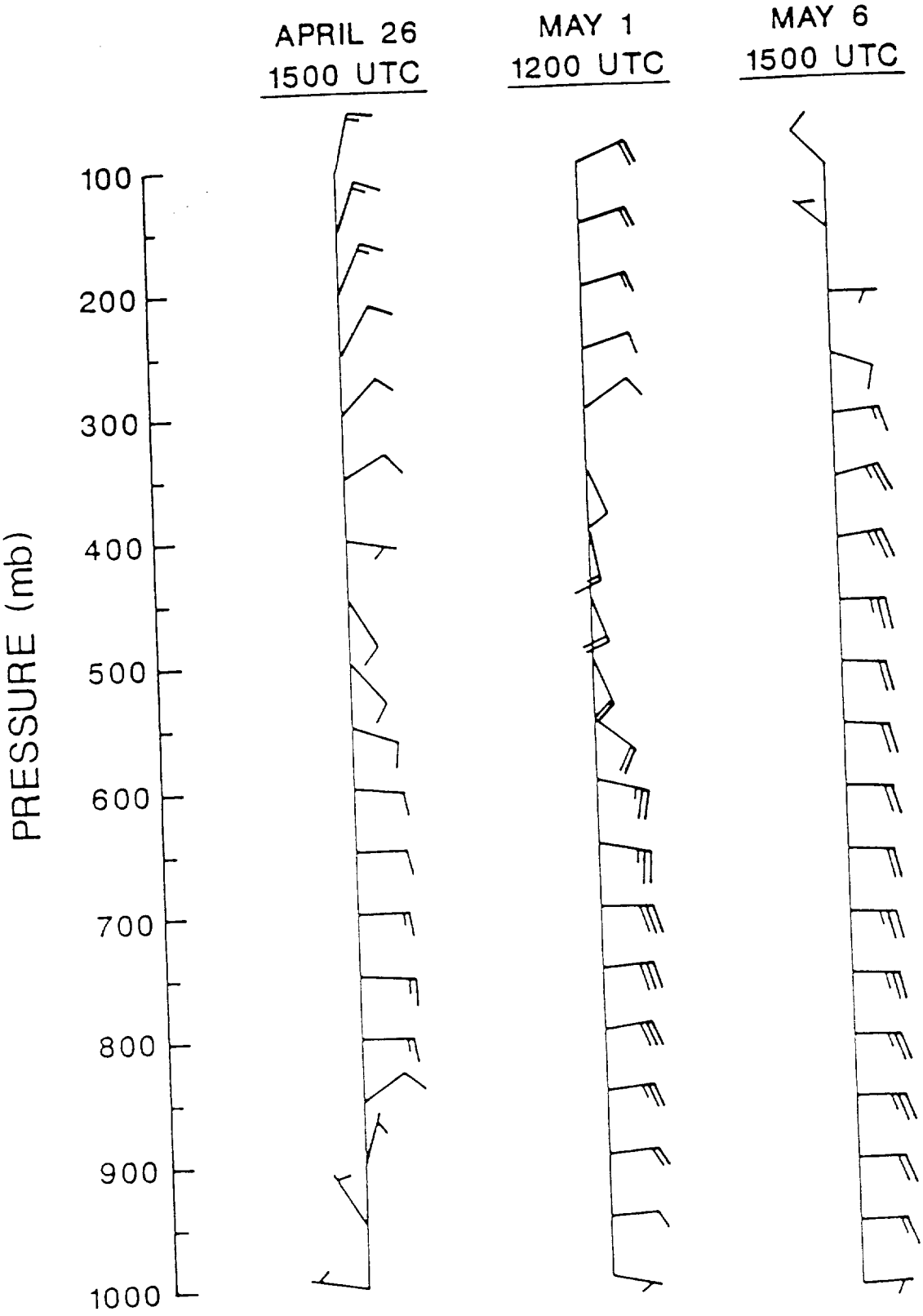
APRIL 26
1500 UTC
MAY 1
1200 UTC
MAY 6
1500 UTC
PRESSURE (mb)
100
200
300
400
500
600
700
800
900
1000

Fig 13

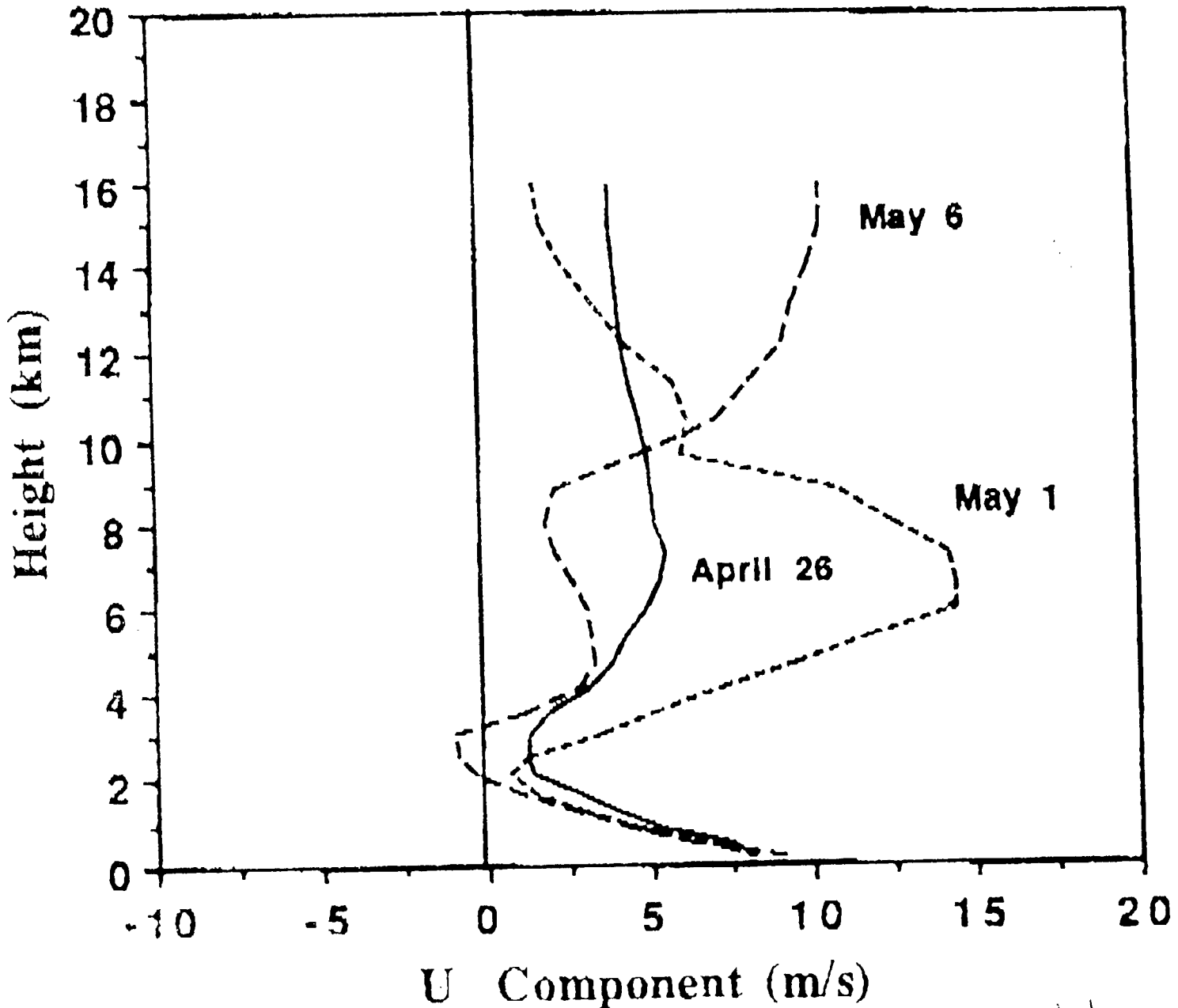
20
18
16
14
12
10
8
6
4
2
0
Height (km)
May 6
May 1
April 26
-10
-5
0
5
10
15
20
U Component (m/s)

Acq 14

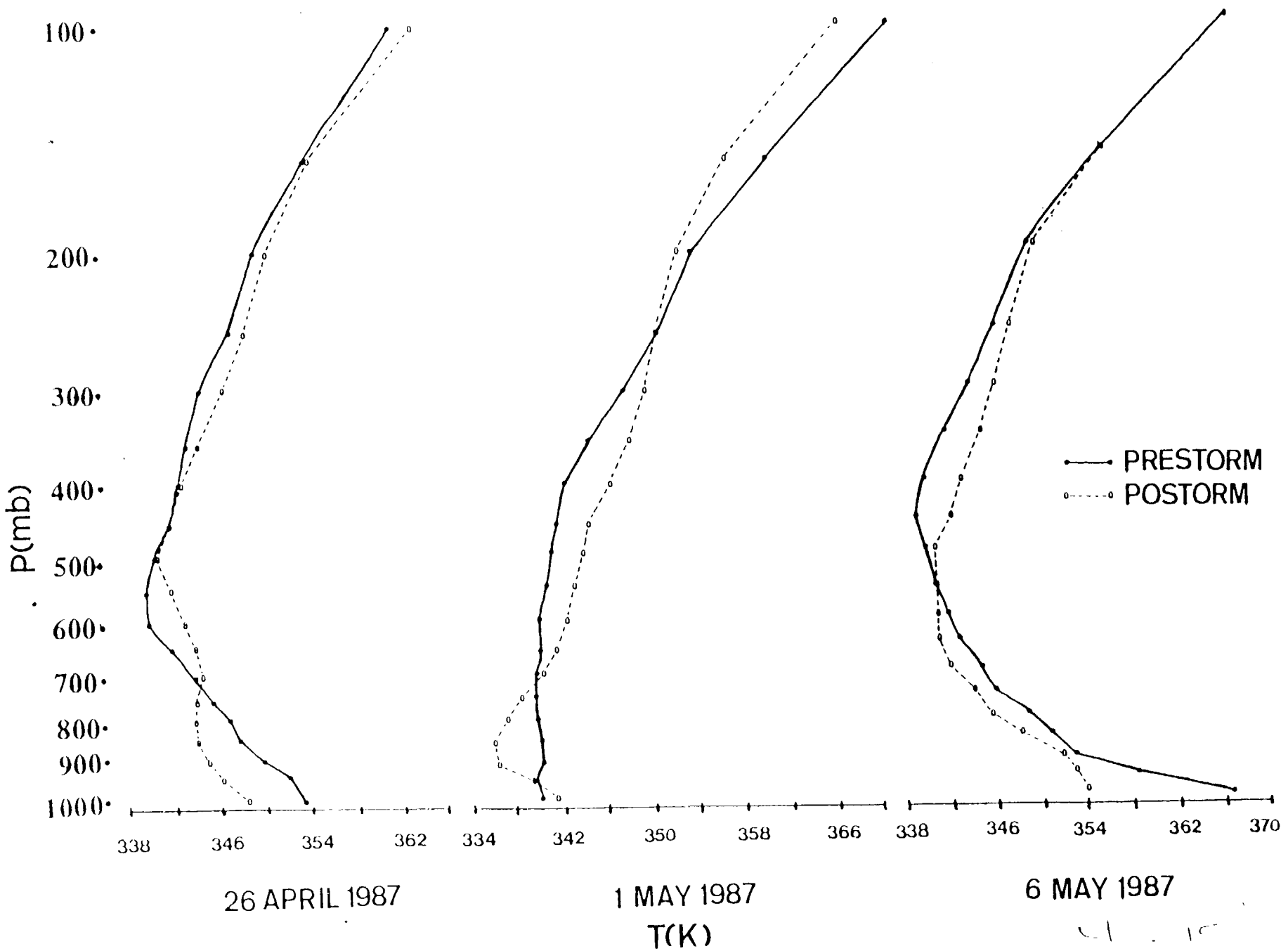
100
200
300
400
500
600
700
800
900
1000
P(mb)
338
346
354
362
334
342
350
358
366
338
346
354
362
370
PRESTORM
POSTORM
26 APRIL 1987
1 MAY 1987
6 MAY 1987
T(K)

AMAZON COASTAL SQUALL LINES
PART II: HEAT AND MOISTURE TRANSPORTS

Steven Greco, Harold L. Massie, Jr.[1], Michael Garstang,
Jeffrey Halverson, John Scala[2] and Wei-Kuo Tao[2]

Department of Environmental Sciences
University of Virginia
Charlottesville, VA 22903

[1]Air Weather Service Headquarters, Scott Air Force Base, IL 62225.

[2]Severe Storms Branch, NASA Goddard Space Flight Center, Greenbelt, MD 20771

Abstract

The role of the Amazon basin as a global center of action for deep convection is quantified in the context of the planet's heat balance. Mesoscale heat and moisture budgets are presented for three synoptic scale Amazon coastal squall lines (ACSL) over the central Amazon basin during the 1987 wet season. The budgets are obtained from volumetric analyses of mesoscale rawinsonde data from the second Amazon Boundary Layer Experiment (ABLE 2B). Classification of cloud and rainfall components are based on data from Portable Automated Mesonet (PAM) towers, GOES images, and radar. Satellite estimates of the total active cloud area, coupled with the mesoscale budget calculations, are used to determine the upper level vertical heat transport for an entire ACSL as a function of life cycle.

The instantaneous upper level heat transport in a mature ACSL equals nearly 20% of the theoretical export requirement for the equatorial trough zone. A little more than half of the system-wide transport occurs in the dynamically active anvil cloud. Amazon coastal squall lines are shown to exist over the basin simultaneously in various stages of formation, maturity and decay. When three stages are present, the combined instantaneous production of heat exceeds one third of the requirement to balance the global heat budget.

1. Introduction

Amazon Coastal Squall Lines (ACSL), classified as "Coastal Occurring Systems (COS)" by Greco et al. (1990), "Propagating Squall Lines (PSL)" by Cohen et al. (1989), and identified as lines of instability by Kousky and Molion (1981), rank among the largest of tropical synoptic disturbances. These systems can reach a total length of 2000-3000 km, with over 1000 km being active deep convection. More importantly, Greco et al. (1990) found that these "COS" were responsible for at least 40% of the total precipitation which fell over the Central Amazon Basin (CAB) during the 1987 wet season months of April and May.

In light of this important contribution to rainfall production, Part I of this study investigated the life cycle and kinematic structure of the ACSL over the CAB. As detailed in Part I, the ACSL develop during late morning-early afternoon along the northern coast of South America within an area of seabreeze-induced convection. They then intensify and propagate inland, possibly as mesoscale waves associated with trapeze instablity (Sun and Orlanski, 1981a, b). At night, due to the cutoff of surface heating, the ACSL and its associated convection weaken. Many of the ACSL dissipate before they enter the CAB. However, a large number (12 during the 1 April-15 May 1987 Amazon Boundary Layer Experiment) of ACSL continue propagating through the night and regenerate the following day in the CAB due to increased surface heating. The average propagation speed of the ACSL before dissipation is 50-65 km h^{-1}. At maturation, ACSL are

usually 1000-2000 km long and 100-300 km wide. These results agree well with the findings of Kousky (1980), Kousky and Molion (1981), Cohen et al. (1989) and Greco et al. (1990).

Divergence, vertical velocity and storm-relative flow calculations presented in Part I suggest a primarily 2-D airflow structure which features deep upward motion in the leading edge convection (LEC) and a region of mid-level speed convergence in the trailing stratiform region (TSR). Mesoscale ascent occurs in the TSR above 500 mb and subsidence below. The vertical motions in the TSR are an order of magnitude smaller than those in the LEC. These findings agree well with the structure and dynamics of other squall lines found both in the tropics and midlatitudes (Houze, 1989).

Part II of this study evaluates the mesoscale heat and moisture transports associated with three ACSL sampled in the CAB during the 1987 Amazon Boundary Layer Experiment (ABLE 2B). Special emphasis will be placed upon investigating the evolution of the heat and moisture transports as a function of both ACSL life cycle and cloud component. A secondary focus will be an evaluation of the relative importance of ACSL heat transports in the context of the total required global export of heat from the tropics.

The Amazon Basin plays a recognized role as a global "center of action" for thunderstorms (Newell et al., 1972), with the storms often concentrated in synoptic disturbances (Kousky, 1979, 1980; Molion, 1987; Greco et al., 1990). Until now, insufficient

rawinsonde measurements from the vast, relatively inaccessible Brazilian rain forests have precluded a definitive treatment of ACSL structure and energetics. This study uses a mesoscale network of surface and rawinsonde observations from the April-May 1987 ABLE 2B field program (Garstang et al., 1990; Harriss et al., 1990) to assess ACSL energetics.

While both Riehl and Malkus (1958) and Riehl and Simpson (1979) invoke the "hot" tower hypothesis to account for the needed upward transfer of heat from the lower to upper atmosphere in the tropics, they do not emphasize the concentration of the towers within any specific region of the tropics. They state that the required convective vertical transport of heat occurs in 1500-5000 giant clouds active at one time and distributed in approximately 30 large disturbances throughout the tropics.

The results presented in this paper suggest that organized meso- to synoptic-scale systems, such as the ACSL, which occur over a large equatorial, continental land mass contribute a significant fraction of the heat required to balance the heat budget of the planet.

The findings reported in the following sections differ from the results of Riehl and Malkus (1958) and Riehl and Simpson (1979) in that we suggest that injections of heat in the equatorial trough can be:

a) concentrated in centers of action over a continental land mass such as South America.

b) concentrated in organized meso- to synoptic-scale systems in which only half of the vertical heat transport is by the "hot tower" mechanism and half by mesoscale stratiform circulation.

The ACSL are further shown to generate multiple stratiform cloud layers in the moist environment of the CAB. Mesoscale circulations associated with the stratiform cloud layers are shown to accomplish up to 50% of heat transported to the upper troposphere. Hot tower transport occurring in the deep convective towers accounts for the remaining 50%.

Recent budget studies of tropical squall lines (Johnson, 1984; Houze, 1989; Ackerman et al., 1988; Gallus and Johnson, 1991) have also substantiated and clarified the important role played by anvil cloud layers. By partitioning their squall line analysis into convective and stratiform components, they show marked mesoscale ascent and vertical transports in the stratiform anvil. The energy needed for this mesoscale ascent has been attributed to the horizontal transport and injection of hydrometeors from the convective regions into the trailing stratiform layers (Rutledge and Houze, 1987). The total amount of heating will be shown to vary as a function of anvil area during the ACSL life cycle.

2. Data

The wet season ABLE 2B was in operation over the CAB from 1 April to 15 May 1987. A detailed description of the type, quality and frequency of meteorological data collected during

ABLE 2B can be found in Part I of this study and in both Garstang et al. (1990) and Harriss et al. (1990). To avoid repetition, only a concise summary of the data collection and measurement networks is presented below.

The ABLE 2B measurement network was designed to capture atmospheric motions ranging from the planetary through the turbulent scale. Geostationary Observational Environmental Satellite (GOES) imagery was used to analyze cloud fields over the entire Amazon Basin and western tropical Atlantic Ocean. Hourly visible and infrared images with both a 2 km and 8 km grid resolution were also employed in partitioning the ACSL into convective and stratiform components.

A four station mesoscale triangle network located in the CAB, 17 km north of the city of Manaus, Brazil (Fig. 1) was comprised of rawinsonde stations at the 3 triangle vertices co-located with Portable Automated Mesonet (PAM) stations. A PAM station was also employed at the center of the mesoscale triangle. Rawinsondes were launched every 3 h and provided wind, temperature, and humidity measurements between the surface and 100 mb. The PAM stations, located on towers 5 m above the forest canopy, recorded measurements of surface parameters such as rainfall, u, v, q, T and θ_e at a frequency of 1 Hz and stored them as 1 min averaged values.

Another component of the ABLE 2B measurement network was a 3 cm radar located at the Eduardo Gomez Airport between Manaus and the mesoscale network. Constant Altitude Planned Position

Indicator (CAPPI) scans of the entire network area were made every 5 min and were used in tracking the convective cells embedded within the ACSL and propagating through the mesoscale triangle.

As presented in Part I, the radar, PAM, rawinsonde and satellite data were used collectively to monitor the ACSL, to discern the stage of life cycle as it passed through the network, and to partition the ACSL into leading edge convection and trailing stratiform components. Heat and moisture transports for the different life cycle stages and the various ACSL components will be computed in the following sections.

3. Budget Equations

Equations presented by Yanai et al. (1973) and used in studies by Thompson et al. (1979), Johnson and Young (1983) and Johnson (1984), among others, are applied in heat and moisture transport calculations for the mesoscale triangle. The equations for sensible heat source (Q_1) and latent heat sink (Q_2) following Yanai et al. (1973) and Johnson and Young (1983), respectively, are:

$$Q_1 = \frac{\partial \overline{s}}{\partial t} + \overline{\mathbf{V}}\cdot\nabla\overline{s} + \overline{\omega}\frac{\partial \overline{s}}{\partial p} \qquad (1)$$

and

$$Q_2 = -L\left(\frac{\partial \overline{q}}{\partial t} + \overline{\mathbf{V}}\cdot\nabla\overline{q} + \overline{\omega}\frac{\partial \overline{q}}{\partial p}\right) \qquad (2)$$

where the symbols are defined as follows:

Q_1 = apparent sensible heat source

Q_2 = apparent moisture sink

s = dry static energy ($= C_pT + gz$)

C_p = specific heat at constant pressure

T = temperature

g = acceleration of gravity

z = geopotential height

q = specific humidity

V = horizontal wind velocity

ω = vertical velocity in pressures coordinates ($= dp/dt$)

p = pressure

t = time

L = latent heat of condensation

$\overline{}$ = area average of a quantity

From Yanai et al. (1973) and Thompson et al. (1979), the equation for the vertical eddy flux of total heat (F) between the tropopause (p_t) and a given pressure level (p) is:

$$F = g^{-1} \int_{P_t}^{p} (Q_1 - Q_2 - Q_R)\, dp \qquad (3)$$

where Q_R is the net radiative heating rate and F is zero at the highest level. The right side of Eq. (3) is a good estimate for F in larger-scale studies such as Yanai et al. (1973) where the horizontal eddy flux convergences are considered negligible. However, as noted by Gallus and Johnson (1991), subgrid horizontal heat and moisture transports between the convective and stratiform components of a squall line may not be negligible on the mesoscale.

Thus, our estimate of F is actually an estimate of the total cloud transport, including both horizontal and vertical eddy fluxes. Although the vertical eddy flux term tends to dominate on the scale and size of systems we are dealing with, our values of F are still an overestimate of the vertical eddy flux of total heat and will be treated as such in later sections.

Calculations of Q_1 and Q_2 include storage ($\partial/\partial t$), horizontal advection ($V\cdot\nabla$) and vertical advection ($\omega\,\partial/\partial p$) of s and q, respectively. Storage calculations use forward-in-time differences while vertical advection calculations use centered-in-space differences. Horizontal advection is found by applying a least squares objective analysis to rawinsonde measurements of s, q, u and v for the network triangle (Thompson et al., 1979; Johnson and Young, 1983).

The relatively small size of the triangle network and well-known limitations of rawinsonde systems cause unavoidable errors in Q_1 and Q_2. These errors are smaller and less significant during convectively active periods (Thompson et al., 1979; Johnson and Young, 1983) when the vertical advection terms increase by an order of magnitude and dominate over storage and horizontal advection.

Tropical budget studies (e.g., Thompson et al., 1979; Chen, 1987) and methods of convective parameterization based upon them (Frank, 1978; Betts, 1986) have emphasized diabatic processes related to water, water vapor, and ice phase changes over radiation. Although the magnitude of Q_R is small in relation to

Q_1 and Q_2, Q_R can play an important role in cloud development as shown by model simulations (Tao et al., 1992), and can account for a 10-20% increase in surface precipitation. Studies by Webster and Stephens (1980), Gray and Jacobson (1977) and Tao et al. (1991) indicate that large differences in net radiation between the base and top of anvil clouds cannot be ignored in the total heat budget of tropical cloud systems. In addition, horizontal gradients resulting from radiation effects between clear and cloudy regions are also important.

The net radiative heating (Q_R) due to both longwave and shortwave radiative processes in the triangular volume is calculated by the methods described in detail by Pielke (1984). Separate equations are used for the calculation of radiative fluxes, both long and short wave, in clear air and in the presence of clouds.

Fractional cloud cover (σ_c) at each pressure level in the mesoscale network is determined from the area-averaged relative humidity measured by rawinsonde. The method is generally based on cloud analysis procedures discussed in Air Weather Service Manual 105-124 (1969). The cloud analysis procedure employs a linear relationship between cloud cover and relative humidity. It is assumed that clouds form at a relative humidity of 90% and that the triangle is totally covered by clouds at a relative humidity of 100%. Relative humidities above the freezing level are based upon the frost point. The cloud analysis is checked for consistency against surface observations and satellite

images.

For levels partially covered by clouds, the longwave radiative flux for the combination of clouds and cloud-free air is

$$\overline{R}_{lw} = \sigma_c \overline{R}_c + (1 - \sigma_c)\overline{R} \qquad (4)$$

while the shortwave irradiance can be represented by

$$\overline{R}_{SWT} = \sigma_c \overline{R}_{SWC} + (1 - \sigma_c)\overline{R}_{SW} \ . \qquad (5)$$

These methods neglect backscattered radiation from the ground and overlying clouds, cloud shading and the effects of cloud shape.

Divergence for the mesoscale triangle is computed from the line integral of the wind components normal to each leg (Gamache and Houze, 1982). The divergence is calculated from 1000 to 100 mb in 25 mb intervals. The vertical velocity at each pressure level is first determined from the vertically integrated divergence and then adjusted by O'Brien's (1970) method.

4. Results

a. Heat and Moisture Transports

Recent work on the total heat budgets of squall lines has shown the importance of partitioning the vertical heating and moisture distributions into convective and stratiform components (Johnson and Young, 1983; Johnson, 1984; Houze, 1989; Chong and Hauser, 1990; Gallus and Johnson, 1991). The rawinsonde network of the ABLE 2B experiment is smaller than either the convective or stratiform components of the ACSL. Thus, the network is capable of giving measurements (surface and upper air) obtained entirely within each component. This enables individual

calculations of heating and moistening profiles for both the convective and stratiform components. Throughout this study, a composite sounding derived from an average of the nearly simultaneously launched rawinsondes from the three corners of the mesoscale triangle (Fig. 1) will be used to compute heating and moisture profiles.

Profiles of total sensible heat source and total apparent moisture sink for the 1 May 1987 squall line are shown in Fig. 2. These budgets were calculated for the system while it was in its mature stage. It should be noted that the profiles and budgets presented here for the 1 May system correspond only to that portion of the squall line that traversed the measurement network during the mature stage and may not be representative of other regions during different life cycles.

The squall system produced net heating and drying throughout the troposphere with peaks at 550 and 500 mb, respectively. The shape of the heating profile closely resembles that diagnosed for mesoscale systems over the Gulf of Carpentaria, which also exhibit their heating peak at 550 mb during maturity (Frank and McBride, 1989).

Unlike the total heating profiles of continental squall lines studied over West Africa (Chong and Hauser, 1990) and the Great Plains (Gallus and Johnson, 1991), the 1 May total Q_1 profile shows no cooling in the low-levels. Such cooling has been attributed to pronounced evaporation of both stratiform and convective rainwater in a relatively deep, dry subcloud air

layer. However, the lowermost troposphere over the Amazon forest canopy is characterized by a strong diurnal cycle of evapotranspiration that produces very large mixing ratios. Furthermore, model results for a similar ACSL system on 6 May (Scala et al., 1991) suggest a relative absence of dry tropospheric air for the production and maintenance of evaporatively cooled downdrafts. Thus, the characteristically high moisture content in the wet season lower troposphere may prevent or severely limit cooling in the convective region of the Amazon systems.

Normalizing the convective apparent sensible heat source by rainfall rate allows comparison of the magnitude of the peak heating rate with other studies (Johnson, 1984). The rainfall rate used in the normalization is expressed in cm d^{-1}. The normalization rate is obtained by extrapolating the convective rainfall rates in mm min^{-1} to 24 h. A rainfall rate of 16 cm d^{-1} on 1 May gives a normalized value for the Q_1 maximum of 17.5°K d^{-1} at 1200 UTC. This value is much larger than earlier estimates (Chong and Hauser, 1990; Gallus and Johnson, 1991; Johnson, 1976; Gamache and Houze, 1985). However, this large value may be partially due to the small size of the sampling network (1000 km^2) relative to other studies.

The profile of total apparent moisture sink in Fig. 2 indicates a weak double peak structure characteristic of many tropical mesoscale convective systems (Johnson, 1984; Frank and McBride, 1989; Gallus and Johnson, 1991). In these systems, the

double peak in Q_2 results from the combined effects of a low-level peak in drying in the convective region and a midlevel drying maximum in the stratiform region (Johnson, 1984). However, Fig. 3, which partitions the total heating and drying profiles into convective and stratiform components, indicates that the peak drying is concentrated in the midlevels (450-650 mb) in both the convective and stratiform regions. The weak double peak structure observed in the total profile is actually due to twin peaks (one at 500 mb, the other at 650 mb) in the convective region. This structure was also found in the deep convective elements over Taiwan (Johnson and Bresch, 1991). As noted in Johnson and Bresh (1991), there are two possible explanations. The double peak may arise from either the strong convergence of eddy moisture flux in the deep convective towers and/or the mesoscale triangle sampled co-existing convective and stratiform cloud types within the budget volume. We are unable to distinguish between these two processes from the available data.

Figure 3 also shows that the centers of convective heating and drying occupy nearly the same level and are approximately equal in magnitude. This suggests a coupling of Q_1 and Q_2 in the absence of pronounced eddy transports and is an indicator of predominantly stratiform processes (Gallus and Johnson, 1991). A study of systems over the Gulf of Carpentaria (Frank and McBride, 1989) showed that, during the period of most intense rainfall (mature phase), total heating and drying were also coincident.

The stratiform region profile, Q_2, in Fig. 3 exhibits two drying peaks, one at 800 mb and the other at 500 mb. While heating coincides with the upper peak as expected, cooling is associated with the lower maximum. In Part I, subsidence was found in this cooling layer. Typically, cooling and moistening characterize the sinking region beneath the melting level of most MCS (Houze, 1989). The reason for the observed drying is uncertain, but may be tied to the cutoff of a moisture source leading to drying of mesoscale downdrafts.

The stratiform region also has a shallow layer of warming and moistening below 950 mb. Since the squall line passed through the sampling network very early in the morning, the warming and moistening may indicate rapid boundary layer recovery processes during the mid-afternoon solar heating of the forest canopy. These recoveries are indeed present, as indicated by the PAM surface time series of such values as q and Θ_e (see Fig. 6, Part I). Nearly instantaneous increases in sensible and latent heat fluxes are often measured just above the forest canopy in the wake of the squall systems. Formation of extensive stratus decks within and above the forest canopy immediately after the convective rain suggests that very large rates of evapotranspiration are occurring.

Figure 4 shows the vertical profile of the total cloud transport flux of heat (F) and its decomposition into convective and stratiform components. Once again, we acknowledge that our results for F are indicative of total cloud transport (both

horizontal and vertical) and are not indicative of the vertical eddy flux of total heat as calculated in larger scale studies (i.e., Yanai et al., 1973). However, in the convection region (LEC), our F may still be a good estimate of vertical transports. In the stratiform region (TSR) though, horizontal motions are much more important and F overestimates the vertical eddy flux.

The total profile shows a broad mid-tropospheric maximum which is composed of two distinct peaks, one at 450 mb and the other at 600 mb. These peaks are the result of the strong maxima in the convective eddy flux. The reason for the double convective maxima is unclear. The stratiform contribution to the total eddy flux is largest in the mid-troposphere, and is maximized at the same level as the convective flux. The large positive eddy surface layer value is associated with fluxes of moisture and heat during boundary layer recovery. Slightly negative values above this surface layer in the stratiform region may be a consequence of the downward transport of warm, dry air from an inversion layer between 700 and 950 mb (refer to Part I for the sounding structure).

The magnitude of the maximum total cloud transport at 600 mb is over 2200 W m^{-2}, a number that nearly equals the maximum vertical eddy heat flux diagnosed between 500 and 650 mb for mid-latitude continental systems (Gallus and Johnson, 1991). However, the mid-latitude total eddy flux does not exhibit a double peak structure. The values reported here are much larger than the 400 W m^{-2} midlevel values found for tropical maritime

systems (Yanai et al., 1973; Esbensen et al., 1988), but it is important to note that in these earlier calculations, these budgets were calculated over much larger space and time scales than used in this study.

Figure 5 presents the total cloud transport for the stratiform regions of three Amazon squall lines. The 1 May case represents a system in its maturity, the 26 April system was weakening and the 6 May case was a system that initially weakened but then began to regenerate. The maxima for all three systems has a similar magnitude, but each differs from the other in its vertical distribution. The 6 May regenerating case includes a secondary maximum located just above the surface at 950 mb. This may be associated with shallow (newly developing) convective processes as the system enters its reorganizing stage.

Although the heat transport in the convective region of the 1 May ACSL is larger and occupies a deeper layer than in the stratiform region, it will be shown that when integrated over the larger horizontal area of anvil cloud, the stratiform region makes a significant contribution to the vertical eddy heat flux of the total squall system.

b. System-wide transports

The total system-wide heat transport of the ACSL is evaluated as a function of cloud component and life cycle with a model developed from the triangle network heat transport calculations and satellite analysis of active cloud area. The term "component" refers to part of the ACSL having features

that can be resolved by ABLE 2b sampling and analysis methods. As shown in Part I of this study, both the cloud component and life cycle stages of the ACSL as it passed through the rawinsonde measurement network were discerned through analysis of both GOES-west satellite imagery and the surface PAM data.

We will show that vertical heat transport by ACSL can equal a substantial amount of the lateral heat export requirement for the tropics as estimated by Riehl and Simpson (1979). Furthermore, it is revealed that the dynamically active ACSL anvil plays an important role in the total system-wide heat transport.

Table 1 gives the total vertical heat transport per unit area in both the LEC and TSR components of the mature 1 May ACSL. These values were obtained by integrating **F** over three separate layers. The integrations were carried out for the entire tropospheric column (1000-100 mb), the upper troposphere (500-100 mb), and the layer of strongest Hadley export from the equatorial trough zone (300-100 mb) (Palmén and Vuorela, 1963).

As mentioned in Section 3, our estimate of F includes both the vertical and horizontal eddy fluxes of heat and is thus an overestimate of the vertical transport of total heat. The improved estimates of F, called F_1 and F_2, have been made. In the F_1 approximation the horizontal flux term is considered negligible. In the F_2 approximation the horizontal flux is set equal in magnitude to the vertical eddy flux. Vertical motions dominate in the LEC, and therefore the true F will lie between F_1

and F_2. In the TSR, where horizontal motions may dominate (see Part I): the horizontal eddy flux term is (1) set equal to the vertical eddy flux (F_1) and (2) twice the vertical eddy flux term (F_2). The vertical eddy flux of total heat (F) for both the convective (LEC) and stratiform (TSR) likely lies between F_1 and F_2.

Although the total vertical heat transport within the LEC is 2-3 times larger than in the TSR region, massive amounts of heat are transported upwards through the entire tropospheric column in both components. There is a substantial decrease in the vertical transport of heat in the 500-100 mb layer within the LEC. This decrease shows that the ACSL converts much of the energy originating in the lower levels to help maintain the convective towers and also to export hydrometeors from the LEC into the TSR where the heat is released. The heat reaching the 300-100 mb layer is only 2% and 6% of the column total in the LEC and TSR, but, as will be shown below, takes on global importance when integrated over the area of an entire ACSL.

Table 2 displays the vertical heat transport per unit area in the TSR of a mature (1 May), weakening (26 April) and regenerating (6 May) ACSL. The general result of Tables 1 and 2 for the ACSL anvil is unmistakable: it is dynamically active.

Riehl and Simpson (1979) concluded that tropical deep convective towers provide the vertical heat transport required for the heat balance of the equatorial trough zone. In their previous study, Riehl and Malkus (1958), argued for the existence

of a midlevel total heat minimum, found throughout the tropics, that prohibited the vertical heat transport via a steady, large-scale upward circulation like that envisioned by Hadley (1735).

Riehl and Malkus (1958) also concluded that undilute transport in the "hot tower" conduits of tropical thunderstorms is the necessary mechanism for the transfer of heat to the upper levels of the atmosphere. Budget studies by Johnson (1984) and model experiments by Scala et al. (1990, 1991, 1992) show that undilute tranpsort is not the only means of vertical heat transport in tropical squall lines over continental rainforests.

Gamache and Houze (1982) and Cohen and Frank (1987) have shown that system-wide vertical transports are shared by cloud components consisting of more than hot towers. The results in Table 2 substantiate Johnson's (1984) recommendation to partition heating and moistening between the hot tower and anvil components.

Substantial vertical heat transports occur in the TSR during all stages of the ACSL life cycle (Table 2). The largest total column (1000-100 mb) heat transports occurred during the regenerating stage of the 6 May ACSL. However, the upper level vertical transports of heat (500-100, 300-100 mb) are strongest in the mature 1 May ACSL. This is especially true in the upper troposphere (300-100 mb) and is a good indicator of the importance of vertical transports in the stratiform region of a mature tropical squall line found over the CAB.

The results of Tables 1 and 2 are extrapolated to the scale

of an entire ACSL with the aid of the Mb-enhanced satellite images. First, the length and width of each convectively active cloud cluster appearing in black (segment 7) is measured on the Mb images. Then the lengths and widths of all active clusters are summed over the length of the entire ACSL to obtain the total active cloud area for the system.

The width of the LEC was derived from ground observations and the measured duration of convective rainfall at the PAM stations. The convective-stratiform rain rate cutoff was set at .25 mm/min. This value is slightly higher than most estimates (see for example, Gamache and Houze, 1982), but was necessitated by the .25 mm resolution of the tipping bucket raingauges employed at the PAM stations. However, the error introduced by this over-estimated cutoff is probably negligible due to the abrupt drop-off in rainfall intensities accompanying the passage of an ACSL (see Fig.6, Part I) and the fast response rainfall measurements utilized on the PAM stations (every minute). The widths obtained by these procedures are consistent with the Gamache and Houze (1982) structural morphology for tropical squall lines.

The anvil width is obtained by subtracting the combined widths of the building cumulus and hot towers from the satellite measurement of the total active width of the system. Large differences in anvil width at different stages of system maturity result in large differences in total active cloud area during the COS life cycle. In the three ACSL evaluated, each had an active

length of about 750 km while passing over the mesoscale network.

Table 3 shows the horizontally integrated system-wide heating in the 26 April, 1 May and 6 May ACSL for the same layers appearing in Tables 1-2. In these tables, it is assumed that vertical heat transport per unit area is uniform throughout each cloud component.

In the case of the mature 1 May ACSL, the importance of the TSR in terms of total and vertical heat transport is clearly evident. Due to both the larger width of the anvil (when compared to the LEC) and the existence of vertical motions (incorporated into the calculations of Q_1, Q_2, and F) within it, there is almost as much total vertical heat transport within the TSR as in the LEC region. In the upper half of the atmosphere (500-100 mb), however, the vertical transports are larger in the TSR than in the LEC. However, a large portion of the energy present in the TSR and available for vertical transport was probably generated in the LEC and transported into the TSR. This is consistent with results from other studies on the heat budgets of tropical squall lines (Tao et al., 1992).

All three ACSL cases show remarkably similar values of total vertical heat transport attributed to the TSR. The results in Table 2 most probably reflect the fact that, although the size (width) of the trailing anvil may change dramatically during the ACSL life cycle evolution, the strength of the circulations and transports within the core of the TSR remain relatively unchanged. Thus, the vertical motions and heat transports within

the TSR of all 3 storms were representative of an ACSL with active stratiform layer(s). In addition, the similar heat transport values support the classification of each storm as an ACSL and underscore some of their common attributes.

The maximum poleward-directed mass flow in the upper-level leg of the Hadley circulation occurs near 200 mb (Palmén and Vuorela, 1963). Riehl and Simpson (1979) calculated an upper-level requirement of 6.6×10^{15} W for the lateral heat export from a 10°-wide belt adjoining the equatorial trough line.

Table 4 presents the relative contributions to the Riehl-Simpson export requirements of the 300-100 mb vertical heat transports within the 1 May LEC and TSR components, and within the TSR component of both the 26 April and 6 May cases. The relative contributions of the pre-storm cumulus heat transports in the 6 May and 26 April ACSL were found to be negligible (< 1%) and thus the total 300-100 mb heat transport is seen as a sum of the contributions made by the TSR and LEC.

In the case of the 1 May ACSL, the 300-100 mb vertical transport of a mature system totals between 10% and 20% of the tropical export requirement. The percentage of the total tropical heat export requirement accomplished by a regenerating (6 May) and weakening (26 April) ACSL is found to be 6-10% and 10-16%, respectively.

According to analyses of ABLE 2b satellite data, up to 3 ACSL at different stages of their life cycle may exist concurrently over tropical South America. Using the results

obtained in Table 4, it can be seen that, during active periods of ACSL formation in the Amazon Basin (April-May and August-September) (Cohen et al., 1989), the total instantaneous upper-level heat transport attributed to the ACSL may equal as much as or higher than one-third of the tropical heat export requirement.

Similar, although slightly smaller values were determined by Connors (personal communication). In a study which classified the weather regimes over the Amazon Basin through analysis of digital data from hourly GOES-6 imagery (1 April 1986-1 April 1987), Connors (personal communication) found several prominent wet season regimes. The wet season weather regimes which existed during the climatological ACSL active months of April-May (Cohen et al., 1989) often contributed 1.0-2.0 x 10^{15} W or 15-30% of the energy required to balance the heat budget of the global tropics.

Riehl and Malkus (1958) argued that 1500-5000 hot towers, distributed among approximately 30 tropical synoptic disturbances could meet the heat export requirements of the equatorial trough at any one time. Our results indicate that 5-10 organized meso- to synoptic-scale disturbances such as the ACSL can meet the instantaneous upper-level heat transport requirement for the tropics.

5. Summary and Conclusions

In Part II of our investigation of the Amazon Coastal Squall Lines (ACSL) we have analyzed the heat and moisture transports of the ACSL in terms of convective and stratiform components, instantaneous and storm-wide energetics, and in relation to the

energy required to balance the heat budget of the global tropics.

Using rawinsonde data collected from a 4-station mesoscale network (approximately 1000 km^2) located in the CAB during the 1 April-15 May 1987 ABLE 2b experiment, vertical profiles of Q_1, Q_2 and F were determined for the convective (LEC - Leading Edge Convection) and stratiform (TSR - Trailing Stratiform Region) regions of a mature ACSL (1 May 1987) and the stratiform region of a weakening (26 April 1987) and regenerating (6 May 1987) ACSL. These instantaneous profiles were extrapolated to storm-wide energetics using rainfall rate and satellite imagery data to delineate the individual components of the ACSL and estimate their size and active cloud area.

Analysis of the mature 1 May ACSL indicates net heating and drying through the troposphere. The peak heating was found in the mid-levels (550-500 mb). This is similar to results for mesoscale systems in the Gulf of Carpenteria (Frank and McBride, 1989) but somewhat above the level of peak heating for mature eastern Atlantic systems (Johnson, 1984) and below the level identified for West African (Chong and Hauser, 1990), western Pacific (Johnson, 1984) and U.S. Great Plains (Gallus and Johnson, 1991).

Unlike the double peak structure found in the vertical profiles of Q_2 for many tropical mesoscale systems, the peak drying in the 1 May ACSL is mainly concentrated in mid-levels (450-650 mb). The similarity in magnitude and level of maximum transport found in the profiles of total Q_1 and Q_2 suggests a

coupling of Q_1 and Q_2 in the absence of pronounced eddy transports. This is also indicative of a predominantly stratiform process (Gallus and Johnson, 1991).

The Q_1, Q_2 and F profiles for the TSR of the 1 May, 26 April and 6 May ACSL all displayed similar shapes and magnitudes, with peak values found between 550 and 700 mb. Although the instantaneous heat and moisture fluxes associated with the LEC were much stronger than in the TSR, the horizontal and vertical extent of the TSR over the entire storm system results in significant heat transports for the TSR.

Total cloud transports of heat (F) were obtained for the atmospheric column (1000-100 mb) and the upper troposphere (500-100 mb, 300-100 mb) for both the LEC and TSR of the 1 May ACSL. Previous studies on larger scale networks (i.e., Yanai et al., 1973) have considered horizontal transports negligible and thus F was a representation of total vertical eddy flux of heat. However, in the present mesoscale study, horizontal effects can not be neglected and thus F is a measure of the total cloud transport (horizontal and vertical). Despite this difference, the similarity between our results and other studies indicate the critical role of cloud scale transports in the overall distributions of Q_1, Q_2 and F.

Large amounts of heat were transported in both the LEC and TSR components; 250,000-520,000 W m^{-2} in the LEC and 170,000-340,000 W m^{-2} in the TSR. The heat reaching the 300-100 mb layer was only 3% (LEC) of the total column heating. Thus, much of the

low-level energy is used to both maintain the convective towers and to export hydrometeors into the anvils.

The TSR of the regenerating (6 May) and weakening (26 April) ACSL also produced substantial heat transport of over 200,000 W m^{-2}. Thus, a dynamically active anvil region is a characteristic of the ACSL. In all three TSR, only 2-6% of the total column heat transport reaches the 300-100 mb layer for export from the Amazon Basin. However, calculations show that these small amounts are significant when integrated over the active area of the entire ACSL.

ACSL lengths and widths were determined through analysis of surface and satellite data. Typical dimensions of an active ACSL were 750-1000 km long by 100-200 km wide. In all 3 cases, the TSR occupied over 65% of the ACSL width.

On a storm-wide basis, the TSR region of the 1 May ACSL was responsible for more total vertical heat transport than the LEC region. This is especially true in the 500-100 mb layer. Similar heat transports were also found in the TSR of the 26 April and 6 May ACSL, underscoring their importance to the dynamics and energetics of the ACSL as a whole.

The relative contribution to the global heat budget was determined. The upper levels of a single, mature ACSL could account for 15-20% of the total amount of heat export required to balance the heat budget of the global tropics (Riehl and Simpson, 1979).

Although our calculations of F represented total cloud scale

transports, an estimate of the total vertical eddy flux of heat was obtained by assuming in the convective region (LEC) that, (1) as in larger scale studies (Gallus and Johnson, 1991; Yanai et al., 1973), horizontal transports are negligible; and (2) the vertical and horizontal transports are equal in magnitude. In the stratiform region (TSR), the horizontal flux was (1) set equal to and (2) 2X larger than the vertical flux. The true value of F likely lies somewhere between the 2 values.

Analysis of ABLE 2b satellite data indicates the presence of three ACSL over the Amazon Basin on several occasions. Calculations show that, in these instances, the ACSL may be responsible for up to one-third of the required upper level heat export from the global tropics. Thus, it appears that, in addition to the Riehl and Malkus (1958) hot tower hypothesis, 5-10 organized meso- to synoptic-scale disturbances (such as the ACSL) can meet the instantaneous heat export requirement for the tropics.

Acknowledgements

We gratefully acknowledge the sustained support provided by the Tropospheric Chemistry Program of NASA. This support, following the field work in ABLE 2a and 2b, has made analysis of extensive and unique data sets possible. We would also like to recognize the substantial computer resources support provided by the Goddard Space Flight Center.

A large part of this paper is drawn from Harold L. Massie's doctoral dissertation and from the doctoral research of Jeffrey Halverson.

References

Air Weather Service Manual 105-24, 1969: Use of the Skew-t, log P diagram in analysis and forecasting. Dept. of the Air Force, Headquarters Air Weather Service, Scott AFB, IL.

Ackerman, T.P., K.-N. Liou, F.P.J. Valero, and L. Pfister, 1988: Heating rates in tropical anvils. J. Atmos. Sci. 45, 1606-1623.

Betts, A.K., 1986: A new convective adjustment scheme. Part I: Observational and theoretical basis. Quart. J. Roy. Meteor. Soc., 112, 677-691.

Chen, Y.-L., 1987: Thermodynamic effects of mesoscale convective systems on the environment over the eastern Atlantic. J. Meteor. Soc. Japan, 65, 391-400.

Chong, M., and D. Hauser, 1990: A tropical squall line observed during the COPT 81 experiment in West Africa. Part III: Heat and moisture budgets. Mon. Wea. Rev., 118, 1696-1706.

Cohen, C., and W.M. Frank, 1987: Simulation of tropical convective systems. Part II: Simulations of moving cloud lines. J. Atmos. Sci., 44, 3800-3820.

Cohen, J.C.P., C.A. Nobre, and M.A.F. da Silva Dias, 1989: Mean distribution and characteristics of the squall lines observed over the Amazon Basin. Proc. Third Internat. Conf. Southern Hemisphere Meteor. and Oceanogr., Buenos Aires, Argentina, pp. 205-207.

Esbensen, S.K., J.T. Wang, and E.I. Tollerud, 1988: A composite life cycle of non-squall mesoscale convective systems over the tropical ocean. Part II: Heat and moisture budgets. J. Atmos. Sci., 45, 537-548.

Frank, W.M., 1978: The life cycle of GATE convective systems. J. Atmos. Sci., 35, 1256-1264.

Frank, W.M., and J.L. McBride, 1989: The vertical distribution of heating in AMEX and GATE cloud clusters. J. Atmos. Sci., 46, 3463-3478.

Gallus, W.A., Jr., and R.H. Johnson, 1991: Heat and moisture budgets of an intense midlatitude squall line. J. Atmos. Sci., 48, 122-146.

Gamache, J.F. and R.A. Houze, Jr., 1982: Mesoscale air motions associated with a tropical squall line. J. Atmos. Sci., 48, 122-146.

_____, and _____, 1985: Further analysis of the composite wind and thermodynamic structure of the 12 September GATE squall line. Mon. Wea. Rev., 113, 1241-1259.

Garstang, M., S. Ulanski, S. Greco, J. Scala, R. Swap, D. Fitzjarrald, D. Martin, E. Browell, M. Shipham, V. Connors, R. Harriss and R. Talbot, 1990: The Amazon Boundary Layer Experiment (ABLE 2B): A meteorological perspective. Bull. Amer. Meteor. Soc., 71, 19-32.

Gray, W.M., and R.W. Jacobson, 1977: Diurnal variation of deep cumulus convection. Mon. Wea. Rev., 105, 1171-1188.

Greco, S., R. Swap, M. Garstang, S. Ulanski, M. Shipham, R.C. Harriss, R. Talbot, M.O. Andreae, and P. Artaxo, 1990: Rainfall and surface kinematic conditions over central Amazonia during ABLE 2B. J. Geophys. Res., 93, 17001-17014.

Hadley, G., 1735: Concerning the cause of the general trade winds. Phil. Trans. Roy. Soc. London, 39, 58; reprinted in Smithsonian Inst. Misc. Collec., 51, 5-7 (1910).

Harriss, R.C., M. Garstang, S.C. Wofsy, S.M. Beck, R.J. Bendura, J.R.B. Coelho, J.W. Drewry, J.M. Hoell, P.A. Matson, R.J. McNeal, L.C.B. Molion, R.L. Navarro, V. Rabine, and R.L. Snell, 1990: The Amazon Boundary Layer Experiment: Wet season 1987. J. Geophys. Res., 93, 16721-16736.

Houze, R.A., Jr., 1982: Cloud clusters and large-scale vertical motions in the tropics. J. Meteor. Soc. Japan, 60, 396-410.

_____, 1989: Observed structure of mesoscale convective systems and implications for large-scale heating. Quart. J. Roy. Meteor. Soc., 115, 425-461.

Johnson, R.H., 1976: The role of convective-scale precipitation downdrafts in cumulus and synoptic scale interactions. J. Atmos. Sci., 33, 1890-1910.

_____, 1984: Partitioning tropical heat and moisture budgets into cumulus and mesoscale components: Implications for cumulus parameterization. Mon. Wea. Rev., 112, 1590-1601.

_____, and G.S. Young, 1983: Heat and moisture budgets of tropical mesoscale anvil clouds. J. Atmos. Sci., 40,

2138-2147.

_____, and J.F. Bresch, 1991: Diagnosed characteristics of precipitation system over Taiwan during the May-June 1987 TAME. Mon. Wea. Rev., 119, 2540-2557.

Kousky, V.E., 1979: Frontal influence on northeast Brazil. Mon. Wea. Rev., 107, 1140-1153.

_____, 1980: Diurnal rainfall variation in northeast Brazil. Mon. Wea. Rev., 108, 488-498.

_____, and L.C.B. Molion, 1981: Umq contribuicao a climatologia dinamica da troposfera sobre a Amazônia. INPE-2030-RPI/050, Sao Jose dos Campos, S.P. Brazil.

Molion, L.C.B., 1987: On the dynamic climatology of the Amazon basin and associated rain-producing mechanisms. In The Geophysiology of Amazonia: Vegetation and Climate Interactions, R. Dickerson (ed.), John Wiley, New York, pp. 391-407.

Newell, R.E., J.W. Kidson, D.G. Vincent, and G.J. Boer, 1972: The General Circulation of the Tropical Atmosphere and Interactions with Extratropical Latitudes, Vols. 1 and 2, MIT Press, Cambridge, MA.

O'Brien, J.J., 1970: Alternative solutions to the classical vertical velocity problem. J. Appl. Meteor., 9, 197-203.

Palmén, E., and L.A. Vuroela, 1963: On the mean meridional circulations in the Northern Hemisphere during the winter season. Quart. J. Roy. Meteor. Soc., 89, 131-138.

Pielke, R.A., 1984: Mesoscale Meteorological Modeling. Academic Press, New York, 612 pp.

Riehl, H., and J.S. Malkus, 1958: On the heat balance in the equatorial trough zone. Geophys., 6, 503-538.

_____, and J. Simpson, 1979: The heat balance in the equatorial trough zone, revisited. Contrib. Atmos. Phys., 52, 287-305.

Rutledge, S.A., and R.A. Houze, 1987: A diagnostic modeling study of the trailing statiform region of a midlatitude squall line. J. Atmos. Sci., 44, 2640-2656.

Scala, J.R., M. Garstang, W.-K. Tao, K.E. Pickering, A.M. Thompson, J. Simpson, V.W.J.H. Kirchhoff, E.V. Browell, G.W. Sachse, A.L. Torres, G.L. Gregory, R.A. Rasmussen, and M.A.K. Khalil, 1990: Cloud draft structure and trace gas transport. J. Geophys. Res., 93, 16721-16736.

Scala, J.R., W.-K. Tao, K. Pickering, A. Thompson, and M. Garstang, 1991: The effect of tropical squall-type convection on the vertical transport and redistribution of trace gases. Proc. AMS Seventh Joint Conf. on Appl. Air Poll. Meteor., with AWMA, New Orleans, LA, January, 228-231.

_____, W.-K. Tao, and J. Simpson, 1992: Transport dynamics in the convective and stratiform regions of a tropical squall line: Results of a two-dimensional numerical investigation. Proc. AMS 5th Conf. on Mesoscale Processes, Atlanta, GA, 303-306.

Sun, W.-Y., and I. Orlanski, 1981a: Large mesoscale convection and seabreeze circulation. Part I: Linear stability analysis. J. Atmos. Sci., 38, 1675-1693.

_____, and _____, 1981b: Large mesoscale convection and seabreeze circulation. Part II: Nonlinear numerical model. J. Atmos. Sci., 38, 1694-1706.

Tao, W.-K., J. Simpson and S.-T. Soong, 1991: Numerical simulation of a subtropical squall line over Taiwan Straits. Mon. Wea. Rev., 119, 2699-2723.

_____, _____, C.-H. Sui, L. Lang, J. Scala, B. Ferrier, M.-D. Chou, and K. Pickering, 1992: Heating, moisture and water budgets in the convective and stratiform regions of tropical and midlatitude squall lines: Their sensitivity to longwave radiation. Submitted to J. Atmos. Sci.

Thompson, R.M., Jr., S.W. Payne, E.E. Recker, and R.J. Reed, 1979: Structure and properties of synoptic-scale wave disturbances in the intertropical convergence zone of the eastern Atlantic. J. Atmos. Sci., 36, 53-72.

Webster, P.J., and G.L. Stephens, 1980: Tropical upper-tropospheric extended clouds: Inferences from winter MONEX. J. Atmos. Sci., 37, 1521-1541.

Yanai, M., S. Esbensen, and J. Chu, 1973: Determination of bulk properties of tropical cloud clusters from large-scale heat and moisture budgets. J. Atmos. Sci., 36, 53-72.

List of Figures

Fig. 1: Location of the ABLE-2B observation network in the Central Amazon Basin.

Fig. 2: Vertical profiles of the total sensible heat source and total apparent moisture sink for the 1 May 1987 squall line.

Fig. 3: Vertical profiles of the sensible heat source and apparent moisture sink for the convective and stratiform components of the 1 May ACSL at 1200 and 1800 UTC.

Fig. 4: Vertical profile of total cloud transport of heat (F) for the entire 1 May ACSL (solid) and both the convective (dashed) and stratiform (dotted) components.

Fig. 5: Vertical profile of total cloud transport of heat (F) for the stratiform components of the 26 April (solid), 1 May (dotted) and 6 May (dashed) ACSL.

TABLE 1. Vertical heat transport (per unit area) in the mature 1 May 1987 ACSL as a function of cloud component.

Pressure Layer (mb)	LEC ($W\ m^{-2}$)		TSR ($W\ m^{-2}$)	
	F_1	F_2	F_1	F_2
1000-100	521,538	260,769	171,588	114,380
500-100	112,350	56,175	64,690	43,122
300-100	12,950	6,475	9,299	6,198

TABLE 2. Vertical heat transports (per unit area) in the TSR region of a weakening (W), mature (M) and regenerating (R) ACSL.

	1000-100 mb ($W\ m^{-2}$)		500-100 mb ($W\ m^{-2}$)		300-100 mb ($W\ m^{-2}$)	
	F_1	F_2	F_1	F_2	F_1	F_2
26 April (W)	182,700	121,787	51,671	34,443	8,297	5,531
1 May (M)	171,588	114,380	64,690	43,122	9,299	6,198
6 May (R)	206,294	137,516	57,167	38,108	6,975	4,650

TABLE 3. Horizontal dimensions and total vertical heat transport in 3 separate layers for a mature (1 May), weakening (26 April) and regenerating (6 May) ACSL. Definitions for F_1 and F_2 are provided in text (Section 4b). Heat transports (W) were computed for the cloud component sampled by the rawinsondes.

Mature: **1 MAY**

	PSC	LEC		TSR	
		F_1	F_2	F_1	F_2
Width (km)	25	50		100	
Length (km)	750	750		750	
1000-100 mb	-	2.0×10^{16}W	1.0×10^{16}	1.3×10^{16}	0.9×10^{16}
500-100 mb	-	4.2×10^{15}W	2.1×10^{15}	4.8×10^{15}	3.2×10^{15}
300-100 mb	-	4.8×10^{14}W	2.4×10^{14}	7.0×10^{14}	4.6×10^{14}

Weak: **26 APRIL**

	PSC		LEC	TSR	
	F_1	F_2		F_1	F_2
Width (km)	25		50	100	
Length (km)	750		750	750	
1000-100 mb	5.2×10^{15}W	2.6×10^{15}	-	1.8×10^{16}	0.9×10^{16}
500-100 mb	3.6×10^{14}W	1.8×10^{14}	-	3.8×10^{15}	2.5×10^{15}
300-100 mb	2.6×10^{13}W	1.3×10^{13}	-	6.2×10^{14}	3.9×10^{14}

Table 3. (cont.)

Regenerating: 6 MAY

	PSC	LEC	TSR	
			F_1	F_2
Width (km)	10	25	75	
Length (km)	750	750	750	
1000-100 mb	-	-	1.1×10^{16}	0.7×10^{16}
500-100 mb	-	-	3.2×10^{15}	2.1×10^{15}
300-100 mb	-	-	3.9×10^{14}	2.6×10^{14}

TABLE 4. The 300-100 mb ACSL heat transport in percent of the equatorial heat export requirement of 6.6×10^{15} W (Riehl and Simpson, 1979). See Table 3 for definition of F_1 and F_2.

	LEC (%)		TSR (%)		TOTAL (%)	
	F_1	F_2	F_1	F_2	F_1	F_2
1 May (mature)	7.3	3.6	10.6	7.0	17.9	10.6
26 April (weakening)	*7.3	3.6	9.0	5.9	*16.3	9.5
6 May (regenerating)	*3.7	1.9	5.9	3.9	* 9.6	5.8

*Assuming the LEC 300-100 mb transport per unit area to be no larger than that occurring in the mature 1 May LEC region.

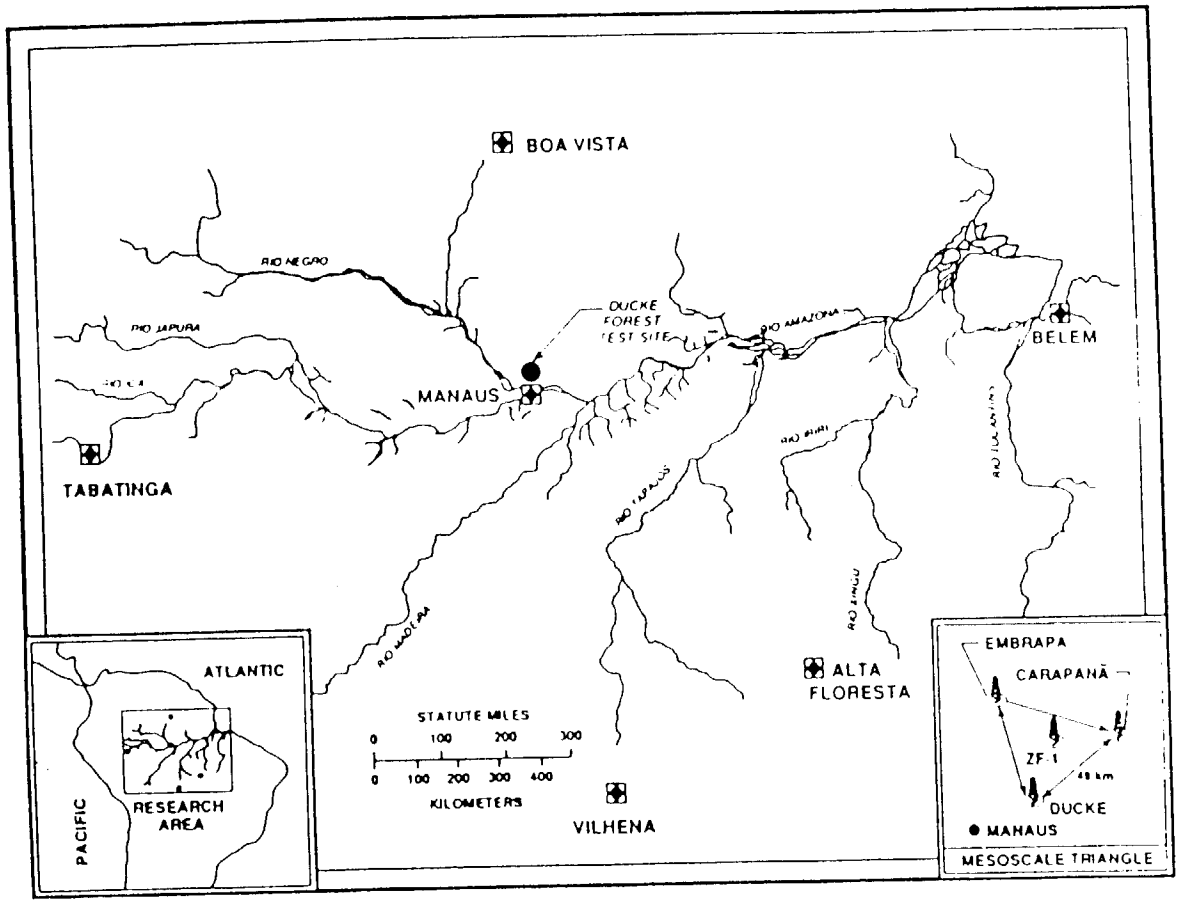
BOA VISTA
RIO NEGRO
RIO JAPURA
DUCKE FOREST TEST SITE
RIO AMAZONAS
BELEM
MANAUS
TABATINGA
RIO MADEIRA
RIO TAPAJOS
RIO XINGU
ALTA FLORESTA
VILHENA
STATUTE MILES
0 100 200 300
0 100 200 300 400
KILOMETERS
ATLANTIC
PACIFIC
RESEARCH AREA
EMBRAPA
CARAPANÃ
ZF-1
48 km
DUCKE
MANAUS
MESOSCALE TRIANGLE

Fig. 1

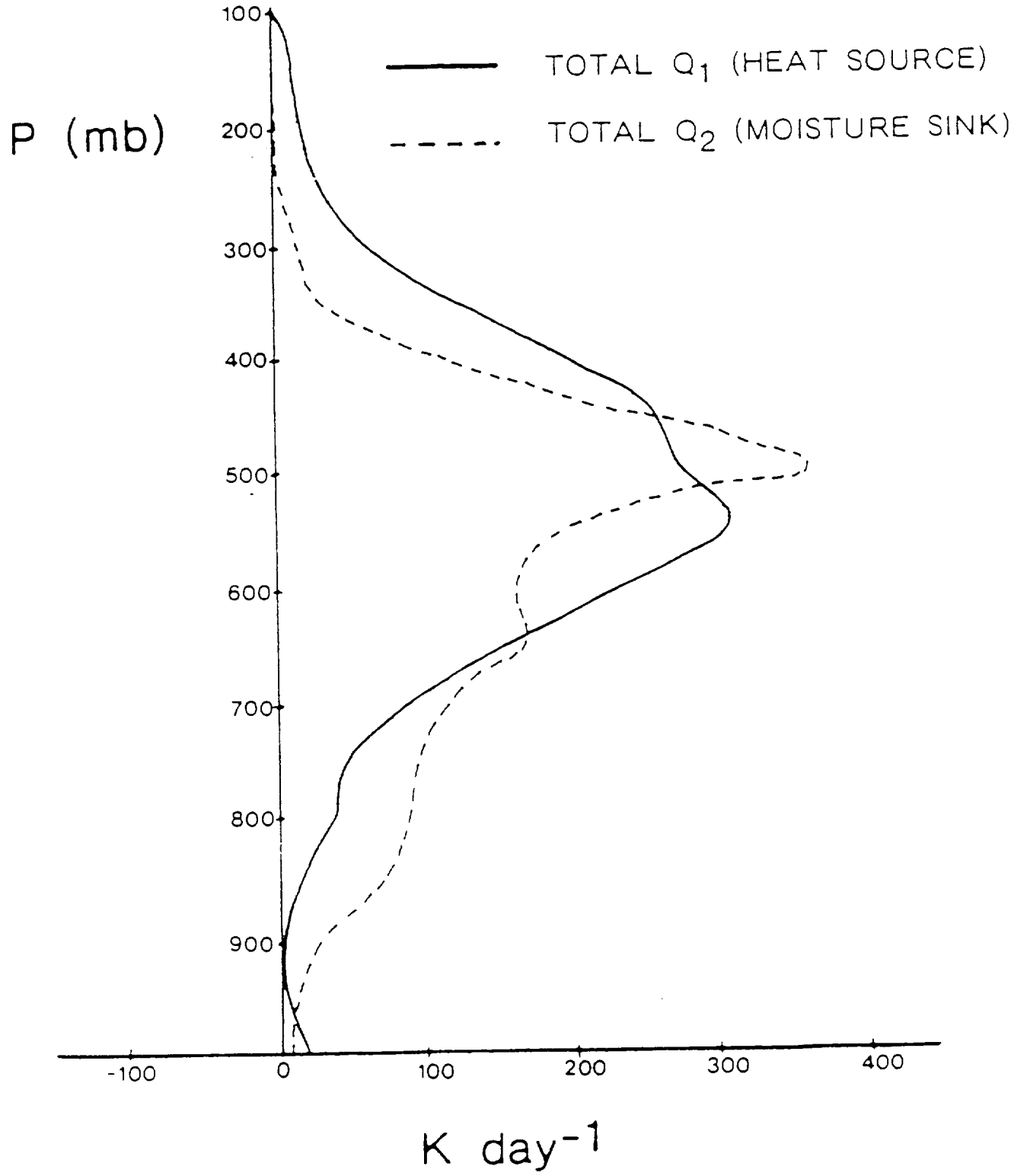
P (mb)
100
200
300
400
500
600
700
800
900
TOTAL Q_1 (HEAT SOURCE)
TOTAL Q_2 (MOISTURE SINK)
-100
0
100
200
300
400
K day^{-1}

Fig 2

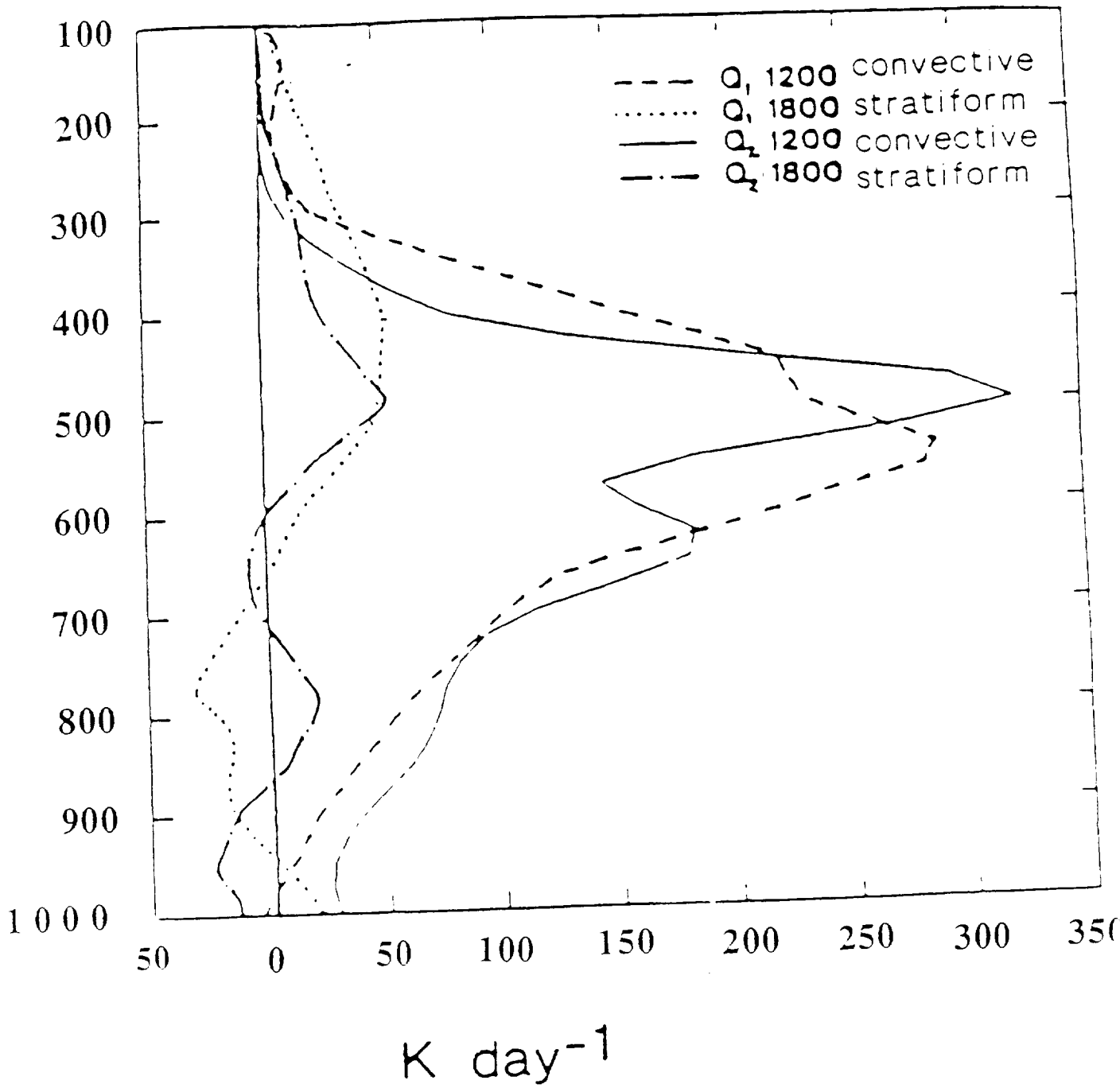
100
200
300
400
500
600
700
800
900
1000
p (mb)
50
0
50
100
150
200
250
300
350
K day-1
Q1 1200 convective
Q1 1800 stratiform
Q2 1200 convective
Q2 1800 stratiform

Fig 3

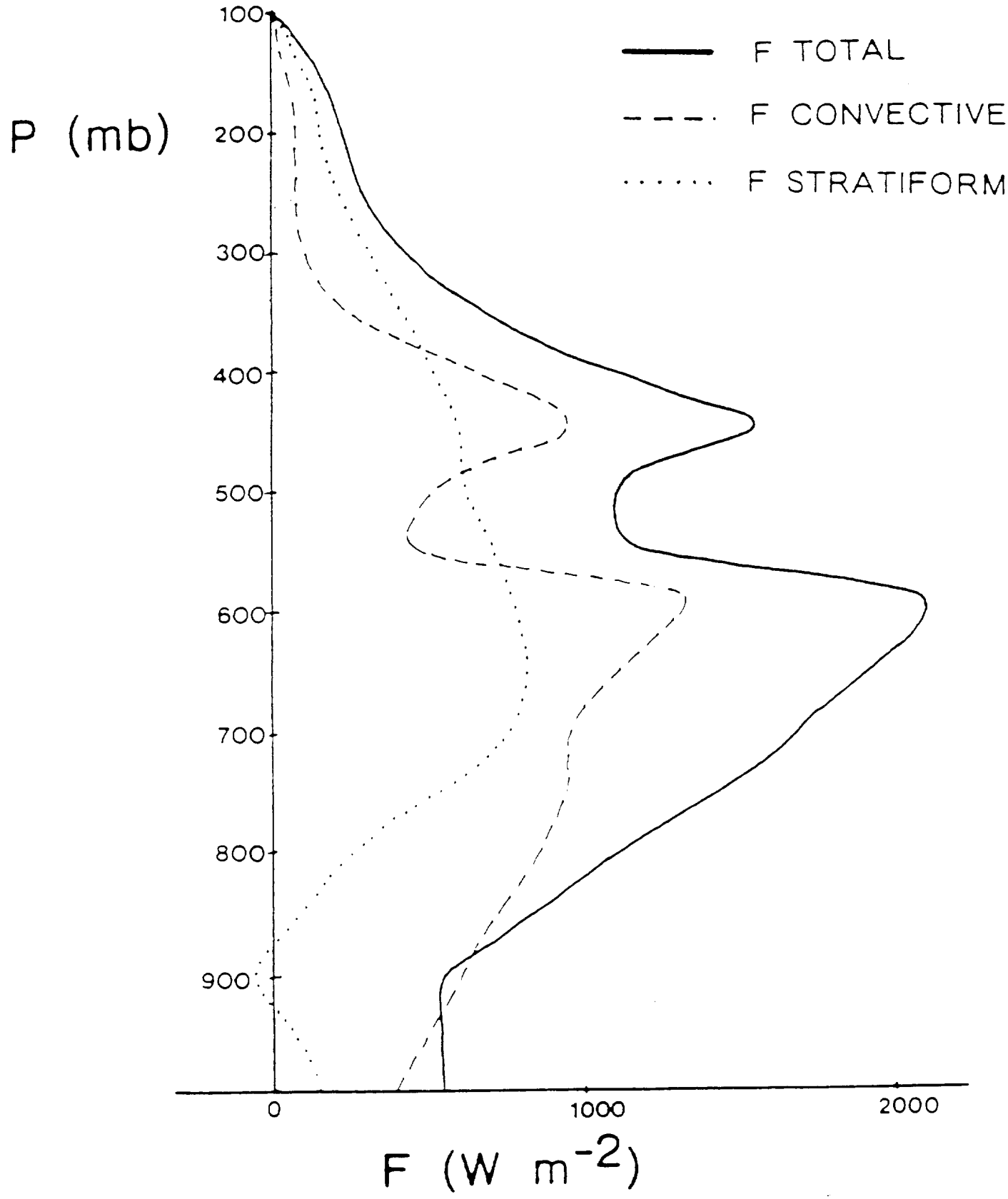
P (mb)
100
200
300
400
500
600
700
800
900
F TOTAL
F CONVECTIVE
F STRATIFORM
0
1000
2000
F (W m-2)

4q 4

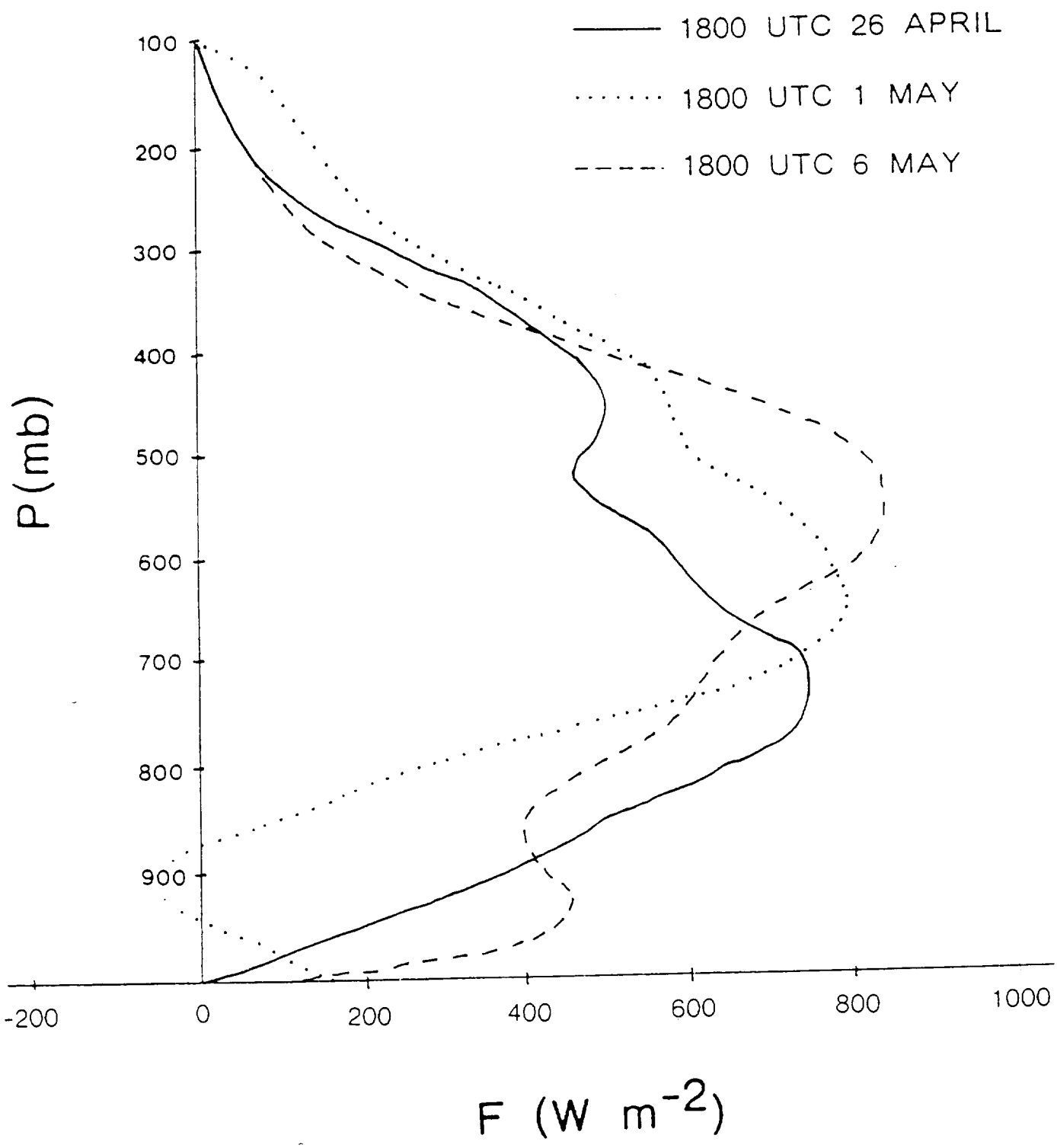
1800 UTC 26 APRIL
1800 UTC 1 MAY
1800 UTC 6 MAY
P(mb)
100
200
300
400
500
600
700
800
900
-200
0
200
400
600
800
1000
F (W m-2)

Fig 5